Atom counting with accelerator mass spectrometry

Walter Kutschera*

Faculty of Physics—Isotope Physics, University of Vienna, Vienna Environmental Research Accelerator (VERA), Waehringerstrasse 17, A-1090 Vienna, Austria

A. J. Timothy Jull

Geosciences and Physics, University of Arizona, Tucson, Arizona 85721-0077, USA and Isotope Climatology and Environmental Research Centre (ICER), Institute for Nuclear Research, 4026 Debrecen, Hungary

Michael Paul

Racah Institute of Physics, The Hebrew University of Jerusalem, Jerusalem 91904, Israel

Anton Wallner

Accelerator Mass Spectrometry and Isotope Research, Helmholtz-Zentrum Dresden-Rossendorf, Institute of Ion Beam Physics and Materials Research, Bautzner Landstrasse 400, D-01328 Dresden, Germany and Institute of Nuclear and Particle Physics, Technische Universität Dresden, D-01062 Dresden, Germany

(published 28 September 2023)

Accelerator mass spectrometry (AMS) was born in the late 1970s, when it was realized at nuclear physics laboratories that the accelerator systems can be used as a sensitive mass spectrometer to measure ultralow traces of long-lived radioisotopes. It soon became possible to measure radioisotope-to-stable-isotope ratios in the range from 10^{-12} to 10^{-16} by counting the radioisotope ions "atom by atom" and comparing the count rate with ion currents of stable isotopes ($1.6\ \mu A = 1 \times 10^{13}$ singly charged ions/s). It turned out that electrostatic tandem accelerators are best suited for this, and there are now worldwide about 160 AMS facilities based on this principle. This review presents the history, technological developments, and research areas of AMS through the 45 yr since its discovery. Many different fields are touched by AMS measurements, including archaeology, astrophysics, atmospheric science, biology, climatology, cosmic-ray physics, environmental physics, forensic science, glaciology, geophormology, hydrology, ice core research, meteoritics, nuclear physics, oceanography, and particle physics. Since it is virtually impossible to discuss all fields in detail in this review, only specific fields with recent advances are highlighted in detail. For the others, an effort is made to provide relevant references for in-depth studies of the respective fields.

DOI: 10.1103/RevModPhys.95.035006

CONTENTS

*Corresponding author: walter.kutschera@univie.ac.at

I. INTRODUCTION

A. History

1. Isotopes

The concept of isotopes was introduced by Frederick Soddy when it turned out that certain newly discovered radioactive species could not be separated by chemical means. They were therefore assigned to the same element, i.e., to the same place (*isos topos*) on the periodic chart of elements (Soddy, 1913). At about the same time, it was observed that positive rays of neon ions deflected in a magnetic spectrograph split up into a main component at mass 20 and a weaker one at mass 22 (Thomson, 1913). This was the first physical proof that an element consists of at least two stable isotopes. With refined mass-spectrometric techniques, Aston established by 1922 that 18 elements consisted of more than one isotopes, with a total of 58 isotopes (Aston, 1922). In the ensuing years more isotopes were discovered, but it is interesting that these results were achieved before the neutron was discovered (Chadwick, 1932a, 1932b). After this discovery, theoretical considerations quickly led to the conclusion that the atomic nucleus must contain both protons and neutrons (Heisenberg, 1932): Isotopes of a particular element therefore have a fixed proton number in the nucleus but a varying number of neutrons. On the other hand, the term *nuclide* is used whenever a nucleus with an unambiguous proton and neutron number is denoted; see Fig. 5. Recently a compilation of the discovery of all stable and radioactive isotopes known by 2015 (3211 in all) was published (Thoennessen, 2016). The total number of isotopes within the so-called dripline, beyond which the nuclei cannot bind to an additional proton or neutron, may eventually still increase by a factor of 2 by producing them in exotic nuclear reactions at the new generation of heavy-ion accelerators. Although most of them will have short half-lives (<1 s), they are of interest to fully explore the limits of nuclear forces, and to study the synthesis of the elements in stars in the laboratory (Thielemann, 2019). In this review, we concentrate on long-lived radioisotopes with half-lives of a few years to about 10^8 yr, which can be traced by accelerator mass spectrometry (AMS) in minute quantities in many sections of the environment at large (Kutschera, 2016). [Note that in cosmochronolgy and geochronology "long-lived" radioisotopes are sometimes called "short lived" since they did not survive the age of the Solar System (Wasserburg *et al.*, 2006).]

2. Counting atoms rather than decays

It was pointed out early in the development of AMS that "counting atoms rather than decays" results in an unprecedented detection sensitivity of long-lived radioisotopes (Muller, 1977). Although this was contemplated earlier (Oeschger *et al.*, 1970), only AMS made it feasible. Arnold (1987) mentioned in a retrospective paper about decay counting that in the early days of radiocarbon dating mass spectrometry was already suggested to Willard Libby, but the low isotopic ratios of $^{14}C/^{12}C \sim 1.2 \times 10^{-12}$ did not make it feasible at the time. A considerable effort for a mass-spectrometric detection of ^{14}C without an accelerator using CN^- ions was reported by Anbar (1978) at the First Conference on Radiocarbon Dating with Accelerators but fell short by 1 order of magnitude.

As an example of the difference between beta decay counting and direct atom counting, we first consider the detection of ^{14}C (half-life $= 5700 \pm 30$ yr) through its beta decay. [For the slight revision of the traditional half-life of 5730 ± 40 yr (Godwin, 1962) to the new one, see the discussion of the ^{14}C half-life by Kutschera (2019).] A sample of 1 mg organic

carbon with a natural isotope ratio of $^{14}C/^{12}C \sim 1.2 \times 10^{-12}$ (Arnold and Libby, 1949) contains about 6×10^7 ^{14}C atoms. If we denote this number as N, then from the radioactive decay law $dN/dt = -\ln 2 \times (N/\text{half-life})$ one calculates that slightly less than one ^{14}C atom decays per hour out of the 6×10^7 in the sample. With AMS, however, it is possible to directly count in one hour ~2% of the 6×10^7 ^{14}C atoms, which means about 10^6 times more than by decay counting. Thus, a large factor in detection efficiency is gained (for decay counting one actually has to use a few grams of carbon and count for several days). Over the years, the AMS technique has been refined so much that it is now possible to perform ^{14}C measurements with just a few micrograms of carbon (Santos *et al.*, 2007; Cao *et al.*, 2013; Petrenko *et al.*, 2016; Steier *et al.*, 2017). Thus, a factor of 10^6 is gained in the reduction of the sample size, which allows one to take small samples from precious objects. All this is possible only through the particular selectivity of AMS, where both the nuclear charge (atomic number Z) and the mass (mass number A) are determined at sufficiently high beam energies. Since every isotope has a unique combination of Z and N (neutron number $N = A - Z$), an unambiguous detection of trace isotopes down to extremely low concentrations is possible. In contrast, the widely used mass-spectrometric methods without accelerators depend chiefly on high-mass resolution (Ireland, 2013). Since the ultimate limitation is unidentified background events, AMS allows one to measure isotope ratios that are several orders of magnitude lower than what is possible with mass spectrometry without an accelerator (Maher, Jjunju, and Taylor, 2015). A notable exception is the laser-based magneto-optical trap technique called atom trap trace analysis (ATTA), which is described in Sec. II.G (Lu, 2016).

3. Discovery of accelerator mass spectrometry

The first use of an accelerator as a mass spectrometer was in 1939, when Louis Alvarez used the 60 in. cyclotron at Berkeley (Fig. 1) to detect ^3He in helium (Alvarez and Cornog, 1939a). He subsequently showed that tritium (^3H) is radioactive by bombarding deuterium (^2H) with deuterons and separated ^3H from ^3He (Alvarez and Cornog, 1939b). This was an important discovery because it proved that ^3He, not ^3H, was the stable mass-3 nuclide, contrary to what was believed at that time (Bethe and Bacher, 1936). Many years later, Alvarez described these early days of accelerator mass spectrometry in a reminiscent article in Physics Today (Alvarez, 1982), where he also pointed out his discovery of the tandem accelerator principle (Alvarez, 1951), which later became so important for AMS. In 1980, Alvarez *et al.* (1980) also provided evidence that the extinction of the dinosaurs some 6.6×10^7 yr ago were caused by an impact of a large meteorite on Earth; see Sec. IV.B.3.

After a period of almost 40 yr, where accelerators were used mainly to study nuclear reactions, the use of accelerators as mass spectrometers was rediscovered in 1977 at several nuclear physics laboratories (Bennett *et al.*, 1977; Muller, 1977; Nelson, Korteling, and Stott, 1977; Purser *et al.*, 1977). While in Berkeley the 88 in. cyclotron was operated with positively charged ions to detect ^{14}C at natural abundances

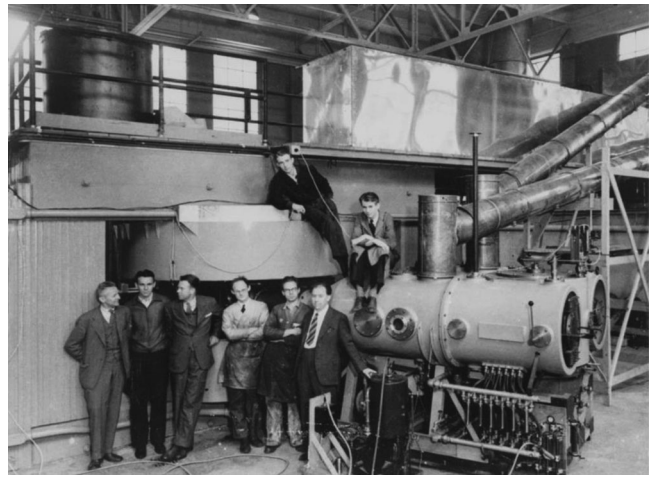

FIG. 1. The 60 in. cyclotron at the Lawrence Radiation Laboratory, Berkeley, soon after completion in 1939. The key figures in its development and use are, from left to right, Dr. D. Cooksey, Dr. D. Corson, Dr. Ernest Orlando Lawrence (the inventor of the cyclotron), Dr. R. Thornton, Dr. J. Backus, W. S. Sainsbury, Dr. L. W. Alvarez, and Dr. Edwin Mattison McMillan.

(Muller, 1977) and to search for quarks with unit charge (Muller *et al.*, 1977), it was recognized at the tandem accelerators of the University of Rochester (Bennett *et al.*, 1977; Purser *et al.*, 1977) and of McMaster University (Nelson, Korteling, and Stott, 1977) that the requirement of negatively charged ions at the injection offered an enormous advantage for ^{14}C detection. The chief reason is the complete suppression of the stable isobar ^{14}N in the ion source, because it does not form stable negative ions. Since we live in an atmospheric "ocean" of ^{14}N and the relative mass difference to ^{14}C is only one hundred thousandth (10^{-5}), it is virtually impossible to separate the isobars by mass discrimination alone. Although abundant negative molecules such as $^{13}CH^-$ and $^{12}CH_2^-$ are formed in the ion source and interfere with ^{14}C at low energy, the stripping process at the terminal of tandem accelerators breaks up the molecules and thus removes this interference effectively; see Sec. II.D.1. The pioneering AMS efforts of 1977 were described in several reminiscences by some of the original participants (Gove, Purser, and Litherland, 2010; Muller, 2010; Nelson, 2010; Purser and Litherland, 2020).

Although detection of ^{14}C with small cyclotrons using negative-ion injection to suppress ^{14}N was pursued for some time (Bertsche *et al.*, 1990; Chen *et al.*, 2000; Zhou *et al.*, 2000), the advantage of tandem accelerators is so great that they now became the basis for essentially all AMS facilities (~150) around the world (Synal, 2013, 2022). In the early days of AMS, though, the Grenoble cyclotron was used with positive-ion injection for the first detection of ^{10}Be with AMS (Raisbeck *et al.*, 1978). The same group subsequently used the accelerator system ALICE [linear accelerator (linac) plus cyclotron] at Orsay to separate ^{26}Al from the stable isobar ^{26}Mg by fully stripping the ions at high energy (Raisbeck, Yiou, and Stephan, 1979). Similarly, ^{41}Ca was separated from the stable isobar ^{41}K (Raisbeck and Yiou, 1980). Now these radioisotopes are all measured with tandem AMS facilities at much lower energy. The detection of the heavy radioisotope

^{205}Pb was pursued early on with positive-ion injection only at the UNILAC heavy-ion linac at GSI Darmstadt (Ernst *et al.*, 1984). Positive-ion injection must be used for noble gases since they do not form negative ions (except for metastable He^-). Examples are the measurements of ^{81}Kr at the superconducting cyclotron of Michigan State University (Collon *et al.*, 2000) and ^{39}Ar at the Argonne Tandem Linear Accelerator System (ATLAS) heavy-ion linear accelerator at Argonne National Laboratory (Collon *et al.*, 2004; Tessler *et al.*, 2018).

Over the years AMS has been reviewed many times, documenting the steady progress in both technical and scientific aspects. Some of these reviews were given by Muller (1979), Litherland (1980), Kutschera (1983, 2005, 2013 2016), Elmore and Phillips (1987), Kutschera and Paul (1990), Finkel and Suter (1993), Tuniz *et al.* (1998), Fifield (1999), Gove (1999), Collon, Kutschera, and Lu (2004), Suter (2004), Jull and Burr (2006), Gove, Purser, and Litherland (2010), Litherland, Zhao, and Kieser (2011), and Synal (2013, 2022).

Progress in AMS was documented in the proceedings of the triannual AMS conferences starting in 1978 at the University of Rochester (Gove, 1978) and continued at Argonne National Laboratory (Henning *et al.*, 1981). Since 1984, the proceedings have been published in Nuclear Instruments and Methods in Physics Research B: AMS 3, Zurich, Switzerland (Wölfli, Polach, and Andersen, 1984); AMS 4, Niagara-on-the-Lake, Canada (Gove, Litherland, and Elmore, 1987); AMS 5, Paris, France (Yiou and Raisbeck, 1990); AMS 6, Canberra-Sydney, Australia (Fifield *et al.*, 1994); AMS 7, Tucson, AZ (Jull, Beck, and Burr, 1997); AMS 8, Vienna, Austria (Kutschera *et al.*, 2000); AMS 9, Nagoya, Japan (Nakamura *et al.*, 2004); AMS 10, Berkeley, CA (Knezovich *et al.*, 2007); AMS 11, Rome, Italy (Calcagnile *et al.*, 2010); AMS 12, Wellington, New Zealand (Zondervan *et al.*, 2013); AMS 13, Aix-en-Provence, France (Braucher and Bourlès, 2015); AMS 14, Ottawa, Ontario, Canada (Kieser *et al.*, 2020); and AMS 15, Sydney, Australia.

B. Long-lived radionuclides

1. Cosmic-ray-produced radionuclides

The seminal work of Lal and Peters (1967) described the production of radioactivity on Earth through a cosmic-ray interaction. Based largely on this work, Fig. 2 summarizes the production of long-lived radioisotopes in the atmosphere (Kutschera, 2013).[1]

The production rate depends on the availability of suitable target atoms, the cosmic-ray flux, and the cross sections of nuclear reactions with primary cosmic rays, which are composed mainly of highly energetic protons (Simpson, 1983). Secondary cosmic rays (neutrons or muons) produce radioactivity in the atmosphere, and some reach the surface of Earth and produce valuable radioactivity in rocks (Lal, 1988), which can be utilized by AMS for surface exposure dating (Lal, 1991) and erosion studies (Dunai, 2010). For recent reviews see Hajdas *et al.* (2021) and Schaefer *et al.* (2022).

[1]For a record of CO_2 in the past, see https://keelingcurve.ucsd.edu.

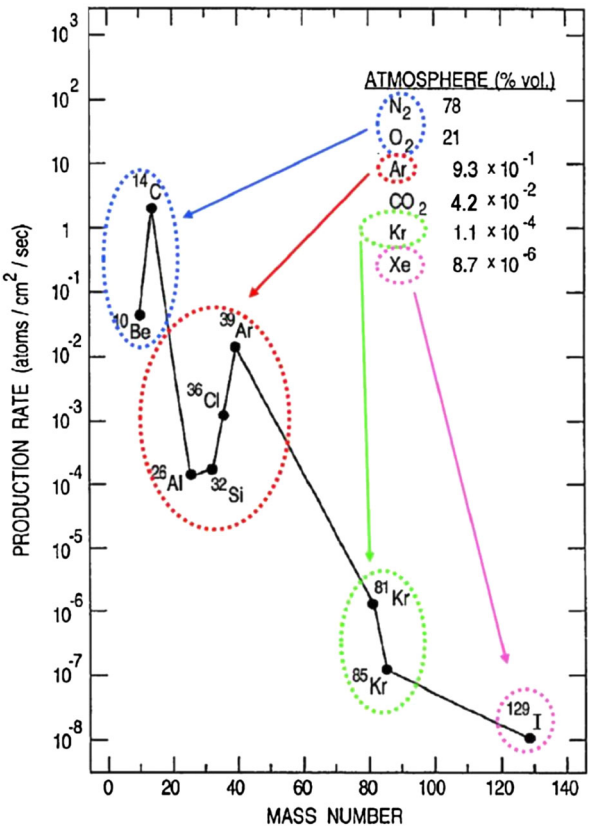

FIG. 2. Production rate of long-lived radionuclides by cosmic rays in the atmosphere. The main target atoms for the production of the respective radionuclides are indicated with different colors. The atmospheric concentration of CO_2 in 2022 is 0.042%. The total production rates in the atmosphere (atoms/s) can be obtained by multiplying the plotted numbers with the surface of Earth (5.1×10^{18} cm^2). Adapted from Kutschera, 2013.

2. Artificial radionuclides

Short-lived radionuclides are widely used in physics and other fields, often as "tracers" of various processes because they mimic the chemical behavior of their stable isotopes. They are also useful for both diagnostic and therapeutic use in the medical field. Sometimes these radioactivities produce a long-lived daughter product. An example is the most used radionuclide in diagnostic medicine, the short-lived metastable ^{99m}Tc (half-life = 6.0 h), fed through the beta decay of the longer-lived "mother" ^{99}Mo (half-life = 66 h). ^{99m}Tc decays to the long-lived ground state of ^{99}Tc [half-life = 2.1×10^5 yr (Browne and Tuli, 2017)]. ^{99}Tc also contributes to the long-lived inventory from nuclear power reactors, because it is the long-lived end product of the mass-99 isobaric chain produced in the fission of ^{235}U and ^{239}Pu.

The intense nuclear weapons testing period between 1952 and 1963 released neutrons and fission products into the atmosphere. The neutrons reacted with ^{14}N to form ^{14}C (Fig. 3), increasing the ^{14}C content in the atmosphere by about a factor of 2 at the time of the Nuclear Test Ban Treaty in 1963 (Levin and Hesshaimer, 2000; Levin *et al.*, 2022). This triggered interesting applications of the so-called ^{14}C bomb peak (Grimm, 2008). Other anthropogenic radionuclides are discussed in Sec. III.G.

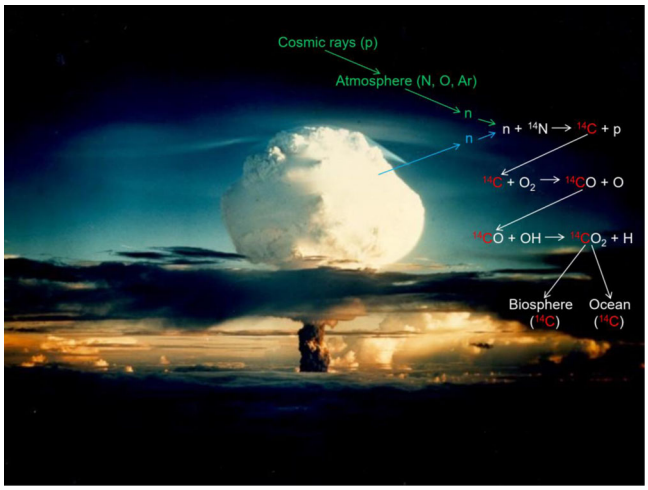

FIG. 3. Schematic presentation of ^{14}C production in the atmosphere through the nuclear reaction $^{14}\mathrm{N}(n,p)^{14}\mathrm{C}$, with neutrons originating from both cosmic-ray-induced spallation of atmospheric nuclei and man-made nuclear explosions. The subsequent two-step oxidation of ^{14}C to $^{14}\mathrm{CO}_2$ and its uptake by the biosphere and the ocean are also indicated. The photo is from the first hydrogen-bomb test "Ivy Mike" in 1952 (National Nuclear Security Administration, Nevada Site Office). Adapted from Wild *et al.*, 2019.

3. Overview of radionuclides suitable for AMS measurements

Early on the long-lived radionuclides ^{10}Be (half-life $= 1.39 \times 10^6$ yr), ^{14}C (5700 yr), ^{26}Al (7.18×10^5 yr), ^{36}Cl (3.01×10^5 yr), and ^{129}I (1.61×10^7 yr) were established as being well suited for AMS measurements with tandem accelerators (Elmore and Phillips, 1987). For a discussion of half-lives see Sec. IV.A.1.

Twenty-five years later, the number of radionuclides measured with AMS had grown to 55 (Kutschera, 2013), and in 2022 had reached 61 (also including the primordial radionuclides ^{40}K, ^{232}Th, ^{235}U, and ^{238}U): ^{3}H, ^{7}Be, ^{10}**Be**, ^{14}**C**, ^{26}**Al**, ^{32}Si, ^{36}**Cl**, ^{39}Ar, ^{40}K, ^{41}Ca, ^{44}Ti, ^{53}Mn, ^{55}Fe, ^{59}Ni, ^{60}Fe, ^{63}Ni, ^{68}Ge, ^{79}Se, ^{81}Kr, ^{90}Sr, ^{92}Nb, ^{93}Zr, ^{99}Tc, ^{126}Sn, ^{129}**I**, ^{135}Cs, ^{137}Cs, ^{146}Sm, ^{151}Sm, ^{166m}Ho, ^{182}Hf, ^{202}Pb, ^{205}Pb, ^{210}Pb, ^{210m}Bi, ^{226}Ra, ^{228}Ra, ^{228}Th, ^{229}Th, ^{230}Th, ^{231}Pa, ^{232}Th, ^{232}U, ^{233}U, ^{234}U, ^{235}U, ^{236}U, ^{237}Np, ^{238}U, ^{239}Pu, ^{240}Pu, ^{241}Pu, ^{241}Am, ^{242}Pu, ^{243}Am, ^{244}Pu, ^{244}Cm, ^{246}Cm, ^{247}Cm, ^{248}Cm, and ^{250}Cm.

Frequently measured radionuclides are marked in bold letters. Among them, ^{14}C is by far the most used one (>90%). This is due to the versatility of ^{14}C for research in many different fields (Kutschera, 2018). The second most used radionuclide is ^{10}Be, followed by ^{26}Al, ^{36}Cl, and ^{129}I. A potentially interesting radionuclide is ^{41}Ca (half-life $= 9.94 \times 10^4$ yr), as it was envisioned early on for the dating of bones (Yamaguchi, 1963) and first considered with AMS

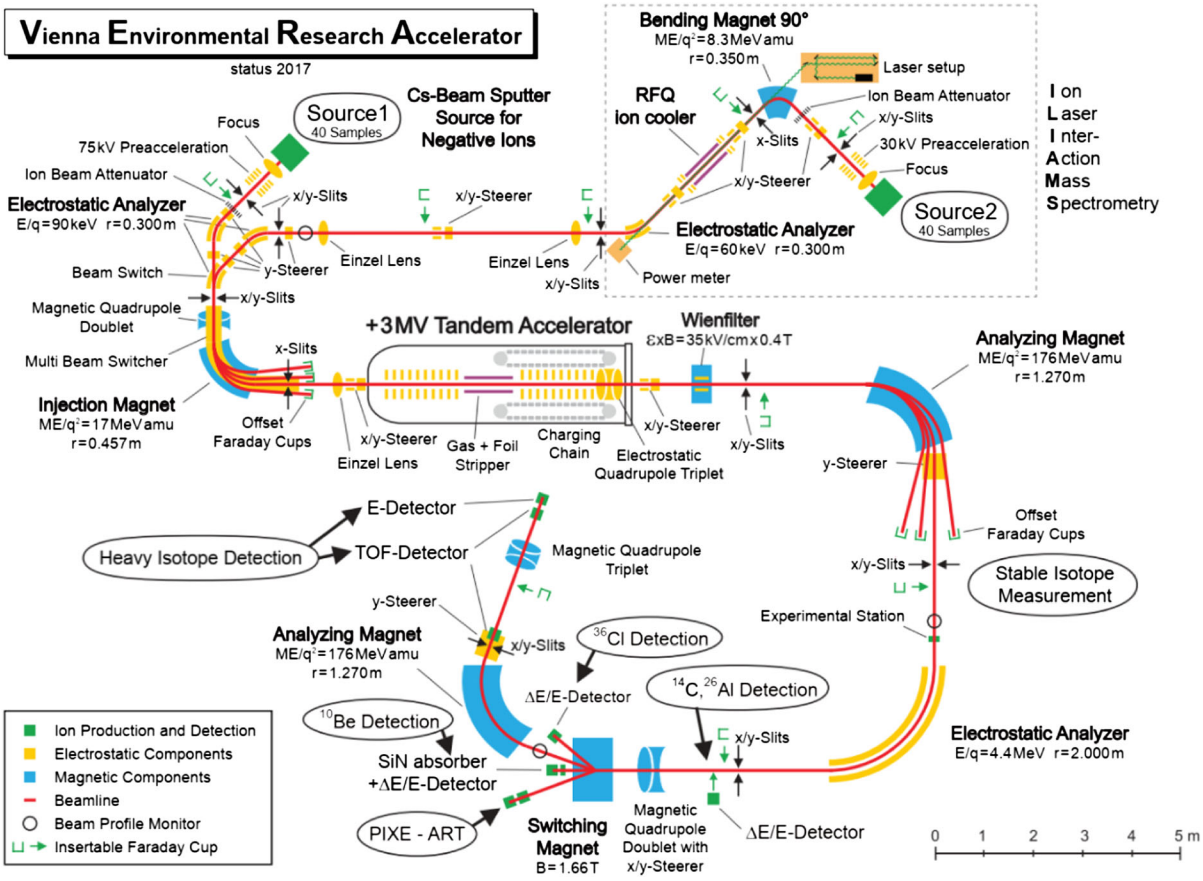

FIG. 4. Schematic layout of the VERA AMS facility in the configuration of 2022. The original facility became operational in 1997 and has since gone through several upgrades in order to accommodate the presently detected isotopes. From Golser and Kutschera, 2017.

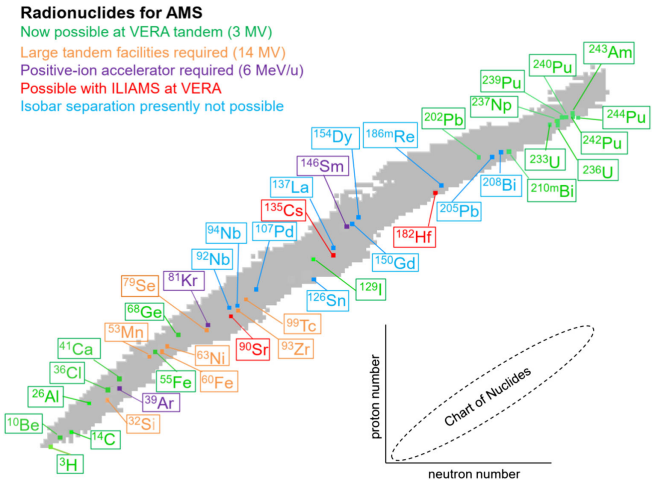

FIG. 5. Display of radionuclides that are of interest for AMS measurements. Radionuclides that can be measured at smaller tandem AMS facilities like VERA are marked in green, whereas those that can currently be measured only at larger tandem facilities are marked in brown. The ones marked in purple require positive-ion production and acceleration via heavy-ion linear accelerators (Collon *et al.*, 2004; Kinoshita *et al.*, 2012; Tessler *et al.*, 2018) or heavy-ion cyclotrons (Collon *et al.*, 2000). The ones marked in red can now be measured at VERA using the new laser-anion interaction system ILIAMS (Martschini, Hanstorp *et al.*, 2019; Martschini *et al.*, 2020, 2022); see also Sec. II.D.3. Previously ^{90}Sr could be measured only at a large tandem facility (Paul *et al.*, 1997). For radionuclides marked in blue, a stable isobar suppression has presently not been achieved.

(Raisbeck and Yiou, 1979, 1980; Henning *et al.*, 1987). Although the detection of ^{41}Ca at natural levels in different environments has been accomplished with AMS (Fink, Klein, and Middleton, 1990; Fink *et al.*, 1990), a radiocalcium dating method for bones is still awaiting a solution; see Sec. III.A.7.

A versatile AMS facility such as the Vienna Environmental Research Accelerator (VERA) based on a 3 MV tandem accelerator (Fig. 4) is capable of measuring a large fraction of the previously listed radionuclides that typically excludes some of the medium-heavy and heavy radionuclides requiring isobaric separation. The situation is depicted in Fig. 5.

II. TECHNICAL ASPECTS OF AMS

A. Isotopic ratios: General principle of AMS measurements

AMS is a mass-spectrometric method that produces an ion beam and separates ions according to their mass, particle energy, and charge state by electric and magnetic components and, moreover, can separate or discriminate nuclides of the same mass number A and different atomic number Z. Rare isotopes are counted with particle detectors one by one, while the beam intensity of stable ions is measured as a current with Faraday cups. By alternating the measurement setup between rare and reference isotope, an isotopic abundance ratio of these two can be obtained. By the use of an accelerator and particle stripping (discussed later), much lower atom concentrations can be measured than with conventional mass-spectrometric techniques [exceptions are some applications using resonance ionization mass spectrometry (RIMS) (Wendt, Trautmann, and Bushaw, 2000; Wendt, 2002]. AMS often allows the measurement of long-lived radionuclides at their natural abundance ratios with respect to their stable isotopes. If no stable isotope exists, such as in the case of Pu AMS, a well-known amount of a spike can be added to the sample, and the rare isotope can then be measured relative to the spike again as the isotopic ratio (both counted with a particle detector). The measured isotope ratio needs to be corrected for measurement background, which may be introduced either during sample preparation (for instance, modern ^{14}C) or as an intrinsic machine (usually ion source) background. The isotopic ratio needs to be normalized by means of standards of well-defined ratios to correct for mass-dependent effects in the measurement setup (such as stripping, tuning differences, or systematic differences in the particle detector versus current measurement).

In AMS, the ion beam is selected for the isotope of interest, and unwanted atoms or molecules are filtered using a series of electrostatic and magnetic deflectors. Utilizing the high particle energies provided by the accelerator (Sec. II.B), particle identification methods of nuclear physics with single-atom detectors can be applied (Sec. II.E). The sample material is sputtered and therefore slowly consumed with consumption rates of less than or of the order of a milligram per hour of measurement. The detector rates can be between more than 1000 events per second for modern carbon and less than one event per day, for instance, for ^{60}Fe- or ^{244}Pu-free blank samples. If only a few counts are expected, it is crucial to suppress completely the interfering background due to stable elements of the same mass called isobars (for example, ^{10}B in the case of ^{10}Be), molecules of the same mass ($^{12}CH_2$ vs ^{14}C), and tails of the more abundant isotopes (for instance, ^{235}U and ^{238}U vs ^{236}U). It is also crucial to suppress other ions (such as m/q ambiguities) that can enter the detector and may be present at much higher count rates but different energies.

The abundance sensitivity in AMS is limited by the overall efficiency of the rare isotope detection (this is the fraction of radionuclides in the sample that is counted eventually with the detector), and also by any residual isobaric and isotopic interferences in the detector mimicking a rare radionuclide detector signal. Many methods have been developed to make AMS measurements possible for a number of isotopes or for improving the measurement sensitivity to facilitate its wide range of applications. The typically 10–16 orders of magnitude or so higher intensity of stable neighboring isotopes makes it more and more probable for heavier masses to pass the mass-selective filters due to scattering and charge-exchange reactions when the relative mass difference becomes smaller. Isobars cannot be separated by mass and a number of techniques are applied to remove or identify the isobaric content in the beam. In the following, we discuss different types of accelerators (Sec. II.B) and how to prepare samples and produce negative ions (Sec. II.C). Optimizing measurement sensitivity by source output and some methods to suppress interfering background are also discussed (Secs. II.D and II.E). For more details on the specific techniques used in AMS, see Synal (2013, 2022).

B. The choice of accelerator

1. Tandem accelerators

Accelerator mass spectrometry is a good example of the use of accelerators for a purpose they were not built for (Alvarez, 1982). Although early on AMS was performed with both cyclotrons and tandem accelerators, it was soon realized that AMS can best be performed with the latter (Litherland, 1980), especially in combination with cesium-beam negative-ion sputter sources (Middleton, 1984a, 1984b). This type of accelerator therefore became the preferred system for AMS experiments. Over the years, a dramatic reduction in the size of AMS facilities has been achieved (Fig. 6), driven by systematic investigations of ion beam physics at ETH Zurich (Suter, Jacob, and Synal, 1997; Synal *et al.*, 2004; Synal, Stocker, and Suter, 2007).

The main reasons why tandem accelerators are well suited for AMS are as follows.

(a) For several important radionuclides (^{14}C, ^{26}Al, ^{36}Cl, and ^{129}I), the otherwise strongly interfering stable isobars (^{14}N, ^{26}Mg, ^{36}Ar, and ^{129}Xe) do not form stable negative ions. Other examples are ^{55}Fe, ^{68}Ge, and ^{202}Pb, where the stable isobars (^{55}Mn, ^{68}Zn, and ^{202}Hg) also do not form stable negative ions.

(b) The stripping process in the terminal of tandem accelerators, converting negative ions to positive ones, breaks up interferences of molecules of the same mass number (such as $^{12}CH_2^-$ and $^{13}CH^-$) for ^{14}C detection.

(c) It is possible to stabilize the terminal voltage of the tandem accelerator with a feedback loop from a generating voltmeter guaranteeing a well-defined particle energy without the need for a slit control feedback signal from a "real" beam on the high-energy end of the accelerator. Alternative methods used position-sensitive Faraday cups (White *et al.*, 1981). In power supply driven low-energy AMS, high-voltage stability is intrinsically provided from the power supply itself.

(d) The cesium-beam negative-ion sputter source (Middleton, 1983) is capable of producing negative ions for most elements. Molecular negative ions can be used in cases where atomic ions are unstable and/or weakly bound (such as $^{10}BeO^-$, $^{41}CaH_3^-$, and $^{41}CaF_3^-$).

(e) Detailed studies of the stripping process in tandem accelerators (Suter, Jacob, and Synal, 1997;

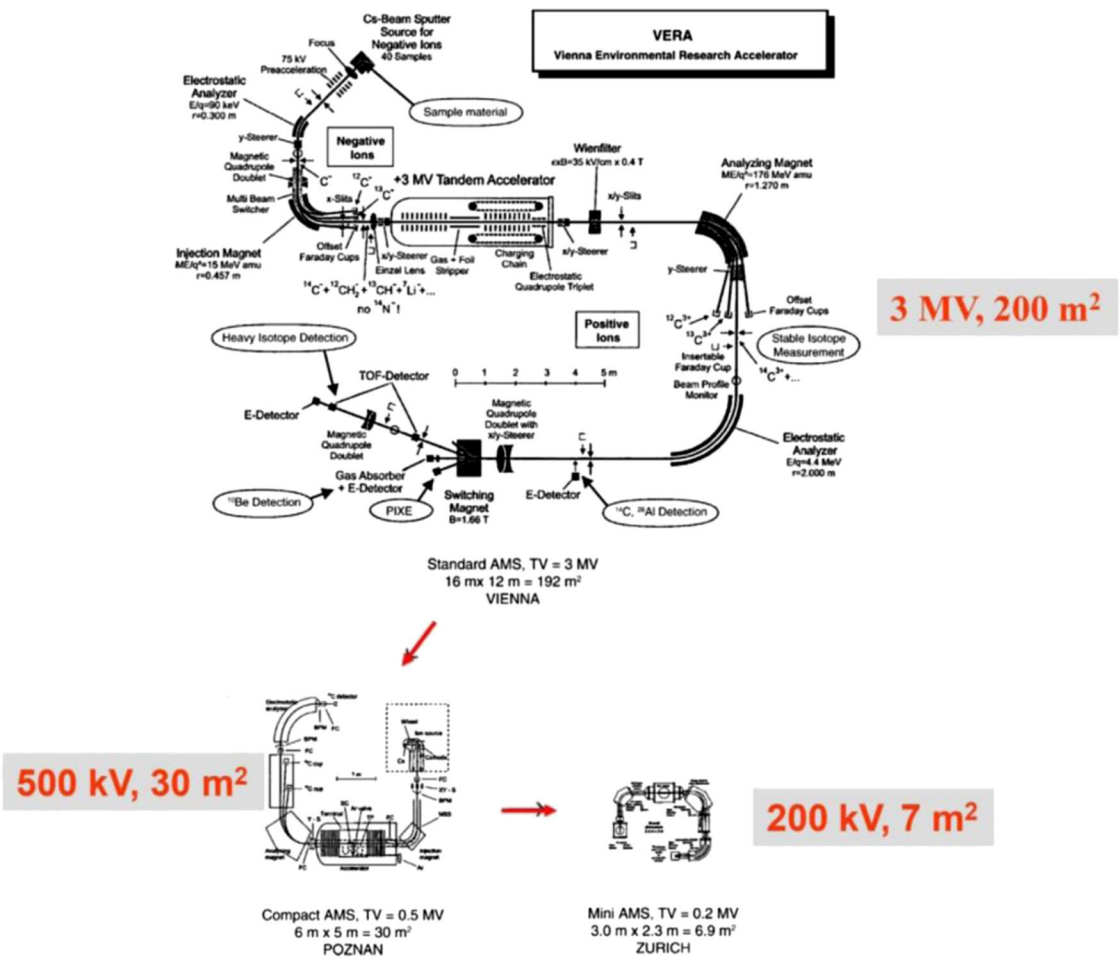

FIG. 6. Illustration of the size reduction of AMS facilities strongly depending on the terminal voltage of the tandem accelerator. Terminal voltage and floor space requirement are indicated with red labels. Note that "Mini AMS" is now known as the mini radiocarbon dating system (MICADAS). Adapted from Kutschera, 2016.

Synal *et al.*, 2004; Synal, Stocker, and Suter, 2007) have led to the development of ever smaller AMS facilities (Fig. 6).

(f) Finally, an important point is to obtain a high overall efficiency, i.e., the fraction of radionuclide atoms in the ion source sample that actually arrive in the final detector system. This can be as high as 5% for ^{14}C, but as low as 0.1% to 0.01% for more difficult cases where radionuclides do not easily form negative ions.

2. Low-energy cyclotrons

For some time, ^{14}C measurements were pursued with negative-ion injection into a small 35 keV cyclotron (the "Cyclotrino") at Berkeley (Welch *et al.*, 1986; Bertsche *et al.*, 1990). Later this concept was pursued with a 50 keV mini-cyclotron at Shanghai (Chen *et al.*, 1994), culminating in a minicylotron-based AMS facility capable of performing ^{14}C measurements at natural levels (Chen *et al.*, 2000), with first applications using archaeological samples (Zhou *et al.*, 2000). However, small radiocarbon facilities based on the tandem accelerator principle such as MICADAS (Synal, Stocker, and Suter, 2007) turned out to be better suited for ^{14}C measurements than the minicyclotron and thus dominate AMS facilities worldwide; see Sec. II.H.

3. High-energy cyclotrons

At sufficiently high energy, it is possible to separate radionuclides from stable isobars by complete stripping; see also Sec. II.D. At the ALICE facility of Orsay it was shown early on (Raisbeck, Yiou, and Stephan, 1979) that at 200 MeV fully stripped $^{26}Al^{13+}$ ions can be separated from the stable isobar interference $^{26}Mg^{12+}$ in a magnetic spectrometer after the cyclotron.

Since noble-gas radionuclides do not form negative ions, they have to be measured at accelerators with positive-ion injection. Electron cyclotron resonance (ECR) sources produce multiply charged positive ions for proper injection into high-energy cyclotrons and linear accelerators (Geller, 1990). At the superconducting cyclotron facility of Michigan State University, an AMS experiment was performed with ^{81}Kr (half-life $= 2.3 \times 10^5$ yr) at 3.6 GeV by separating fully stripped $^{81}Kr^{36+}$ ions from the stable isobar $^{81}Br^{35+}$ with a magnetic spectrometer (Collon *et al.*, 1997). Subsequently this method was used for ^{81}Kr dating of old groundwater in the Great Artesian Basin of Australia (Collon *et al.*, 2000). Although a successful dating was achieved, the overall efficiency was low (10^{-5}), and the operation of a large accelerator facility was complex. In recent years, a laser-based method called atom trap trace analysis (Chen *et al.*, 1999) has advanced to a stage where ^{81}Kr detection with much higher efficiency and laboratory-size equipment became feasible; see Sec. II.G.

At the UNILAC accelerator at GSI in Darmstadt, Germany, the detection of ^{205}Pb (half-life $= 1.7 \times 10^7$ yr) has been pursued for some time (Ernst *et al.*, 1984). At an energy of 2.3 GeV, a separation from ^{205}Tl was possible with a combination of a passive gas absorber, a time-of-flight measurement, and a magnetic spectrograph. The goal of this effort is to eventually determine the integrated flux of pp solar neutrinos through the reaction $^{205}\mathrm{Tl}(\nu, e^-)^{205}\mathrm{Pb}$ by measuring accumulated ^{205}Pb atoms in the thallium-bearing mineral lorandite (Pavicevic *et al.*, 2018).

C. Negative-ion sources and sample preparation

The overwhelming importance of electrostatic tandem accelerators in AMS and the principle of negative-ion injection resulted in an intense effort to develop versatile, intense, and practical negative-ion sources. The widely used source is the cesium-sputter ion source. Production of negative ions from the surface of a solid by sputtering with Cs^+ ions was conceived much before its application to AMS by Krohn (1962); see also the prior research on negative ions (Massey, 1950). The singular role of Cs in the production of negative ions is lowering the work function of a material surface, an effect observed by Krohn to be enhanced by covering the surface with a layer of Cs atoms. The Aarhus negative-ion source (Tykesson, Andersen, and Heinemeier, 1976) based on the Cs sputtering was first developed for the acceleration of heavy ions in tandem accelerators. However, the major development of the modern Cs-sputter negative-ion source was made by Middleton (1983), who contributed in large part to the successful expansion of AMS. The principle of the Middleton high-intensity negative-ion source is illustrated in Fig. 7 for the ion source used by the AMS Hebrew University group (Gelbart *et al.*, 1997). Most AMS facilities use multisample Middleton-type sources built commercially (between ~20 and 200 samples), allowing for automatized sample changing and providing intense negative ionic or molecular ion beams. Together with their quasiuniversal use in AMS, common shortcomings with this type of source are the need for regular cleaning and so-called ionizer poisoning by deposition of refractory materials. Possible memory and crosstalk effects between samples are also observed and are critically dependent on the physical and chemical properties of the sample material and the ion produced; see Pavetich *et al.* (2014) for the case of ^{36}Cl.

Sample preparation techniques for use with negative-ion sources constitute a major part of AMS and often dominate efforts to ensure that successful measurements and large efforts were dedicated to them. For ^{14}C measurements, certainly the most numerous and demanding, the main considerations in preparation are (i) C^- negative-ion intensity, required mostly in the 10 to 100 μA range, (ii) reduction of sample size, sometimes down to the microgram range, and (iii) strict control of contamination from atmospheric or environmental modern carbon. Combustion of an organic material to gaseous CO_2 (for instance, by heating with CuO to ≈900 °C) and following graphitization with a reducing agent were shown early on to be an efficient method of preparation of milligram-size sputter targets (Jull, Donahue, and Zabel, 1983) producing C^- beams at microampere intensity. An important development was an automized graphitization system at the ETH Zurich (Wacker, Nemec, and Bourquin, 2010), which is now widely in use at AMS ^{14}C facilities. Even smaller-size samples of a few micrograms are prepared and used, as mentioned in Sec. I.A.3 (Santos *et al.*, 2007; Cao *et al.*, 2013; Petrenko *et al.*, 2016; Steier *et al.*, 2017).

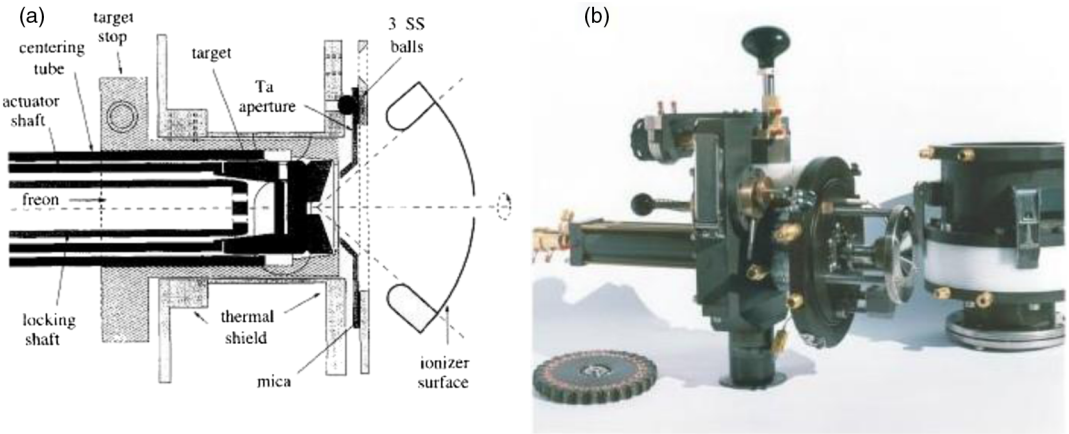

FIG. 7. (a) Schematic illustration of a custom-built Middleton-type high-intensity negative-ion source used by the Hebrew University AMS group (Gelbart *et al.*, 1997). Cs vapor delivered into the source volume by an oven (internal in this design) and Cs^+ ions produced on the resistively heated hemispherical ionizer surface (tantalum) are accelerated and focused onto the target at a negative potential of about 5 kV. The solid AMS sample is pressed in a 1.5 or 1 mm diameter hollow in the conical target, which is cooled by Freon circulation. Negative ions ejected by the same potential through the central 4 mm diameter hole in the ionizer are eventually extracted and transported toward the injection system of the accelerator. (b) Photographs (from left to right) of the ion source components: (i) A sample wheel containing positions for 28 targets. The target is rotated using a computer-controlled pneumatic motor for insertion into the source body. (ii) Ion source assembly. The wheel is located in the flat box (separately pumped via the lower port) and can be isolated from the ion source volume by a hand gate valve (black handle) for fast replacement. (iii) Ion source chamber with its extractor insulator (white).

A more direct method of sample preparation for ^{14}C AMS measurements was pioneered at Oxford with the development of a gas ion source (Bronk and Hedges, 1987, 1990; Bronk Ramsey and Hedges, 1997) using CO_2 obtained by burning of a sample and eliminating the additional contamination risks involved with graphitization. This method was refined by Ruff *et al.* (2010) and became quite common for small AMS machines (Molnár *et al.*, 2021). Other considerations important for sample preparation are related to the selection of chemical compounds from which production of negative molecular ions either is abundant enough for a useful AMS measurement or provides isobaric discrimination at the ion source stage. Important examples are BeO^- ions used for AMS of ^{10}Be and oxides or fluorides for uranium and other actinide isotopes. Also notable is the case of ^{41}Ca AMS, which cannot rely on the low intensity of Ca^- ions [see Schwarzschild (1988)], which itself is due to the extremely small electron affinity of Ca (24.55 ± 0.10 meV) (Petrunin *et al.*, 1996). Raisbeck *et al.* (1981) discovered that the molecular ion CaH_3^- can be used with fair intensity and considerably reduces ^{41}K isobaric interference owing to the instability of the KH_3^- ion. It was later shown that the CaF_3^- ion can be similarly employed using fluoride anions observed for their elemental selectivity and high beam intensity; see Sec. II.D.1.

D. Background suppression

The unique abundance sensitivity provided by AMS follows from the ability to measure ratios between low counting rates of the rare ion (in some cases 0.1–1 count/d) and rates of stable ions measured by charge current, typically in the range of e nA to e μA (10^9 to 10^{12} ions/s). In addition, ion detectors for AMS energies ($> \sim 1$ MeV) have no dark current, and therefore no intrinsic background. In this section we discuss methods to sustain high count rates by applying efficient methods to reduce intense background from stable isotope and isobar contributions before the beam enters the final detector system. It is then possible to identify the remaining components in the beam including the rare isotope with this detector system (such as a multianode ionization chamber).

Mass spectrometry is a destructive method, meaning that the sample material is consumed during the measurement. Sample preparation seeks to reduce the isobar content in the measurement sample but also to concentrate the element of interest such that a high source output is ensured, which leads to reasonable count rates in the detector. For example, the sample matrix is often reduced from a gram size or hundreds of grams to a milligram sputter sample, and the radionuclide concentration correspondingly increases by several orders of magnitude.

With few exceptions [such as an online radiocarbon (^{14}C) analysis of carbonate records via laser-ablation AMS (Welte *et al.*, 2016; Welte, Wacker *et al.*, 2016)], for some cross section measurements in nuclear physics and astrophysics (Wallner *et al.*, 2003, 2014) the sample material needs to be processed and the element including the isotope of interest isolated from the bulk material, for instance, C from bones (Deviese *et al.*, 2018), Be from rocks or sediment (Horiuchi *et al.*, 2013; Corbett, Bierman, and Rood, 2016), and Pu from soil samples (Tims *et al.*, 2016).

The typical consumption rates in a sputter ion source for AMS are of the order of 10^{15} atoms and molecules per second, equivalent to sputtering rates between a few μg/ min and up to several mg/h. In the following, a few examples are presented for natural radionuclide concentrations: 1 mm^3 modern wood or modern bone contain approximately 10^7 ^{14}C atoms. In principle, such material would allow sputtering of the sample

directly, but at the cost of reduced measurement accuracy and source output. Modern dedicated AMS systems produce detector count rates exceeding 1000 ^{14}C detector events/s for modern radiocarbon samples, equivalent to 100 μA of stable C currents extracted from the ion source. In contrast, other nuclides might yield only ten to a few 100 nA (for instance, Al, although new methods allow the ^{26}Al count rate to be increased significantly; see Sec. II.D.2). At the other extreme, AMS systems manage to handle detector count rates of fewer than one event per day for the lowest measurable concentrations of extraterrestrial nuclides (for instance, if natural production on Earth is negligible, such as for ^{60}Fe or ^{244}Pu; see Sec. IV.B.3). This vast difference in beam intensity spanning 7 orders of magnitude highlights the dynamic range of AMS and its flexibility for a wide range of applications.

For the goal of the "Old Carbon Project" (Beukens *et al.*, 2004; Litherland, Zhao, and Kieser, 2011) ^{14}C enrichment allowed the measurement of ^{14}C/^{12}C isotope ratios down to $\sim 10^{-18}$. Many other examples based on substantial matrix reduction by dedicated chemistry in combination with sophisticated particle detection methods have achieved similar concentration levels. Examples are ^{63}Ni AMS measurements from Cu samples exposed to fast neutrons in the Hiroshima atomic bomb explosion with a concentration ratio ^{63}Ni:^{63}Cu of $\sim 1:10^{18}$ (Rugel *et al.*, 2000; Straume *et al.*, 2003, 2004; Rühm *et al.*, 2007) and the detection of interstellar ^{244}Pu in deep-sea crusts with quantifications even down to the zeptoscale range ($<10^{-20}$ g ^{244}Pu/g deep-sea crust); see Sec. IV.B.3.

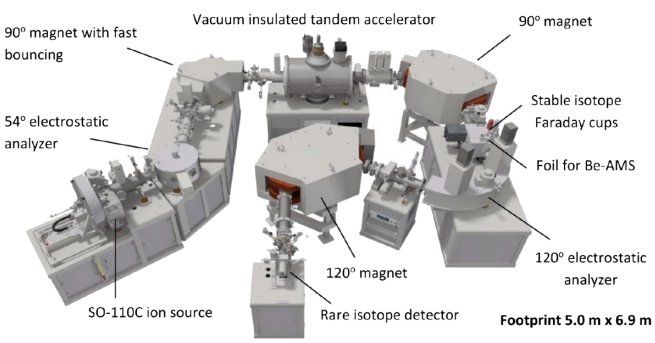

FIG. 8. Example of a compact AMS system. The 4103Bo AMS multielement system is shown operating with a vacuum insulated tandem accelerator as produced by HVE. The vacuum insulated tandem accelerator principle was pioneered at ETH Zurich (Synal *et al.*, 2004) and is being used in the MICADAS facilities (Synal, Stocker, and Suter, 2007); it is now manifactured by Ionplus. In our example, a 200-sample sputter ion source delivers negative ions that are energy (electrostatic analyzer) and mass filtered (90° magnet) and injected into the tandem accelerator. Collisions in the gas stripper at the terminal strip off electrons and eliminate molecular ions. Positively charged ions are then accelerated a second time, and the mass and energy are again analyzed at the high-energy side of the system. A degrader foil (such as for Be AMS) results in isobars with different energies (higher energy loss for B than for Be) that are then separated by the electrostatic deflector. A second 120° magnet reduces the background further, including isotopic interference, and often does not require an additional TOF system (even for actinide measurements). The rare radionuclides are counted in the final gas-ionization chamber, while stable isotopes are measured as currents after the low-energy and high-energy magnets. Adapted from Scognamilio *et al.*, 2021.

The overall particle detection efficiency depends on the chemical yield in sample preparation, the fraction of the desired atoms in the sample that are extracted as negative ions from the ion source (see the proper choice of molecules in Sec. II.C), the charge-state yield in the stripping process, and the ion-optical transmission through the spectrometer. State-of-the-art AMS facilities (see Fig. 8) are optimized systems reaching an ion-optical transmission of above 90%; another important improvement, particularly for heavy-ion AMS at small AMS facilities, is high charge-state yields combined with complete molecule destruction owing to the use of He as the stripper gas (Vockenhuber *et al.*, 2013).

1. Reduction of isobaric interference

Isobars by definition have the same mass number and consequently nearly the same mass and will often pass all mass and energy filters identically to the rare isotopes. Isobar intensity reduction can be achieved in a number of different ways; see also Table I.

- By dedicated chemical sample preparation procedures (at levels down to ~ppm).
- The proper selection of negative ions or molecules can reduce isobaric interference, for instance, CaH_3^- for ^{41}Ca (Raisbeck *et al.*, 1981) and HfF_3^- for ^{182}Hf (Vockenhuber, Feldstein *et al.*, 2004).
- Isobars extracted from the ion source can be removed from the beam by atom selective processes. Such methods include selective laser photodetachment and chemical reaction cells, both at the low-energy side of the facility; see Sec. II.D.3. Both methods are additions that promise a huge potential for new applications of new radionuclides to become measurable in the future; see Fig. 5 in Sec. I.B.3.
- By taking advantage of the differing energy losses for particles with different atomic numbers (as the isobar has a different atomic number), the so-called dE/dx–E method is widely used in the final detector system for AMS measurements (Elmore *et al.*, 1984). For more on these detector systems see Sec. II.E.
- By losing a different amount of energy, isobars can be separated out from the beam by subsequent energy-selective filters before they enter the final particle detector (the degrader foil technique; for instance, B vs Be or Cl vs S). This method was introduced by Kutschera *et al.* (1980) as early as 1980 in large AMS systems for ^{32}Si and applied to ^{10}Be AMS performed with a 2 MV tandetron accelerator by Raisbeck *et al.* (1984).
- An interfering isobar with a higher Z than the rare radionuclide experiences a higher energy loss and can therefore be stopped before entering the detector (for instance, B vs Be; see Fig. 9) while still leaving sufficient energy for the rare radionuclide to be counted (the passive absorber). Gas cells or thick foils are being used. This method as well as the degrader foil technique

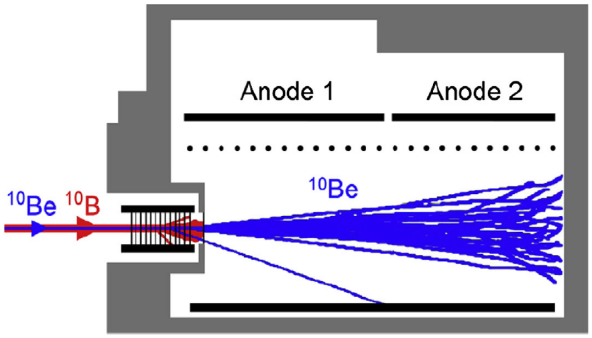

FIG. 9. Simulation of isobar reduction for ^{10}Be AMS via a thick absorber in front of the detector. A stack of silicon nitride membranes stops boron with its higher atomic number ($Z = 5$), while beryllium ($Z = 4$) enters the ionization chamber, where they are stopped in the gas volume. The remaining background (scattered ions or residual ^{10}B) can be identified by the differing energy losses along the two anodes of the chamber. Adapted from Steier *et al.*, 2019.

benefited enormously from the invention of so-called silicon nitride membranes (Döbeli *et al.*, 2004). These foils are produced homogeneously, in particular, for particle identification in low-energy AMS (Müller *et al.*, 2010). See also their use as an entrance window for ionization chambers in Sec. II.E.

- The measurement of characteristic x rays emitted from excited ions after passing a thin foil can be used to tag an event as either an isobaric background or a rare isotope event (projectile x-ray detection) (Artigalas *et al.*, 1993; McAninch *et al.*, 1997).
- If high particle energies are available, the particles can be fully stripped with reasonable yields; thus, the naked radionuclide can have a unique charge state if the atomic number is higher than the isobar and can be separated (Raisbeck, Yiou, and Stephan, 1979; Ernst *et al.*, 1984; Kutschera *et al.*, 1994; Collon *et al.*, 2000).

Finally, also requiring high particle energies and therefore a large accelerator, the gas-filled magnet technique reduces beam intensities of isobars by several orders of magnitude while keeping the intensity of the rare isotope essentially at 100%; for more details see Sec. II.D.4.

For heavier masses, the relative differences in mass and particle energy get closer and the energy resolution of the particle detectors does not allow sufficient discrimination between the stable and radioactive isotope. This leads to an increased background from such leaking stable isotopes.

2. Isotopic background reduction and identification

This isotopic background can be reduced significantly by adding an additional magnet with high-mass resolution at the high-energy side of the system (Suter *et al.*, 2007; Christl *et al.*, 2014; Hotchkis *et al.*, 2019; Steier, Hain *et al.*, 2019); alternatively, a so-called Wien filter (a velocity selector) can separate isotopes from the transmitted beam albeit with lower effectivity. Both methods reduce the beam intensity of the interfering background ions. This has advantages as it reduces detector count rates in contrast to pure isotope identification methods.

Time-of-flight (TOF) detectors measure the particle flight time, which can be combined with particle energy measurements for isotope identification. This method was introduced early on for the separation of ^{127}I for the detection of ^{129}I (Elmore *et al.*, 1980). TOF can be done with much better resolution compared to energies in a particle detector (Paul *et al.*, 1997; Knie *et al.*, 2000; Vockenhuber *et al.*, 2003; Fifield *et al.*, 2010) and thus has much higher discrimination power. Because the flight time (i.e., the velocity) depends on the particle mass, it can be used to discriminate between different masses. TOF systems will not reduce the background count rates; they allow the background ions to be identified with high resolution, but often at the cost of reduced beam transmission.

Adding more energy- and mass-selective components with high resolving power before the particle detector can separate out these background ions more efficiently. Therefore, for cases where no stable isobar exists in the beam (such as actinides), small and compact AMS systems now outperform the larger AMS systems (because charge-state yields are higher and the beam optics allows nearly 100% ion-optical beam transmission). New compact AMS systems

TABLE I. Examples of isobar suppression methods in routine measurements for selected radionuclides. PA, passive absorber; DF, degrader foil; GFM, gas-filled magnet; LIC, laser photodetachment and ion cooler or chemical reaction cell; FS, full stripping; dTOF, delta E TOF (energy loss + TOF); PXD, projectile x-ray detection; TV, terminal voltage.

Radionuclide	Z	Stable isobar	Z	Isobar reduction	Typical TV
^{10}BeO	4	^{10}BO	5	PA, DF, GFM	0.25–8 MV
^{26}AlO	13	^{26}MgO[a]	12	LIC, GFM, FS	0.25–14 MV
^{36}Cl	17	^{36}S	16	DF, GFM, FS, LIC	1.75–14 MV
^{41}CaF$_3$	20	^{41}KF$_3$	19	DF, GFM, LIC	2.5–14 MV
^{53}MnO	25	^{53}CrO	24	GFM, PA	>10 MV
^{60}FeO	26	^{60}NiO	28	GFM	>10 MV
^{59}Ni	28	^{59}Co	27	PXD, GFM	>10 MV
^{146}SmO	62	^{146}NdO	60	GFM	LINAC (6 MeV/u)
^{182}HfF$_5$	72	^{182}WF$_5$	74	LIC (dTOF)	3 (14) MV

[a]The traditional way to detect ^{26}Al is to use ^{26}Al$^-$ from the ion source, which can be measured at low energies due to the instability of ^{26}Mg$^-$ ions. However, ^{26}AlO$^-$ ions are favorable due to a >10 times higher ion yield. The ^{26}MgO isobars can be suppressed at TV ~ 3 MV using LIC, and at TV > 13 MV with the GFM and FS techniques.

(see Figs. 6 and 8) can run fully automatically and allow precise and efficient measurements of many routine isotopes. This also makes AMS attractive for more applications due to more competitive sample preparation costs.

In the following, two effective methods for isobar suppression are discussed: (1) laser interaction within an ion cooler that promises new applications in AMS for a number of new isotopes, and (2) the gas-filled magnet (GFM), which has proven to be an extremely useful tool for isobar suppression, particularly for medium-mass isotopes (such as in nuclear astrophysics applications; see Sec. IV.B).

3. Ion laser interaction mass spectrometry and gas reaction cells

Negative ions can be neutralized by photons via electron detachment if the photon energy is higher than the electron affinity (EA), which is an intrinsic property of a negative ion. This process is a threshold process, and anions with EAs higher than the photon energy are therefore unaffected. The typical EA is of the order of an eV, between fractions of eV and several eV. With 1 eV corresponding to a 1240 nm wavelength, commercial lasers of suitable photon energy are usually readily available.

This method (laser accelerator mass spectrometry) was introduced in a proof-of-concept study in the 1980s by Berkovits *et al.* (1989, 1990). Laser photodetachment is a nonresonant process and, together with a short interaction time (limited by the interaction length between the laser photons and fast-moving ions), the duty factor of the laser-ion interaction made the efficiency too low for practical purposes.

A significant step forward was the implementation of a radio-frequency quadrupole (RFQ) ion beam cooler at Oakridge National Laboratory to slow down the ions, leading to a substantial increase of the interaction time (milliseconds) (Liu *et al.*, 2005). The gas-filled RFQ ion cooler slows down the negative ions to kinetic energies in the few eV range. Inside the quadrupole the ions will be further slowed down by reduction of their kinetic energy by interaction with a buffer gas, often helium. The laser beam runs collinear with the beam line of the ion beam. Liu *et al.* (2005) achieved 95% suppression of ^{59}Co ions by photodetachment, while under identical conditions 10% of ^{58}Ni ions were neutralized. Eventually such a method achieved suppression by more than 99.99% for Co^- ions (Andersson *et al.*, 2010).

Based on these ideas, the AMS group at the VERA facility refined these setups and installed the so-called Ion-Laser Interaction Mass Spectrometry (ILIAMS), which was then coupled to their 3 MV AMS facility (Forstner *et al.*, 2008, 2015; Martschini *et al.*, 2017, 2022; Martschini, Hanstorp *et al.*, 2019). With the availability of new tunable lasers, the VERA facility has now applied this method for the first time successfully to a number of isotopes and demonstrated suppression of isobars close to 100% for ^{36}Cl (Lachner *et al.*, 2019) and ^{26}Al (Lachner *et al.*, 2021); see Fig. 10. For example, for MgO^- isobar suppression factors exceeding 10^{10}, i.e., "complete" isobar suppression, had been achieved for ^{26}Al AMS, paving the way for the use of the more prolific molecule AlO^- instead of isobar-free Al^- (Martschini *et al.*, 2022). Besides the fully developed nuclides ^{26}Al and ^{36}Cl, the nuclides ^{90}Sr and ^{135,137}Cs are also ready for applications. Additional isotopes under investigation are ^{41}Ca, ^{99}Tc, and ^{182}Hf, and many more isotopes are under consideration for utilizing this promising method. If the isobaric background is completely removed from the beam before entering the particle accelerator, high particle energies are no longer required and a small accelerator (for instance, 1 MV or less) will be sufficient, with stripping providing molecule dissociation.

An alternative but similar method for isobar suppression is the interaction of the negative ions with special reactive gases in the cooler due to ion reactions with the gas. Such gases can also provide a selective neutralization of unwanted ions. A resonant charge transfer, initiated by the reactive gas in an ion

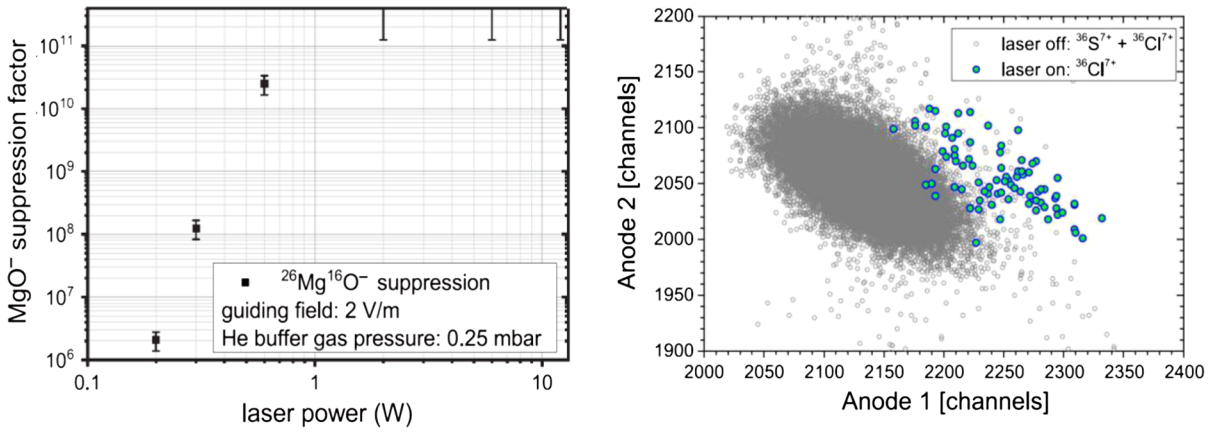

FIG. 10. Left panel: isobar reduction of ^{26}Mg via laser-ion interaction and a gas reaction cell for ^{26}AlO AMS. The molecular isobar MgO^- is suppressed by ~5 orders of magnitude in the simple passage through a He-filled ion cooler. Adding an appropriate laser for selective photodetachment of MgO^- results in additional suppression of up to 11 orders of magnitude and combined yields a suppression factor exceeding 10^{14} at an injected laser power of 12 W. The use of AlO^- increases the detection efficiency relative to the use of Al^- extraction by a factor of between 3 and 5. Adapted from Lachner *et al.*, 2021. Right panel: ^{36}Cl AMS. Effect of the laser interaction for suppression of $^{36}S^-$: both ^{36}Cl and ^{36}S reach the detector without a laser (gray circles). If the laser is turned on (blue symbols), only ^{36}Cl events are recorded (here at a laser power of 1 W). Adapted from Lachner *et al.*, 2019.

guide, was utilized by the Toronto-Ottawa group through their isobar separator for anions (ISA) (Litherland *et al.*, 2007). An RFQ produced by Isobarics Group, Inc., was used as a test system at IsoTrace Laboratory (Toronto) and is now installed at the University of Ottawa. Their method suggests suppression factors of 5 to 6 orders of magnitude (Eliades *et al.*, 2010, 2015) using NO_2 as a reactive gas. This group focuses on the superhalogen anions SrF_3^-, YF_4^-, and ZrF_5^-, which stay largely unaffected in such a gas while suppressing the isobars by orders of magnitude. ISA results demonstrate further that substantial suppression of KF_3^-vs CaF_3^- is possible inside their ion guide.

4. Gas-filled magnet

Among the detection methods useful to AMS and, in particular, to isobaric separation, the gas-filled magnetic spectrograph stands out (Paul *et al.*, 1989). While a magnetic spectrograph in vacuum disperses and analyzes ions by their mass-to-charge ratio, ions traveling in a magnetic field region filled with low-pressure gas collide with atoms or molecules of that gas and can charge exchange by capture or loss of one or more electrons. For a statistically sufficient number of charge-changing collisions (which are still much less frequent than elastic or inelastic atomic collisions), the ion trajectories are governed by the mass-to-mean charge state $m/\langle q\rangle$. Thus, ion trajectories that are separated according to their charge state in vacuum merge into a broad path in the gas-filled magnet (Fig. 11). The degree of merging into a mean charge state depends on the length of the path in the gas-filled magnetic region and the gas pressure because a pressure increase results in a better defined average charge state. This charge focusing competes with the broadening due to multiple small-angle scattering, defining a range of optimal gas pressures. Spatial separation of the trajectories of two isobaric ions results from the dependence of $\langle q\rangle$ on the atomic number Z of the ion $\langle q\rangle \propto vZ^{\gamma}$, where v is the ion velocity and Z is its atomic number with $\gamma \approx 0.3$–0.4; see Dmitriev and Nikolaev (1965). A comprehensive review on charge states and charge-changing cross sections of fast heavy ions penetrating through gaseous and solid media was given by Betz (1972).

The concept of the gas-filled magnet originated in the search for separation of isobaric nuclei in a fission product chain (Cohen and Fulmer, 1958; Fulmer and Cohen, 1958; Sistemich, 1975) and is in fact still used for that purpose (Chebboubi *et al.*, 2016; Kim *et al.*, 2020). It was applied to AMS at the University of Rochester (Kubik *et al.*, 1989) and Argonne National Laboratory (Paul *et al.*, 1989) owing particularly to the fact that the physical separation of a rare radionuclide from its stable isobar enables the latter (or part thereof) to be blocked in front of the particle detector, thus avoiding possibly excessive count rates. Moreover, the gas-filled magnet acts as a passive absorber, which discriminates among isobaric ions by their different residual energies after passage through the gas. As shown by Hain *et al.* (2018), the dual action of the gas-filled magnet as a separator together with a passive absorber leads to higher radionuclide sensitivity.

The gas-filled magnet technique was successfully applied to the detection of cosmogenic and artificial radionuclides,

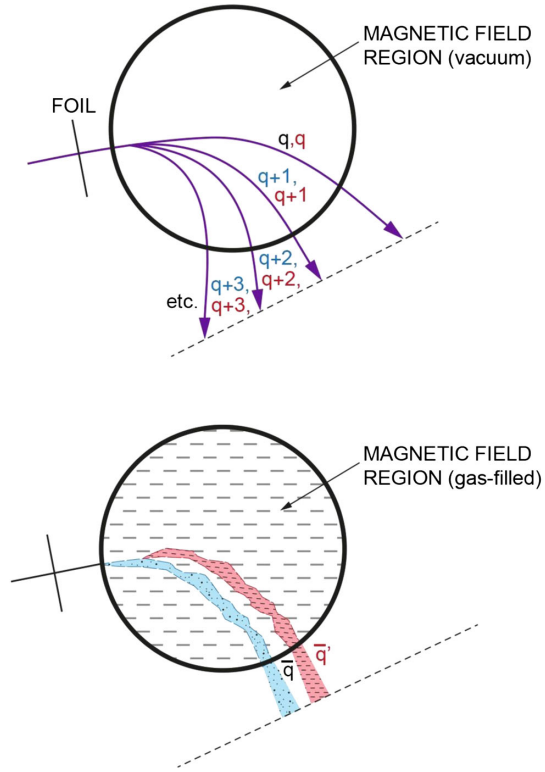

FIG. 11. Schematic illustration of the gas-filled magnet principle. Trajectories followed by heavy ions in a magnetic field region are shown. Top panel: trajectory in vacuum. Two isobaric ions (blue and red) with the same charge states have degenerate trajectories [unless under exceptionally high magnetic resolving power $(m/q)/d(m/q) \sim 10^5$]. Bottom panel: trajectory in a gas-filled magnetic field region. The ions follow two broadened paths governed by their mean ion charge state in the gas that are different owing to their differing ionic charges as a result of differences in Z, and additionally owing to the different energy loss that they experience through their flight through the gas.

allowing in general isobaric separation for heavier radionuclides more effective than would otherwise be possible on the basis of measurements of differential energy loss alone. A further advantage of the gas-filled magnet method compared to a passive absorber followed by conventional magnetic analysis (Finkel *et al.*, 2013) consists of an improved yield: while in a magnetic analysis in vacuum the yield is divided between several charge states (usually three or four), the gas-filled magnet merges all yields in a single group. The technique has thus been continually used since its development in many AMS laboratories, both to improve isobaric discrimination at low-energy accelerators and to investigate ever heavier ions with larger machines. The gas-filled magnet technique was applied soon after its first use in AMS to ultrasensitive analyses of ^{32}Si and ^{36}Cl at ETH Zurich (Zoppi *et al.*, 1994) and in other laboratories for ^{36}Cl (Hatori *et al.*, 2000; Alfimov and Possnert, 2004; Aze *et al.*, 2007; Vockenhuber, Miltenberger, and Synal, 2019), with electrostatic tandem accelerators operating at 5–6 MV terminal voltage.

The technique was also suggested for separation of ^{26}Al from the stable isobar ^{26}Mg when one uses an injection of AlO^-;

the molecular ion AlO^- is much more efficiently produced than the Al^- ion normally used for ^{26}Al because of the instability of the isobaric Mg^- ions (Arazi *et al.*, 2004; Fifield *et al.*, 2007). Large programs of detection of heavier AMS nuclides based on higher-voltage accelerators were developed at Technical University of Munich with the gas-filled analyzing magnet system (Mueller *et al.*, 1992; Knie, Faestermann, and Korschinek, 1997) for detection of ^{53}Mn (Korschinek *et al.*, 2020), ^{59}Ni (Rugel *et al.*, 2007), ^{60}Fe (Knie *et al.*, 2004; Ludwig *et al.*, 2016; Koll *et al.*, 2019; Koll, Korschinek *et al.*, 2019), ^{63}Ni (Knie *et al.*, 2000; Rugel *et al.*, 2000; Straume *et al.*, 2003), ^{79}Sr (Dillmann *et al.*, 2006; Rugel *et al.*, 2007), ^{93}Zr (Hain *et al.*, 2018), and ^{99}Tc (Quinto *et al.*, 2019), at the Australian National University (ANU) (Gladkis *et al.*, 2007; Fujioka *et al.*, 2010; Wallner, Bichler *et al.*, 2015; Wallner *et al.*, 2016a, 2021, 2023; Leya *et al.*, 2020) for nuclear astrophysics and environmental research (^{10}Be, ^{26}Al, ^{32}Si, ^{53}Mn, ^{60}Fe, and ^{93}Zr), and at the PRIME Lab (Caffee, Granger, and Woodruff, 2015). See also Sec. II.F for use of the Enge gas-filled magnetic spectrograph at the ATLAS accelerator (Argonne National Laboratory) for the detection of ^{39}Ar (Collon, Kutschera, and Lu, 2004; Collon *et al.*, 2004; Tessler *et al.*, 2018) and the medium-heavy nuclide ^{146}Sm (Kinoshita *et al.*, 2012).

E. Radionuclide detection and background identification

Rare radionuclide detection is rarely just simply counting the ions; in most cases total particle energy, differential energy loss, or flight time are measured for additional particle identification. These detection methods include solid-state detectors, gas-ionization detectors, and time-of-flight detectors. With AMS facilities moving toward lower particle energies, Si detectors became of interest due to their excellent energy resolution, especially for light ions, but radiation damage degrades their performance and limits their lifetimes. These detectors measure the total energy of the incoming particle, and hence do not differentiate against isobars, because, if not discriminated by other means, the isobars have the same energy.

Ionization chambers are versatile and robust particle detectors. They have been available since the beginning of AMS owing to their use in nuclear physics applications. Multianode ionization chambers play an important role in ion identification and detection for AMS (Elmore *et al.*, 1984). They consist of a refinement of the classical gridded ionization chamber (Bunemann, Cranshaw, and Harvey, 1949). In this type of detector, ions slow down in a chamber filled with gas and lose energy by ionization of the atoms or molecules of the gas whereby electrons and positive ions drift between two electrodes. The electrostatic charge signal induced by electrons on the anode (positive potential) is in principle proportional to the energy lost by the ion via ionization. An intermediate electrode in the form of a so-called Frisch grid located between anode and cathode was shown (Frisch, 1942; Bunemann, Cranshaw, and Harvey, 1949) to shield the charge of opposite sign induced on the anode by the positive ions, which are of much slower mobility than the electrons. This shielding results in a faster signal that is truly representative of the total ionization energy and mostly independent of the distance between the ion track and the anode and of its angle of incidence.

The multianode ionization chamber hosts an anode segmented in several independent sections (at the same potential but insulated from each other) along the general direction of the ion trajectory and was originally developed for heavy-ion nuclear physics experiments (Sann *et al.*, 1975; Shapira *et al.*, 1975; Fulbright, 1979). This principle was also adopted for AMS experiments (Elmore *et al.*, 1984; Synal *et al.*, 1987). In addition, sawtooth-shaped electrodes give position-sensitive signals, as first demonstrated at ANU for the detection of ^{36}Cl (Fifield *et al.*, 1987). The individual signals of the anode segments are therefore proportional to the respective energy losses along the trajectory and provide a powerful signature of the ion atomic number Z for isobaric identification, as shown in Fig. 12 for the case of ^{41}Ca. Multianode ionization chambers are used as a stand-alone detector (Fink, Klein, and Middleton, 1990; Fink *et al.*, 1990) or in more sophisticated detector systems such as the gas-filled magnet; see Sec. II.D.4. Figure 13 illustrates such a detector used at Australian National University (Martschini, Fifield *et al.*, 2019) for the detection of heavy radionuclides (such as ^{53}Mn and ^{60}Fe) in the focal plane of a gas-filled Enge split-pole magnetic spectrograph.

Optimized designs can provide energy resolutions as low as 0.5% (Fifield *et al.*, 2010; Martschini, Fifield *et al.*, 2019; Wallner *et al.*, 2023). However, in the course of the development of universal and compact AMS facilities with lower particle energies at range <1 MeV$/u$, the available detectors were not sufficient for proper particle identification. New designs driven, in particular, by ETH Zurich use exceptionally homogeneous silicon nitride entrance windows, and a detailed understanding of the physics allowed the development of compact special gas-ionization detectors (Suter *et al.*, 2007; Müller *et al.*, 2010; Scognamiglio *et al.*, 2016). In combination with low-noise preamplifiers, significant improvements in the performance have been obtained, especially at low

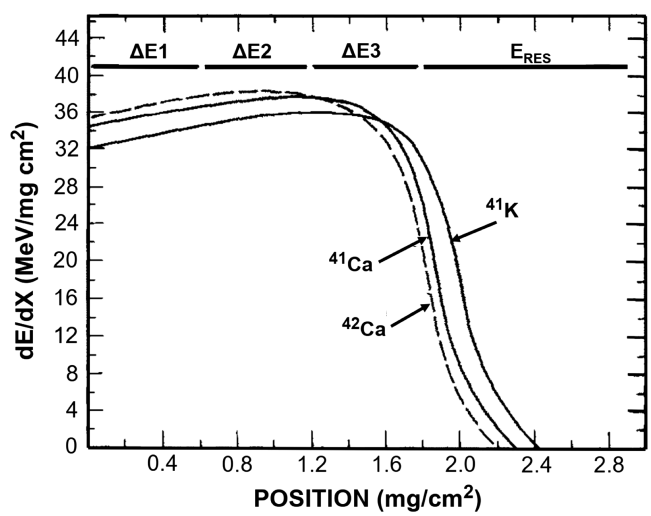

FIG. 12. (a) Depth profile of the differential energy loss in a multianode ionization chamber for ^{41}Ca, its isobar ^{41}K, and a neighboring isotope ^{42}Ca. The profile is probed by the successive ΔE and E_{RES} anodes. Adapted from Fink *et al.*, 1990.

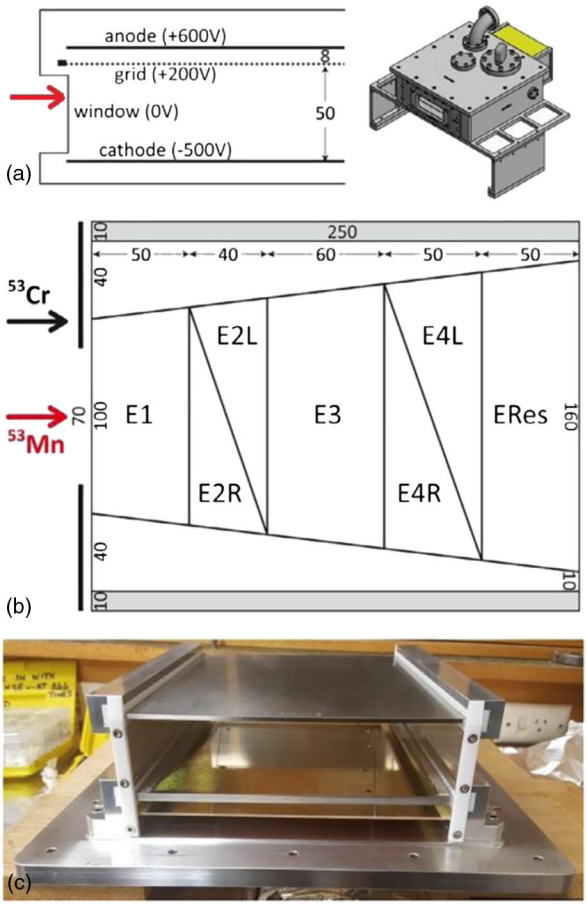

FIG. 13. (a) Schematic illustration (side and top views) of the multianode ionization chamber used at Australian National University for AMS detection of ^{53}Mn and ^{60}Fe. (b) Photograph of the detector showing (from bottom to top) anode, grid, and cathode planes. Dimensions are in mm. Adapted from Martschini, Fifield *et al.*, 2019.

energies, and these detectors now outperform even Si detectors in their energy resolution; see Fig. 14.

F. AMS with positive ions and a heavy-ion linear accelerator

While almost all AMS facilities and research are based on injection of negative ions into electrostatic accelerators, the use of positive ions offers important particularities. As noted, the discovery of stable ^{3}He was made in a 1939 experiment predating modern AMS by injecting positive $^{3,4}He^{2+}$ ions into the 60 in. Berkeley cyclotron (Alvarez and Cornog, 1939a, 1939b). The use of the Berkeley cyclotron (by then 88 in.) was among the first to demonstrate the potential of accelerators for ^{14}C dating (Muller, 1977) and more generally what was to become accelerator mass spectrometry. The dominance of negative-ion injection and use of tandem accelerators for AMS stemmed from the development and availability of the versatile and intense cesium-sputter source (Middleton, 1983, 1984a, 1984b), accompanied in several important cases like ^{14}C and ^{129}I by stable isobar elimination due to the instability of the respective negative-ion isobars. More recently the isobar selectivity offered by fluoride anions was also discovered (Zhao and Litherland, 2007). The tandem accelerator based on the stripping of ions after acceleration to the high-voltage terminal provides the way to destroy and eliminate or greatly reduce the interference of molecular ions of stable species (for instance, $^{12}CH_2$ and ^{13}CH in the case of ^{14}C detection).

It was realized in the early 2000s at Argonne National Laboratory that the ATLAS accelerator system, which consisted of an ECR ion source (Geller, 1990, 1996) producing highly charged positive ions and the ATLAS superconducting heavy-ion linear accelerator, could fulfill the requirements of accelerator mass spectrometry. The production of highly charged ions in the ECR ion source occurs in a low-density plasma confined within a vacuum chamber ($10^{-8} - 10^{-7}$ torr) by static multipolar magnetic fields into which rf microwave power (in the gigahertz range) is fed, creating a surface where the ECR condition

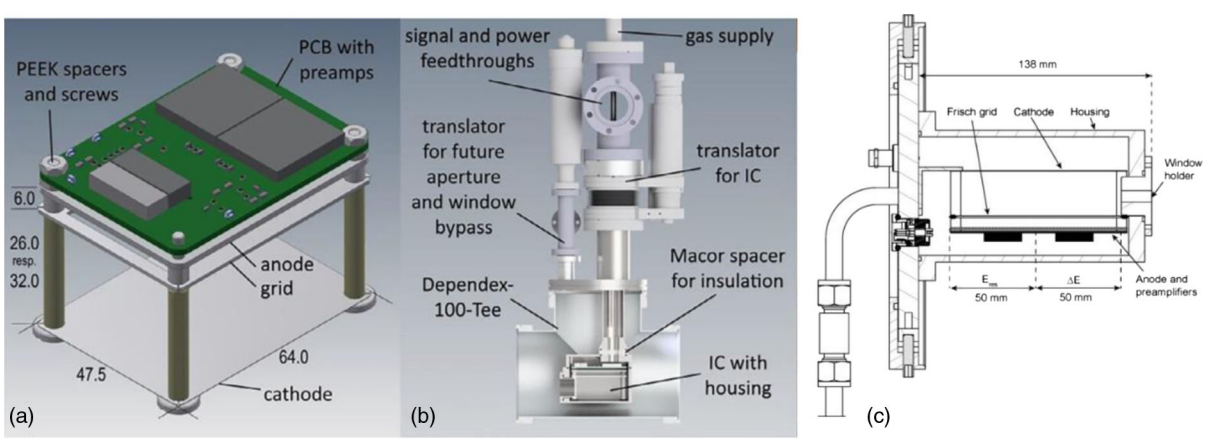

FIG. 14. (a) Schematic drawing of a compact ion chamber (dimensions in mm). (b) The assembly as an insertable-retractable version, as applied at ANU, Canberra (Martschini, Fifield *et al.*, 2019), and based on designs developed at ETH Zurich (Suter *et al.*, 2007; Müller *et al.*, 2010) and VERA (Forstner *et al.*, 2008). (c) Diagram of a compact gas counter for AMS at low energies [provided by ETH and installed at CNA (Spain)] mounted at the end of a beamline. Low-noise preamplifiers are mounted directly on the electrical feedthrough. The detector housing is electrically insulated. Adapted from Scognamiglio *et al.*, 2016.

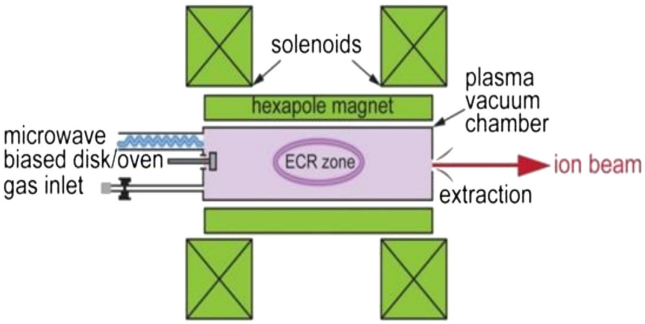

FIG. 15. Schematic diagram of the electron cyclotron resonance ion source originally developed by Geller (1990, 1996); see the text. The ellipse shown in the plasma chamber depicts the cross section of the surface onto which the electron cyclotron resonance [Eq. (1)] is met. Adapted from Paul *et al.*, 2019.

$$f_{\mathrm{ECR}}\ (\mathrm{GHz}) = eB/2\pi m_e = 0.28B(\mathrm{T}) \tag{1}$$

is met. In Eq. (1), f_{ECR} is the microwave frequency, e and m_e, respectively, are the charge and the mass of the electron, and B is the static magnetic field (in tesla). Electrons are accelerated at cyclotron resonance to kinetic energies above the ionization energies of charged ions, and breeding to high-charge states depends on the ion density and the confinement time. A schematic illustration of an ECR ion source is shown in Fig. 15.

The process by which accelerated high-energy electrons breed high ionic charge states in the ECR plasma can be viewed as analogous to the electron stripping of high-velocity ions passing through gas or foil in the high-voltage terminal of an electrostatic tandem. In the same way, molecular ions in the ECR plasma are dissociated as a result of the fast electrons accelerated by the ECR resonance. However, while ionized molecular fragments do exit the tandem terminal of an electrostatic accelerator and possibly further change charge in the high-voltage acceleration tube, ionized fragments in the ECR plasma are separated from the beam at the exit of the ion source by magnetic analysis. The elimination of molecular ions and their fragments from the ECR beam is especially favorable in the case of hydride ions of medium-heavy and heavy elements, which can produce the background in "conventional" tandem-based AMS.

Two main benefits make the use of an ECR ion source and a linear accelerator interesting for AMS compared to a tandem electrostatic accelerator: (i) the possibility to study and detect rare radioisotopes of noble gases: the instability of negative ions of noble gases, except metastable He^-, prevents their use in "classical" AMS accelerators, and (ii) the possibility to achieve isobaric discrimination for heavier radionuclides in the ultrahigh sensitivity range typical for AMS: the capability of producing and extracting highly charged positive ions from an ECR plasma and coupling of the ECR ion source with a heavy-ion linear accelerator enables in principle acceleration to higher energies than an electrostatic accelerator, which is bounded by achievable terminal voltages for similar energies. A practical limitation, however, is the high cost and limited number of available ECR heavy-ion accelerators, none of which are dedicated to AMS. We review here research done with noble gases and heavy radionuclides at the ATLAS facility of Argonne National Laboratory; see a recent review on the subject by Paul *et al.* (2019) for additional details.

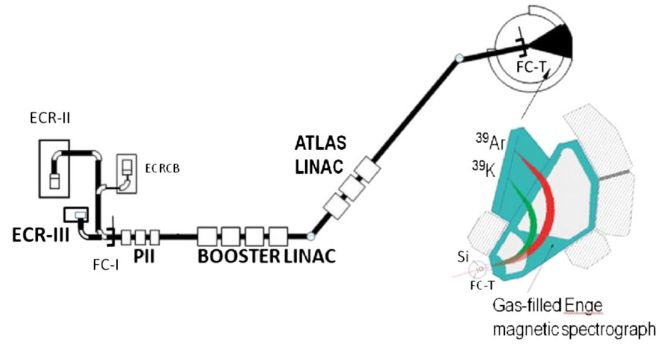

FIG. 16. Schematic illustration of the ATLAS facility and the Enge gas-filled magnetic spectrograph for ^{39}Ar ($t_{1/2} = 269$ yr) detection by AMS (Tessler *et al.*, 2018; Paul *et al.*, 2019). The ECR sources ECR II and ECR III, presently in use, are shown; ECRCB is an ECR charge breeder for externally fed ions. The rare ions (^{39}Ar) are identified and counted in a position-sensitive detector and ionization chamber along the spectrograph focal plane; see Fig. 17. A retractable Faraday cup at the target position (FC-T) is located in front of the spectrograph and is used to measure the charge current of a stable Ar ion (^{38}Ar or ^{40}Ar), allowing one to measure the transmission efficiency between a front end Faraday cup (FC-I) and target position for stable isotopes and, eventually, the quantitative determination of the isotopic ratio ^{39}Ar/Ar. In addition, a rotatable Si detector (Si) is used to optimize the transmission of the rare ions.

A schematic illustration of the ATLAS accelerator facility as it was used in an AMS experiment is shown in Fig. 16. Highly charged ions are extracted and magnetically mass analyzed before injection in the positive-ion injector (PII). The PII was originally composed (at the time of the first AMS experiments) of a harmonic buncher and low-β resonators; an RFQ (mass-to-charge $m/q \leq 7$) was later inserted as the first accelerating unit. Ions are successively accelerated in superconducting rf cavities along two sections (historically named booster and ATLAS linacs) whose individual phases are independently tuned. The cavities thus define an ion velocity profile specific to the mass-to-charge ratio of the accelerated ion.

The accelerator setup for a rare AMS radionuclide is tuned with the help of a so-called pilot beam of ions having a nearby m/q. In the case of the later mentioned $^{39}Ar^{8+}$, a beam of stable $^{78}Kr^{16+}$ ions was used as a pilot beam and optimized on a Faraday cup in front of the magnetic spectrograph. However, the fact that ions of the same m/q ratio are accelerated and transported along the linear accelerator and ion-optical components starting from the ECR ion source often results in interference, not only of isobaric ions but also of ions of stable elements with nearby m/q ratios. Such contaminants are more probable the heavier the ions are. The ambiguity can then be resolved if necessary by an intermediate stripping along the accelerator at the cost of a lower transmission efficiency. For a successful measurement, the beam contaminants eventually need to be separated or discriminated using a sophisticated detection system and the identified rare radionuclide counted. The rare radionuclide count rate is then normalized by the

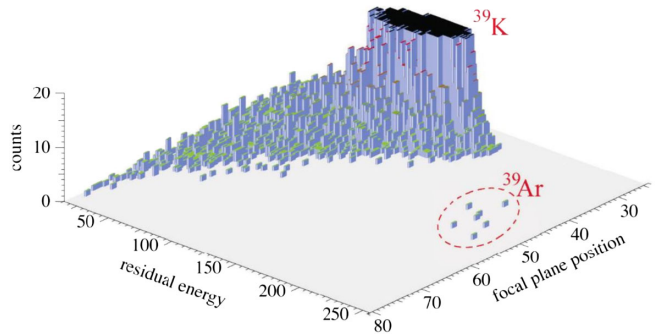

FIG. 17. Identification spectra of ions for an Ar sample extracted from deep oceanic water where the ^{39}Ar concentration $^{39}\mathrm{Ar}/^{40}\mathrm{Ar} = 2.6 \times 10^{-16}$ compared to atmospheric 8.1×10^{-16} is a measure of the age of the water sample (~400 yr) since atmospheric Ar dissolution. The ^{39}K contaminant, spatially separated from ^{39}Ar in the focal plane of the gas-filled magnet (see Fig. 11), was partially shielded in front of the focal-plane detector due to its extremely high count rate. Adapted from Collon *et al.*, 2004.

charge current of a neighboring isotope, transported through ATLAS using a different tuning scaled by the respective m/q ratios and optimized. The charge current is measured with a retractable (suppressed) Faraday cup located at the entrance of the spectrograph (Fig. 16). This normalization procedure was verified in several experiments when the isotopic ratio was known (Nassar *et al.*, 2005; Tessler *et al.*, 2018).

The first successful AMS experiments at ATLAS involved the detection of ^{39}Ar at the extremely low cosmogenic abundances in atmospheric Ar [$^{39}\mathrm{Ar}/\mathrm{Ar} = 8.1 \times 10^{-16}$ (Loosli and Oeschger, 1968)] and in deep ocean water (Collon *et al.*, 2004). The extremely low cosmogenic abundances necessitated operation of the ECR ion source at high power with extracted beams ($^{40}\mathrm{Ar}^{8+}$) of the order of 10 μA, with a special quartz shield covering the walls of the plasma chamber to reduce isobaric ^{39}K interference. Figure 17 shows spectra of ^{39}Ar from a sample of Ar extracted from seawater collected during the South Atlantic Ventilation Experiment cruises from station 95 (−17.997 S, 30.983 W) at a depth of 4717 m (Collon *et al.*, 2004). The measured $^{39}\mathrm{Ar}/\mathrm{Ar}$ ratio of 2.6×10^{-16} is a measure of the water age (~400 yr) since atmospheric Ar dissolution. The Ar sample was extracted from ocean water samples of 20 l volumes, demonstrating the value of atom counting versus the traditional low-level β decay counting (Loosli, Oeschger, and Wiest, 1970), which needs about 1000 l of water. A further reduction in sample size to just 5 l of water was achieved by counting ^{39}Ar atoms with the ATTA method (Ebser *et al.*, 2018); see Sec. II.G.

The positive-ion AMS method was used more recently (Tessler *et al.*, 2018) to measure the cross section of the astrophysically interesting reactions $^{36,38}\mathrm{Ar}(n,\gamma)^{37,39}\mathrm{Ar}$ by counting ^{37,39}Ar atoms; see Sec. IV.B.2. While ^{39}Ar was detected via the same technique as previously described, ^{37}Ar ions were identified by a full stripping to $^{37}\mathrm{Ar}^{18+}$ separating the stable isobar $^{37}\mathrm{Cl}^{17+}$ by magnetic analysis, taking advantage of the high acceleration energy of the linear accelerator. Figure 18 illustrates the AMS setup for this measurement, which was the first direct identification and detection of the

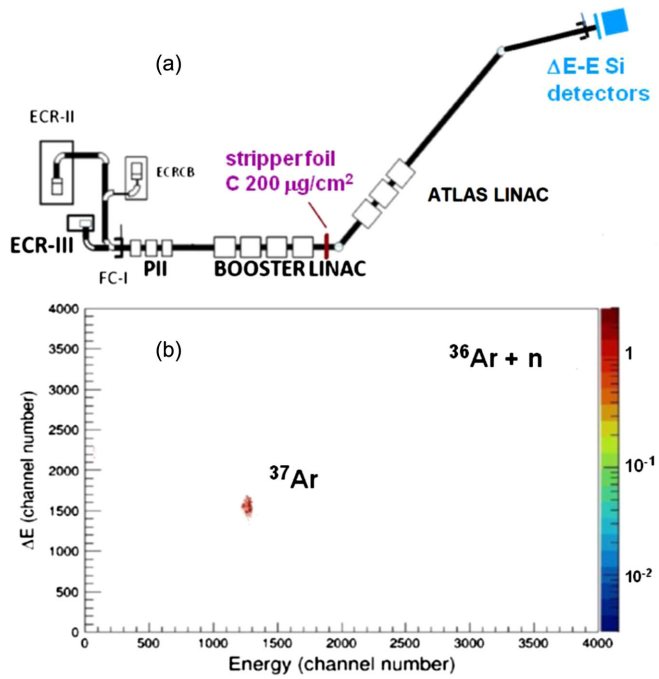

FIG. 18. ^{37}Ar ions detected background free by a full stripping to $q = 18^+$ after midacceleration at the ATLAS positive-ion AMS.

short-lived ^{37}Ar ($t_{1/2} = 35.0$ d). ^{37}Ar is notable for being the nuclide detected by Davis via Auger electron counting to measure the flux of solar neutrinos via the reaction $^{37}\mathrm{Cl}(\nu, e^-)^{37}\mathrm{Ar}$ (Davis, 1994).

In a different experiment, the high acceleration energy achievable with the ATLAS accelerator at ANL enabled complete isobaric discrimination for the medium-heavy radionuclide ^{146}Sm. In a work dedicated to a redetermination of the half-life of the α-decaying nuclide ^{146}Sm [see Sec. IV.A.1 and Kinoshita *et al.* (2012)], the radionuclide was prepared artificially by three independent nuclear reactions, starting with the naturally occurring long-lived, and also α-decaying, nuclide ^{147}Sm [$t_{1/2} = 106.25 \pm 0.38$ Gyr (Villa *et al.*, 2020)]: $^{147}\mathrm{Sm}(n,2n)^{146}\mathrm{Sm}$, $^{147}\mathrm{Sm}(\gamma,n)^{146}\mathrm{Sm}$, and $^{147}\mathrm{Sm}(p,2n)^{146}\mathrm{Eu}(\beta^+)^{146}\mathrm{Sm}$ (Kinoshita *et al.*, 2012).

Figure 19 illustrates the isobaric separation enabled by the high energy (6 MeV/u). The experiment, based on the double ratio of ^{146}Sm and ^{147}Sm α activities and atom numbers, led to a value for the ^{146}Sm half-life of $(68 \pm 7) \times 10^6$ yr, which is not consistent with the previously adopted value of $(103 \pm 5) \times 10^6$ yr (see the note added at the end of this review). The ^{146}Sm nuclide belongs to the family of radioactive nuclei discovered to have been extant in the early Solar System via isotope anomalies of its α daughter ^{146}Nd and is an important chronometer of the early–Solar System formation. The discrepancy existing between the measured values of its half-life calls for an additional independent measurement; see Villa *et al.* (2020).

G. ATTA: An alternative method of atom counting

Here we make a digression from the AMS technique to mention an equally ultrasensitive atom counting technique,

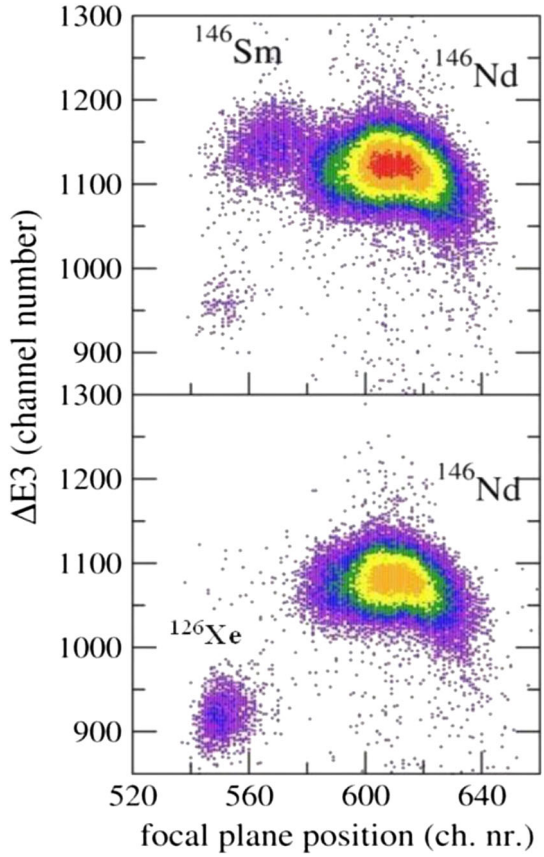

FIG. 19. Isobaric separation of ^{146}Sm and stable ^{146}Nd achieved with highly charged positive-ion AMS at the ATLAS facility (ANL) and the gas-filled Enge magnetic spectrograph. The Sm and Nd ions were accelerated to 6 MeV/u. Adapted from Kinoshita *et al.*, 2012.

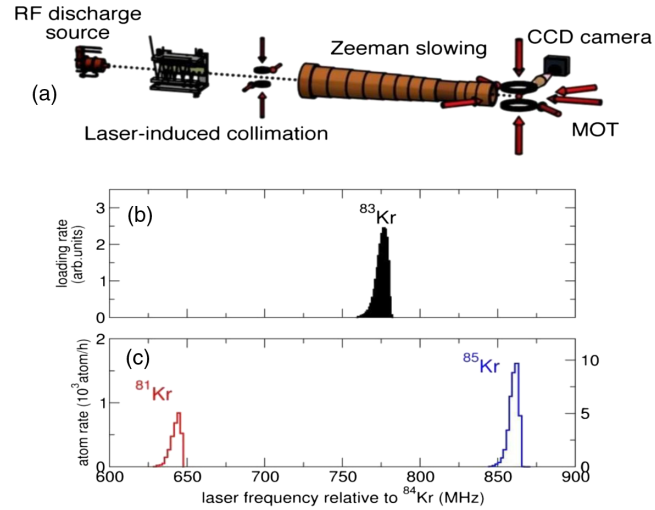

FIG. 20. (a) Schematic of the ATTA atomic beamline. Atoms (dotted line) travel from left to right, starting at the radio-frequency discharge source, passing through the laser-induced collimation and Zeeman slowing stages, and ending in the magneto-optical trap (MOT), where they are imaged using a CCD camera. (b),(c) Typical spectra of the trap capture rate of ^{81}Kr, ^{83}Kr, and ^{85}Kr vs the laser frequency shift (relative to a reference transition in stable ^{84}Kr) measured for an atmospheric Kr sample ($^{81}\mathrm{Kr}/\mathrm{Kr} = 9.3 \times 10^{-13}$) (Zappala *et al.*, 2020). Adapted from Jiang *et al.*, 2012.

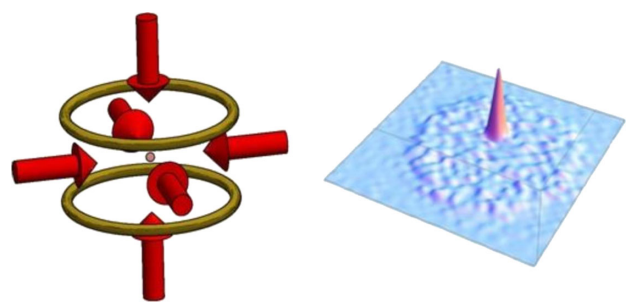

FIG. 21. Fluorescence signal from a single unambiguously identified atom of a noble-gas ^{81}Kr atom in a MOT. Adapted from Lu, 2016.

namely, the ATTA, which has thus far been used to detect noble-gas radionuclides that are cosmogenically or artificially produced: ^{81,85}Kr and ^{39}Ar (Chen *et al.*, 1999).

ATTA uses laser cooling and atom trapping techniques to capture and detect nonionized atoms of the rare isotopes of interest. It exploits the frequency difference between isotopes (isotope shifts) as well as the narrow-band resonant nature of the atomic transitions for atomic excitation, leading to laser manipulation, trapping, and eventually detection in a so-called magneto-optical trap (MOT) with extreme elemental and isotopic discrimination. Thus, by tuning the frequency of the laser light to match a transition in the isotope of interest (see Fig. 20 for the case of Kr isotopes), laser interactions with any other species are exponentially suppressed to the point that ATTA is completely free from a background due to any other isotope, isomer, isobar, atomic, or molecular species. Once atoms are captured in the magneto-optical trap at the heart of the instrument, the many thousand fast-cycling photon-atom interactions allow detection down to the single-atom level via laser-induced fluorescence. This single-atom sensitivity is crucial for the detection of the extremely rare krypton radioisotopes of interest; see the illustration of a single-atom detection in Fig. 21.

Owing to its ultrahigh discrimination power and isotopic selectivity (down in some cases to 10^{-16}–10^{-17} and comparable with the best reported AMS selectivities), the ATTA technique has been employed extensively for geophysical studies of hydrological and ancient ice dating using mainly the ^{81}Kr cosmogenic isotope; see Lu *et al.* (2014) for a review and Lu (2022) for a compilation of references and more recent articles (Purtschert *et al.*, 2021; Ram *et al.*, 2021; Yokochi *et al.*, 2021). Detection of ^{39}Ar ($t_{1/2} = 239$ yr) for geophysical dating was recently added to the routine ATTA capabilities (Ebser *et al.*, 2018; Tong *et al.*, 2021; Ritterbusch *et al.*, 2022).

H. Worldwide AMS facilities

As mentioned, currently almost all AMS facilities utilize the tandem accelerator principle. As depicted in Fig. 22, the

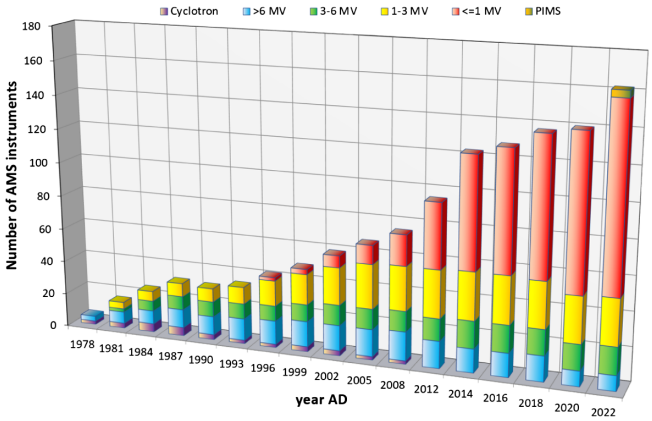

FIG. 22. The growth of the number of tandem AMS facilities since 1978, prepared by Synal (2022) and formulated as a continuation of an earlier version (Synal, 2013). Prior to this, Fink (2010) presented a similar compilation in his talk during AMS11 in Rome. The colors of the column sections indicate the range of tandem terminal voltages in MV. Cyclotrons (green sections at the bottom) were in use only until 2008. The increase in the number of small tandem AMS facilities in the later years is clearly visible. At the top of the last column, the new development of positive-ion mass spectrometry (PIMS) facilities (Freeman *et al.*, 2015) is indicated. A more recent report on PIMS by the AMS group of SUERC is expected to appear in the Proceedings of the AMS-15 Conference in Sydney (Freeman *et al.*, 2021). The unique use of an ECR ion source coupled to a heavy-ion linear accelerator (Collon, Kutschera, and Lu, 2004; Collon *et al.*, 2004; Paul *et al.*, 2019) is not depicted but is described in Sec. II.F.

trend goes from larger (higher terminal voltage) to smaller facilities, as indicated in Fig. 6.

In 2022, the total number of AMS facilities in the world was approaching 160 (Fig. 22, Table II); their distribution is displayed in the world map in Fig. 23. Most of them are situated in countries of the Northern Hemisphere: the U.S., Europe, and the Far East (China, Japan, and South Korea). In the Southern Hemisphere, New Zealand, Australia, and Argentina have been active in the field of AMS for over 30 yr. More recently there have been the additions of one AMS facility in South Africa (Johannesburg) and two newer ones in Brazil (Niteroi) and Argentina (Jujuy). In Central America, a fairly new AMS facility now operates in Mexico.

In Table II, the individual facilities are listed with information on country, accelerator model, terminal voltage, and institution and location of the AMS laboratories. The last column gives the main radionuclides being measured at the respective AMS facilities. Additional radionuclides may also be measured at some of the facilities where the large majority of samples are for radiocarbon measurements. Only the principal possibilities of radionuclide measurements are indicated in the last column for the respective facilities, without any further qualification. Since the status of the facilities, including operational readiness and overall quality of the AMS measurements for specific radionuclides, involves changing commodities and cannot be given in Table II, those interested in the current status of a specific facility should contact the facility directly.

TABLE II. AMS facilities of the world in 2022 compiled to our knowledge, with input from Henri van Oosterhout (HVE), Mark Sundquist (NEC), Joel Bourquin (Ionplus), and Hans-Arno Synal (ETHZ). The list is orderered alphabetically by country and then by increasing terminal voltage. From Kutschera, 2023.

Country	Accelerator (TV)	Laboratory	Radionuclides
Argentina	Tandetron (1.0 MV)	Institute of Dating and Archaeometry, National University of Jujuy	^{14}C, ^{10}Be, ^{26}Al
	FN Tandem (8.0 MV)	Nuclear Regulatory Authority, Buenos Aires	^{129}I, actinides, status unclear
	TANDAR (20 MV)	Department of Experimental Physics, National Atomic Energy Commission, Buenos Aires	^{10}Be, ^{36}Cl
Australia	MICADAS (0.20 MV)	Chronos ^{14}Carbon-Cycle Facility, University of New South Wales, Sydney	^{14}C
	SSAMS (0.25 MV)	Earth Science Department, Australian National University, Canberra	^{14}C
	Pelletron (1.0 MV)	*VEGA* at ANSTO, Menai, Sydney	^{14}C, ^{210}Pb, actinides
	Tandetron (2.0 MV)	Star at ANSTO, Menai, Sydney	^{14}C, IBA
	Pelletron (6.0 MV)	*SIRIUS* at ANSTO, Menai, Sydney	^{10}Be, ^{26}Al, ^{36}Cl, ^{129}I, actinides
	FN Tandem (10 MV)	*ANTARES* at ANSTO, Menai, Sydney	^{14}C
	Pelletron (14 MV)	HIAF, Nuclear Physics Department, Australian National University, Canberra	^{14}C, ^{10}Be, ^{26}Al, ^{32}Si, ^{36}Cl, ^{41}Ca, ^{53}Mn, ^{55}Fe, ^{59}Ni, ^{60}Fe, ^{93}Zr, ^{99}Tc, ^{129}I, ^{210}Pb, actinides
Austria	Pelletron (3.0 MV)	VERA Laboratory, Faculty of Physics, University of Vienna, Vienna	^{14}C, ^{10}Be, ^{26}Al, ^{36}Cl, ^{41}Ca, ^{55}Fe, actinides + more radionuclides with ILIAMS; see Fig. 5
Belgium	MICADAS (0.20 MV)	Royal Institute for Cultural Heritage (RICH), Brussels	^{14}C

(Table continued)

TABLE II. *(Continued)*

Country	Accelerator (TV)	Laboratory	Radionuclides
Brazil	SSAMS (0.25 MV)	Department of Physics, Flumense Federal University, Niteroi	^{14}C
	Pelletron (9.0 MV)	Nuclear Physics Department, University of Sao Paolo, Sao Paolo	^{36}Cl, status unclear
Canada	MICADAS (0.20 MV)	A. E. Lalonde AMS Laboratory University of Ottawa, Ottawa	^{14}C
	Tandetron (3.0 MV)	A. E. Lalonde AMS Laboratory University of Ottawa, Ottawa	^{14}C, ^{10}Be, ^{26}Al, ^{41}Ca, ^{129}I, ^{210}Pb
China	MICADAS (0.20 MV)	XAAMS, Xi'an AMS Centre, Xi'an	^{14}C
	MICADAS (0.20 MV)	Lanzhou University, Lanzhou	^{14}C
	MICADAS (0.20 MV)	Nanjing University, Nanjing	^{14}C
	MICADAS (0.20 MV)	Ocean University of China, Quingdao	^{14}C
	Tandem (0.20 MV)	Coaxial form, China Petroleum and Chemical Corporation, Beijing	^{14}C, delayed due to COVID-19
	SSAMS (0.25 MV)	Homemade AMS, China Institute of Atomic Energy, Beijing	^{14}C, ^{3}H
	SSAMS (0.25 MV)	Homemade AMS, Guangxi Normal University, Guilin	^{14}C
	Tandem (0.30 MV)	Homemade AMS: under development, China Institute of Atomic Energy, Beijing	^{129}I,^{236}U, ^{239}Pu
	CAMS (0.50 MV)	Institute of Heavy Ion Physics, Peking University, Beijing	^{14}C
	CAMS (0.50 MV)	Guangzhou Institute of Geochemistry, Chinese Academy of Sciences	^{14}C
	XCAMS (0.50 MV)	Tianjin University, Tianjin	^{14}C, ^{10}Be
	XCAMS (0.50 MV)	National Laboratory for Marine Science and Technology, Quingdao	^{14}C, ^{10}Be
	XCAMS (0.50 MV)	Southern Marine Science and Engineering Laboratory, Zhuhai	^{14}C, ^{10}Be
	Tandetron (1.0 MV)	Xi'an and Beijing Normal University	^{14}C, ^{10}Be, ^{26}Al, actinides
	Tandetron (1.0 MV)	Institute of Hydrology and Environmental Geology, Chinese Academy of Geological Science (IHEG-CAGS), Shijiazhuang City	^{14}C, ^{10}Be, ^{26}Al, ^{129}I building not yet ready
	UAMS (1.0 MV)	Institute of Geochemistry, Chinese Academy of Sciences, Guizhou, Guiyang	^{14}C, ^{10}Be, ^{26}Al, ^{129}I, actinides
	Tandetron (3.0 MV)	XAAMS, Xi'an AMS Centre, Xi'an	^{14}C, ^{10}Be, ^{26}Al
	EN Tandem (6.0 MV)	Institute of Heavy Ion Physics, Peking University, Beijing,	^{14}C, ^{10}Be
	Pelletron (6.0 MV)	Institute of Geology and Geophysics Chinese Academy of Sciences, Beijing	^{14}C, ^{10}Be, ^{26}Al, ^{36}Cl,^{41}Ca, ^{129}I
	MP tandem (13 MV)	China Institute of Atomic Energy, Beijing	Medium-mass radionuclides, $^{239–242}Pu$
Czech Republic	MILEA (0.30 MV)	Nuclear Physics Institute, Czech Academy of Sciences, Prague	^{14}C, ^{10}Be, ^{26}Al, ^{41}Ca, ^{129}I, actinides
Denmark	Tandetron (1.0 MV)	Institute of Physics and Astronomy Aarhus University, Aarhus	^{14}C, ^{10}Be, ^{26}Al, ^{41}Ca, ^{129}I, actinides
Egypt	Tandetron (2.5 MV)	Nuclear Research Centre, Egyptian Atomic Energy Authority, Inshas, Cairo	^{14}C, status unclear
England, UK	MICADAS (0.20 MV)	*BRAMS* facility, School of Chemistry, University of Bristol, Bristol	^{14}C
	MICADAS (0.20 MV)	Oxford Radiocarbon Accelerator Unit (ORAU), University of Oxford, Oxford	^{14}C
	SSAMS (0.25 MV)	GlaxoSmithKline, Ware (London) Biomedical applications	^{14}C, not in use
	Tandetron (3.0 MV)	Oxford Radiocarbon Accelerator Unit (ORAU), University of Oxford, Oxford	^{14}C, decommisioned
Finland	Tandem (5.0 MV)	Department of Physics, University of Helsinki, Helsinki	^{14}C, status unclear

(Table continued)

TABLE II. *(Continued)*

Country	Accelerator (TV)	Laboratory	Radionuclides
France	MICADAS (0.20 MV)	Aix-MICADAS, Aix-Marseille University, Aix-en-Provence	^{14}C
	MICADAS (0.20)	*ECHO-MICADAS*, Laboratoire de Science du Climat et Environment, Gif-sur-Yvette	^{14}C
	Pelletron (3.0 MV)	*ARTEMIS*, CEA, Saclay, Gif-sur-Yvette	^{14}C
	Tandetron (5.0 MV)	*ASTER*, CEREGE, Aix-Marseille University, Aix-en-Provence	^{10}Be, ^{26}Al, ^{36}Cl, ^{129}I
Germany	MICADAS (0.20 MV)	DatingMICADAS, Curt Engelhorn Centre of Archaeometry, Mannheim	^{14}C
	MICADAS (0.20)	Alfred-Wegener-Institut, Bremerhafen	^{14}C
	Pelletron (1.0 MV)	ExACT AMS, Helmholtz-Zentrum Dresden-Rossendorf, Dresden	^{14}C, ^{10}Be, ^{26}Al, ^{129}I, actinides plus "all isotopes" with ILIAMS
	Tandetron (3.0 MV)	Leibniz-Labor, University of Kiel, Kiel	^{14}C
	MICADAS (0.20 MV)	Max Planck Institute for BioGeo- Chemistry, Jena	^{14}C
	Tandetron (3.0 MV)	Institute for Nuclear Physics, University of Cologne, Cologne	^{14}C
	Tandetron (6.0 MV)	Institute for Nuclear Physics, University of Cologne, Cologne	^{14}C, ^{10}Be, ^{26}Al, ^{36}Cl,^{129}I, actinides
	Tandetron (6.0 MV)	DREAMS, Helmholtz-Zentrum-Dresden-Rossendorf (HZDR), Dresden Germany	^{10}Be, ^{26}Al, ^{36}Cl, ^{41}Ca, ^{55}Fe
	FN Tandem (10 MV)	Institute for Nuclear Physics, University of Cologne, Cologne	^{53}Mn, ^{60}Fe, ^{63}Ni, ^{90}Sr
Hungary	PIMS (0.07 MV)	Isotoptech Zrt., Debrecen	^{14}C + coupled IRMS stable isotopes
	MICADAS (0.20 MV)	Isotope Climatology and Environmental Reasearch Centre, ATOMKI, Debrecen	^{14}C
India	XCAMS (0.5 MV)	Inter University Accelerator Centre, New Delhi	^{14}C, ^{10}Be, ^{26}Al
	Tandetron (1.0 MV)	Physical Research Laboratory (PRL) Ahmedabad	^{14}C, ^{10}Be, ^{26}Al
	Tandetron (1.0 MV)	Mumbai University, Mumbai	^{14}C, ^{10}Be, ^{26}Al
	Pelletron (3.0 MV)	Multi Disciplinary Research Accelerator, Institute of Physics, Bhubaneswar	^{14}C
	Pelletron (15 MV)	Inter-University Accelerator Centre, New Delhi	^{10}Be, ^{36}Cl
Israel	CAMS (0.50 MV)	Kimmel Centre for Archaeology, Weizmann Institute of Science, Rehovot	^{14}C
Italy	Tandetron (3.0 MV)	*INFN-LABEC*, National Institute of Nuclear Physics, Sesto Fiorentino	^{14}C, ^{10}Be, ^{26}Al, ^{129}I
	Tandetron (3.0 MV)	*CEDAD*, Department of Mathematics and Physics, University of Salento, Lecce	^{14}C, ^{129}I, IBA
	Pelletron (3.0 MV)	*CIRCE*, Department of Mathematics and and Physics, University of Campania, Caserta	^{14}C, ^{10}Be, heavier isotopes
Japan	SSAMS (0.25 MV	Atmospheric and Ocean Research Institute, University of Tokyo	^{14}C
	Tandem (0.3 MV)	Coaxial form, Tono Geoscience Center, Japan Atomic Energy Agency, Toki	^{14}C, ^{10}Be, ^{26}Al, ^{129}I
	CAMS (0.5 MV)	Paleo Labo Co., Ltd., Kurohone, Kiryu	^{14}C
	CAMS (0.5 MV)	*BIO-AMS*, Institute for Accelerator Analysis, Motomiya	^{14}C
	CAMS (0.5 MV)	Yamagata University, Kaminoyama	^{14}C
	CAMS (0.5 MV)	National Institute of Environmental Studies (NIES), Tsukuba	^{14}C
	CAMS (0.5 MV)	The University Museum, University of Tokyo, Tokyo	^{14}C
	Tandetron (2.5 MV)	Dating and Material Research Center Nagoya University, Nagoya	^{14}C, ^{10}Be, not in operation
	Tandetron (3.0 MV)	Institute for Space-Earth Environmental Research, Nagoya University, Nagoya	^{14}C
	Pelletron (3.0 MV)	Institute for Accelerator Analysis (IAA), Shirakawa	^{14}C, ^{10}Be

(Table continued)

TABLE II. *(Continued)*

Country	Accelerator (TV)	Laboratory	Radionuclides
	Tandetron (3.0 MV)	Aomori Research and Development Center, Japan Atomic Energy Institute, Mutsu	^{14}C, ^{129}I
	Pelletron (5.0 MV)	Tono Geoscience Center, Japan Atomic Energy Agency, Toki	^{14}C, ^{10}Be, ^{26}Al, ^{36}Cl, ^{129}I
	Pelletron (5.0 MV)	Research Center for Nuclear Science and Technology, University of Tokyo, Tokyo	^{14}C, ^{10}Be, ^{26}Al
	Pelletron (5.0 MV)	Micro Analysis Laboratory, Tandem accelerator (MALT), University of Tokyo, Tokyo	^{14}C, ^{10}Be, ^{26}Al, ^{36}Cl, ^{41}Ca, ^{129}I, ^{236}U
	Pelletron (5.0 MV)	National Institute of Environmental Studies (NIES), Tsukuba	^{14}C
	Pelletron (6.0 MV)	Research Facility Center for Science and Technology, University of Tsukuba, Tsukuba	^{14}C, ^{10}Be, ^{26}Al, ^{36}Cl, ^{41}Ca, ^{90}Sr, ^{129}I
Lithuania	SSAMS (0.25 MV)	Center for Physical Sciences and Technology, Vilnius University, Vilnius	^{14}C
Mexico	Tandetron (1.0 MV)	Institute of Physics, National Autonomous University of Mexico, Mexico City	^{14}C, ^{10}Be, ^{26}Al
Netherlands	MICADAS (0.20 MV)	Center for Isotope Research, University of Groningen, Groningen	^{14}C
	Tandetron (1.0 MV)	BIO-AMS, TNO BIO Science Park, Netherlands Organisation for Applied Scientific Research	^{14}C, ^{10}Be, ^{26}Al, ^{41}Ca
	Tandetron (3.0 MV)	Center for Isotope Research, University of Groningen, Groningen	^{14}C, decommissioned
New Zealand	XCAMS (0.5 MV)	Rafter Radiocarbon Laboratory, GNS Science, Lower Hutt	^{14}C, ^{10}Be, ^{26}Al
Northern Ireland, UK	MICADAS (0.20 MV)	*CHRONO* Center, Queen's University Belfast	^{14}C
	CAMS (0.5 MV)	*CHRONO* Center, Queen's University Belfast	^{14}C
Norway	Tandetron (1.0 MV)	National Lab for Age Determination, Norwegian University for Science and Technology, Trondheim	^{14}C, ^{10}Be, ^{26}Al
Poland	PIMS (0.07 MV)	Academy of Mining and Metallurgy, Department of Geology, Krakow	^{14}C
	CAMS (0.50 MV)	Faculty of Physics, Adam Mickiewicz University, Poznan	^{14}C
	CAMS (0.50 MV)	Faculty of Physics, Adam Mickiewicz University, Poznan	^{14}C
Portugal	Tandetron (3.0 MV)	The Technological and Nuclear Institute (ITN), Sacavem, Lisbon	^{14}C, ^{10}Be, ^{26}Al,
Romania	Tandetron (1.0 MV)	National Institute of Physics and Nuclear Engineering (IFIN-HH), Bucharest	^{14}C, actinides
	FN Tandem (8.0 MV)	National Institute of Physics and Nuclear Engineering (IFIN-HH), Bucharest	^{26}Al, ^{129}I
Russia	MICADAS (0.20 MV)	Novosibirsk State University, Novosibirsk	^{14}C
	Tandem (1.0 MV)	*AMS-BINP*, homemade, Budker Institute for Nuclear Physics, Novosibirsk	^{14}C
Scotland, UK	PIMS (0.07 MV)	*Positive Ion AMS*, Scottish Universities Environmental Research Centre (SUERC), East Kilbride	^{14}C
	SSAMS (0.25 MV)	Scottish Universities Environmental Research Centre (SUERC), East Kilbride	^{14}C
	Pelletron (5.0 MV)	Scottish Universities Environmental Research Centre (SUERC), East Kilbride	^{14}C, ^{10}Be, ^{26}Al, ^{41}Ca, ^{129}I
Slovakia	Pelletron (3.0 MV)	Centre for Nuclear and Accelerator Technologies, Comenius University, Bratislava	^{10}Be, ^{26}Al, IBA

(Table continued)

TABLE II. *(Continued)*

Country	Accelerator (TV)	Laboratory	Radionuclides
South Africa	EN Tandem (6.0 MV)	iThemba LABS, Gauteng, Johannisburg	^{14}C, ^{10}Be, ^{26}Al, ^{129}I
South Korea	MICADAS (0.20 MV)	Department of Creative Convergence Engineering, Dongguk University, Gyeongju City	^{14}C
	MICADAS (0.20 MV)	Korean Apparel Testing and Research Institute (KATRI), Seoul	^{14}C
	MICADAS (0.20 MV)	National Research Institute of Cultural Heritage (NRICH), Daejeon	^{14}C
	MICADAS (0.20 MV)	Korean Research Institute of Chemical Technology (KRICT), Ulsan	^{14}C
	CAMS (0.50 MV)	Korea Institute of Radiological and Medical Sciences (KIRAMS), Seoul	^{14}C
South Korea	Tandetron (1.0 MV)	Korean Institute of Geosciences and Mineral Resources (KIGAM), Deajeon	^{14}C, ^{10}Be, ^{26}Al
	Tandetron (3.0 MV)	Korea Multi-purpose Accelerator Complex (KOMAC), Gyongj	^{14}C
	Tandetron (6.0 MV)	Korea Institute of Science and Technology (KIST), Seoul	^{10}Be, ^{26}Al, IBA
Spain	MICADAS (0.20 MV)	National Centre of Accelerators (CAN), University of Seville, Seville	^{14}C
	MICADAS (0.20 MV)	University of Salamanca, Salamanca	^{14}C
	Tandetron (1.0 MV)	CAN, University of Seville, Seville	^{10}Be, ^{26}Al, ^{129}I, actinides
	Tandetron (1.0 MV)	University of Vigo, Vigo	^{14}C, ^{10}Be, ^{26}Al, status unclear
Sweden	SSAMS (0.25 MV)	GeoBiosphere Science Centre, University of Lund, Lund	^{14}C
	MICADAS (0.20 MV)	Tandem Laboratory, University of Uppsala, Uppsala	^{14}C
	Pelletron (5.0 MV)	Tandem Laboratory, University of Uppsala, Uppsala	^{14}C, ^{10}Be, ^{129}I
Switzerland	LEA (0.05 MV)	Low Energy AMS, Laboratory of Ion Beam Physics, ETH Zurich, Zurich	^{14}C
	MICADAS (0.20 MV)	*ProtoMICADAS*, Laboratory of Ion Beam Physics, ETH Zurich, Zurich	^{14}C
	MICADAS (0.20 MV)	*LIPMICADAS*, Laboratory of Ion	^{14}C
		Beam Physics, ETH Zurich, Zurich	^{14}C
	MICADAS (0.20 MV)	*Lara*, Institute for Environmental Physics, University of Bern, Bern	^{14}C
	MILEA (0.30 MV)	Multi Element Low Energy AMS, Laboratory of Ion Beam Physics, ETH Zurich, Zurich	^{14}C, ^{10}Be, ^{26}Al, ^{129}I, actinide isotopes
	CAMS (0.50 MC)	Compact AMS, Laboratory of Ion Beam Physics, ETH Zurich, Zurich	^{14}C, ^{10}Be, ^{26}Al, ^{41}Ca, actinide isotopes
	EN Tandem (6.0 MV)	Laboratory of Ion Beam Physics, ETH Zurich, Zurich	^{14}C, ^{10}Be, ^{26}Al, ^{32}Si, ^{36}Cl, ^{41}Ca, ^{129}I
Taiwan	Tandetron (1.0 MV)	Department of Geoscience, National Taiwan University, Taipei	^{14}C
Turkey	Pelletron (1.0 MV)	*U-AMS*, Scientific and Technological Research Council of Turkey, Istanbul	^{14}C, ^{10}Be, ^{26}Al, ^{41}Ca,
Ukraine	Tandetron (1.0 MV)	Institute of Applied Physics, National Academy of Science of the Ukraine, Sumy	^{14}C
USA	PIMS (0.07 MV)	NEC in house, Middleton, WI	^{14}C
	MICADAS (0.20)	Northern Arizona University, Flagstaff, AZ	^{14}C
	MICADAS (0.20 MV)	Johns Hopkins University Applied Physics Lab, Laurel, MD	^{14}C
	MICADAS (0.20 MV)	Yale Analytic and Stable Isotope Center, Yale University, New Haven, CT	^{14}C, planned for 2023
	SSAMS (0.25 MV)	Beta Analytic, Miami, FL	^{14}C

(Table continued)

TABLE II. *(Continued)*

Country	Accelerator (TV)	Laboratory	Radionuclides
	SSAMS (0.25 MV)	Beta Analytic, Miami, FL	^{14}C
	SSAMS (0.25 MV)	Beta Analytic, Miami, FL	^{14}C
	SSAMS (0.25 MV)	Beta Analytic, Miami, FL	^{14}C
	SSAMS (0.25 MV)	Xceleron, now part of Pharmanon (China), Germantown, MD	^{14}C, biomedical applications
	SSAMS (0.25 MV)	Center for Applied Isotope Studies University of Georgia, Athens, GA	^{14}C
	SSAMS (0.25 MV)	Center for AMS, LLNL, Livermore, CA	^{14}C
	SSAMS (0.30 MV)	SIMS + SSAMS, Naval Research Laboratory, Washington, D.C.	Trace elements
	CAMS (0.50 MV)	Center for Applied Isotope Studies University of Georgia, Athens, GA	^{14}C
	CAMS (0.50 MV)	Keck-Carbon Cycle AMS Facility, University of California, Irvine, CA	^{14}C
	CAMS (0.50 MV)	Accium Biosciences, Seattle Biomedical applications	^{14}C
	CAMS (0.50 MV)	Institut of Energy and the Environment, Pennsylvania State University, University Park, PA	^{14}C
	CAMS (0.50) MV)	*NOSAMS*, Woods Hole Oceanographic Institution, Woods Hole, MA	^{14}C
	I-CAMS (0.5 MV)	Idaho National Laboratory, Idaho Falls, ID	^{14}C, ^{129}I
	Pelletron (1.0 MV)	Biomedical AMS facility, LLNL, Livermore, CA	^{14}C, ^{3}H, status unclear
	Pelletron (1.0 MV)	Earth and Space Sciences, UCLA, Los Angeles, CA	^{14}C, status unclear
	Tandetron (2.5 MV)	NSF AMS facility, University of Arizona, Tucson, AZ	^{14}C, ^{10}Be, not in operation
	Tandetron (2.5 MV)	NOSAMS, Woods Hole Oceangraphic Institution, Woods Hole, MA	^{14}C, decommissioned
	Pelletron (3.0 MV)	NSF AMS facility, University of Arizona, Tucson, AZ	^{14}C, ^{10}Be, ^{26}Al, status unclear
	FN Tandem (10 MV)	PRIME Laboratory, Purdue University, University, West Lafayette, IN	^{14}C, ^{10}Be, ^{26}Al, ^{36}Cl, ^{41}Ca, ^{129}I
	FN Tandem (10 MV)	Center for AMS, LLNL, Livermore, CA	^{14}C, ^{10}Be, ^{26}Al, ^{36}Cl, ^{41}Ca,^{59}Ni, ^{63}Ni, ^{129}I, actinides
	FN Tandem (10 MV)	Physics Department, University of Notre Dame, Notre Dame, IN	^{10}Be, ^{26}Al, ^{36}Cl, ^{41}Ca
	ATLAS (8 MeV/A)	ECR + Linac, Physics Division, Argonne National Laboratory, Argonne, IL	^{39}Ar, ^{146}Sm

FIG. 23. World map with the global distribution of AMS machines. The size of the symbols indicates the number of machines in one particular location. The large symbols are transparent so as to allow smaller symbols to be visible if they overlap with the larger ones. For details on the various AMS facilities see Table II. Courtesy of Christof Vockenhuber of ETH Zuerich.

III. WIDE-RANGING RESEARCH AREAS OF AMS

A. Archaeology

1. Radiocarbon dating

Archaeology is at the crossroads of science and humanities (Renfrew and Bahn, 2020) and benefited significantly from the development of radiocarbon dating (Taylor and Bar-Josef, 2014). To determine the absolute age of an object, measure both ^{14}C and the radiogenic decay product ^{14}N. However, because of the omnipresence of ^{14}N, it is virtually impossible to detect minute traces of radiogenic ^{14}N, even though an attempt was once discussed (Szabo *et al.*, 1997). Since it is not possible to measure the radiogenic ^{14}N "daughter" content in a sample, the initial ^{14}C content as a function of time needs to be known (calibration curve) to determine an absolute age from the measured ^{14}C content. Cosmic-ray-produced ^{14}C is the main natural source in the atmosphere, and exchanges through the CO_2 cycle with the biosphere and the hydrosphere; cf. Fig. 2. Extensive measurements of ^{14}C in archives of known age (tree rings, varved sediments, speleothems, etc.) have established a continuous record of ^{14}C over the past ~55 000 yr. With the help of continuously updated ^{14}C calibration curves, an absolute age of a sample can be calculated from the measured ^{14}C content (Heaton *et al.*, 2020; Hogg *et al.*, 2020; Reimer *et al.*, 2020), and online software can be used to calibrate the radiocarbon measurements. Since ^{14}C in the atmosphere was not constant over time, the resulting fluctuating calibration curve often limits the precision of the absolute age (Guilderson, Reimer, and Brown, 2005). Since that time, considerable improvements on both ^{14}C AMS measurement techniques and calibration procedures happened. For instance, the discovery of the so-called Miyake excursions [see Sec. III.C.7 in Miyake *et al.* (2012)] and extended single-year tree-ring calibrations (Wacker *et al.*, 2020) allowed in some cases natural (Oppenheimer *et al.*, 2017; Hakozaki *et al.*, 2018) and historical events (Wacker *et al.*, 2014; Kuitems *et al.*, 2020, 2022) to be dated to a single year. In addition, if reliable stratigraphic information is available, a Bayesian statistical analysis of radiocarbon dates can help considerably improve the precision (Bronk Ramsey, 2009). The enormous reduction in sample size and in measuring time using AMS has led to countless research possibilities of radiocarbon dating in archaeology (Marom *et al.*, 2013) and other fields. In fact, ^{14}C measurements compose ~90% of all AMS measurements worldwide. A recent comprehensive review on radiocarbon dating was published by Hajdas *et al.* (2021). Here we mention a few highlights from archaeological research.

2. The 5000-year-old Tyrolean iceman

In 1991 a well-preserved human body, quickly nicknamed Ötzi, was accidentally discovered in a small ice patch at a high-altitude pass [3200 m above sea level (a.s.l.)] in the Ötztal Alps at the Austrian-Italian border (Fig. 24). A surprisingly old age of between 5100 and 5300 yr was established for the body from ^{14}C measurements in bone and tissue (Hedges *et al.*, 1992; Bonani *et al.*, 1994). Further ^{14}C measurements on equipment and botanical remains retrieved from the finding site confirmed the old age of the "iceman Ötzi" (Kutschera *et al.*, 2014). This unique find is on display in the South Tyrol Museum of Archaeology in Bolzano, Italy, and has been the subject of many interesting investigations, including ones about the origin of the iceman through isotope measurements (Müller *et al.*, 2003) and whole-genome sequencing (Keller *et al.*, 2012). In a way, the discovery of the iceman initiated the new field of glacial archeology since the receding glaciers are exposing many objects of interest to archeology and geophysics.

FIG. 24. The partly freed body of the Iceman as watched by two well-known mountain climbers from South Tyrol, Hans Kammerlander (left) and Reinhold Messner (right), on September 21, 1993. Kammerlander holds part of a wooden structure later identified as a carrying support of Oetzi. In the upper right corner the bow can be seen, its lower part stuck in the ice and its upper end leaning against the rocks. Just below the tip of the ski pole held by Messner one can see the smashed remains of a container made of bark from a birch tree, probably used to carry equipment for making a fire. Details of the equipment and their age determination with ^{14}C AMS measurements were given by Kutschera *et al.* (2014). The photograph is courtesy of K. Fritz. From Kutschera and Müller, 2003.

3. Rock paintings in the Chauvet Cave

The Chauvet Cave in France harbors arguably the most beautiful artwork (rock paintings) from early modern humans (Fig. 25). Two distinct human occupations from 37 000 to 33 500 and from 31 000 to 28 000 yr ago were determined from radiocarbon dating (Quiles *et al.*, 2016). The rock paintings were fortuitously preserved by several rock slides, the last one sealing off the cave entrance around 21 000 yr ago.[2] The ages of the rock slides were determined by surface exposure dating of rocks with ^{36}Cl (Sadier *et al.*, 2012). These measurements were also performed with AMS and depend on the accumulation of *in situ*–produced ^{36}Cl in calcium by cosmic-ray secondaries (Stone *et al.*, 1996). The pioneering development of this powerful method was described by Lal (1988).

4. Bronze Age eruption of Santorini

During the late Bronze Age in the Eastern Mediterranean some 3500 yr ago, the Greek island of Santorini (ancient Thera)

[2]The paintings can be viewed at http://bradshawfoundation.com/chauvet/.

FIG. 25. Details regarding the well-preserved rock art paintings of the Chauvet Cave in France, which were produced by prehistoric artists some 30 000 yr ago (Quiles *et al.*, 2016).

experienced a cataclysmic volcanic eruption. Sought after by archaeologists as a time beacon, the exact time of the eruption has not been determined (Kutschera, 2020). Considerable effort has recently been spent by several groups to solve this problem with radiocarbon dating and dendrochronology (Pearson *et al.*, 2018, 2020; Friedrich *et al.*, 2020; Manning *et al.*, 2020). However, a plateau in the ^{14}C calibration curve around the time of the eruption and the unreliable structure of annual rings in olive trees (Ehrlich, Regev, and Boaretto, 2021) leads to a large uncertainty of about 100 yr for the eruption date. This includes a possible eruption in the late 17th century BCE up to 100 yr later. The latter date is favored by some archaeologists (Bietak, 2014). It may eventually be possible to solve this issue with ^{40}Ar/^{39}Ar dating of suitable minerals ejected in the eruption (Kutschera, 2020). This method has been used to verify the date of the Mt. Vesuvius eruption, which is known to have happened in 79 CE (Renne *et al.*, 1997).

5. Appearance of modern humans in the Americas

The earliest indications of the presence of modern humans in South and North America stem from around 17 500 yr ago, based on genetic and archaeological data (Waters, 2019). Progress in genomic analysis (Skoglund and Reich, 2016) revealed a complex heritage of early man, with the main influx from Eurasia and Northern Asia via the Bering Strait. This primary influx was migrating through ice-free corridors to the south, split up into branches of northern Native Americans and southern Native Americans, eventually peopling the respective subcontinents. Recently extensive ^{14}C AMS measurements assigned the appearance of the so-called Clovis culture in North America to a narrow time range from $\sim 13,050$ to $\sim 12,750$ cal. B.P. (Waters, Stafford, and Carlson, 2020). However, Clovis is certainly not the last word. For example, Bennett *et al.* (2021) showed clear evidence of human footprints in White Sands, NM, about 21 000 to 23 000 yr ago. This points to other hints in the archaeological record of pre-Clovis cultures. Further, the combination of genetic and archaeological data promises to be a powerful tool in unraveling the history of early humans in the Americas.

6. The age of Peking man

Dating beyond ~50 000 yr, which is the limit of ^{14}C dating, requires different methods. A powerful tool based on AMS measurements is burial dating using cosmogenic radionuclides (Granger and Muzikar, 2001; Balco and Shuster, 2009). This is based on using two isotopes with different half-lives produced *in situ* by cosmic-ray interaction in suitable minerals. A common pair is ^{10}Be ($t_{1/2} = 1.39 \times 10^6$ yr) and ^{26}Al (0.718×10^6 yr), produced in quartz grains (SiO_2) on an exposed rock surface with a production ratio of ^{26}Al/^{10}Be ~ 6 (Nishiizumi *et al.*, 1989). This ratio is relatively independent of latitude and altitude of the exposed rock. The average ratio was recently determined to be ^{26}Al/^{10}Be $= 6.75$ (Halsted, Bierman, and Balco, 2021). Once the exposed material is buried and shielded from further cosmic-ray exposure, the ^{26}Al/^{10}Be ratio decays with an effective half-life of 1.5×10^6 yr. This method was used to determine the age of the sediment layers in the cave where the remains of the Peking man were found (Shen *et al.*, 2009). The result $(0.77 \pm 0.08) \times 10^6$ yr was substantially older than previously assumed. It indicated that early hominids were present at this site in northern China during a relatively mild glacial period around the marine isotope stage (MIS) 18 (Shen *et al.*, 2009).

7. The promise of ^{41}Ca dating

The half-life of ^{41}Ca is close to 100 000 yr: $t_{1/2} = (99.4 \pm 1.5) \times 10^3$ yr (Jörg *et al.*, 2012). Since calcium is a major component of bones, it was speculated early on that a dating method based on ^{41}Ca would be desirable for archaeology (Yamaguchi, 1963). However, low ^{41}Ca/^{40}Ca ratios around 10^{-14} to 10^{-15} estimated from ^{40}Ca$(n,\gamma)^{41}$Ca reactions made a detection of ^{41}Ca in bones at that time unfeasible (Yamaguchi, 1963). When AMS came along, ^{41}Ca dating was again discussed (Raisbeck and Yiou, 1979). Raisbeck and Yiou mentioned there that ^{41}Ca dating of bones might cover an age range from 50 000 to 10^6 yr ago, considerably extending the ^{14}C method. An important step in the actual development of an AMS detection of ^{41}Ca at natural abundances was proposed by Raisbeck *et al.* (1981) in using $^{41}CaH_3^-$ ions to suppress the interference of the stable isobar ^{41}K. The first AMS measurement of ^{41}Ca in contemporary bovine bones, including a ^{41}Ca preenrichment step, was performed at the ATLAS facility at Argonne (Henning *et al.*, 1987). Direct ^{41}Ca measurements on a 2740-year-old *Homo sapiens* bone were later performed at the same facility (Kutschera *et al.*, 1989) and in modern bones at the tandem accelerator of the University of Pennsylvania (Middleton *et al.*, 1989). The latter showed a considerable scatter of the results for different localities on Earth, indicating a nonuniform ^{41}Ca distribution.

In contrast to ^{14}C dating, the major problem for ^{41}Ca dating is the lack of a universal calibration curve. This is due to the fact that ^{41}Ca does not form a gas in the atmosphere like $^{14}CO_2$, which gets well mixed within the troposphere around the world. Without knowing the initial ^{41}Ca/^{40}Ca ratio as a function of time, one would depend on absolute dating, as once proposed for ^{14}C (Szabo *et al.*, 1997). This means that one has to measure both ^{41}Ca and its radiogenic decay

product $^{41}K^*$. With the known half-life of ^{41}Ca and a measured $^{41}Ca/^{41}K^*$ ratio one can then calculate the age of the object, regardless of the initial $^{41}Ca/^{40}Ca$ ratio. The challenge is to measure the expected minute radiogenic $^{41}K^*$ component on top of ^{41}K from ~50 ppm of potassium in bone apatite (Combes, Cazalbou, and Rey, 2016). However, developments in high-precision potassium isotope measurements with thermal ionization mass spectrometry (TIMS) (Wielandt and Bizzarro, 2011) may eventually make this possible. It may also help that ^{41}Ca decays by pure electron capture to ^{41}K, resulting in a small $^{41}K^*$ recoil energy of ~2.2 eV. $^{41}K^*$ should therefore be confined within the small apatite crystals (Weiner and Price, 1986). This may allow a chemical separation of the small bone apatite crystals from the rest of the bone matrix, and thus reduce the interference of environmental ^{41}K with the radiogenic $^{41}K^*$. In addition to the difficult measurement of a $^{41}K^*/^{41}Ca$ ratio, it has to be guaranteed that the bones to be dated are shielded from the buildup of ^{41}Ca through environmental neutrons via the $^{40}Ca(n,\gamma)^{41}Ca$ reaction. Bones buried in caves may provide such a condition. Currently a reliable dating method with ^{41}Ca is still a dream to be fulfilled in the future. On the other hand, in analogy with ^{14}C a local calibration of the $^{41}Ca/Ca$ ratio might be useful for special cases, as shown with teeth samples from Hiroshima survivors (Rühm *et al.*, 2010; Wallner *et al.*, 2010).

B. Biological research

1. Tracing long-lived radioisotopes in the human body

AMS allows one to trace long-lived radioisotopes at concentrations that produce no significant radiation hazards to biological systems. Considering that humans experience at least 10 000 decays/s from natural radioisotopes in their body (^{14}C,^{40}K, and ^{210}Pb), AMS-traceable amounts of radioisotopes that are far below this level can be administered to humans. In this way, biokinetics research with ^{26}Al administered to humans has been performed (King *et al.*, 1997; Kislinger *et al.*, 1997). In another application of ^{26}Al, the long-time Al retention in the human body was studied (Newton and Talbot, 2012). ^{41}Ca was used to study the metabolism of Ca in bones in connection with osteoporosis (Johnson *et al.*, 1994; Freeman *et al.*, 2000; Denk *et al.*, 2006). Research on drug metabolism with ^{14}C-labeled compounds in animals started at Lawrence Livermore National Laboratory (Turteltaub *et al.*, 1990). It developed into a method called human microdosing (Garner, 2010), which considerably speeds up the development of new drugs. The growing demand by the pharmaceutical industry led to the development of small dedicated tandem facilities for biological research (Schulze-König *et al.*, 2010).

2. ^{14}C bomb peak and cell dynamics in humans

Arnold and Libby (1949) and Libby, Anderson, and Arnold (1949) originally assumed that ^{14}C in the biosphere is constant over all times, and can therefore be assessed by measuring it in modern wood. When de Vries (1958) discovered that ^{14}C was not constant at all times, the consequence was the necessity of a radiocarbon calibration for absolute age determinations. The calibration curve is being refined from time to time; the latest version is from 2020 (Reimer *et al.*, 2020). A dramatic man-made increase of ^{14}C on top of the natural ^{14}C level occurred during the atmospheric nuclear weapons testing period, which is depicted in Fig. 26; see also Fig. 3 and Levin *et al.* (2022).

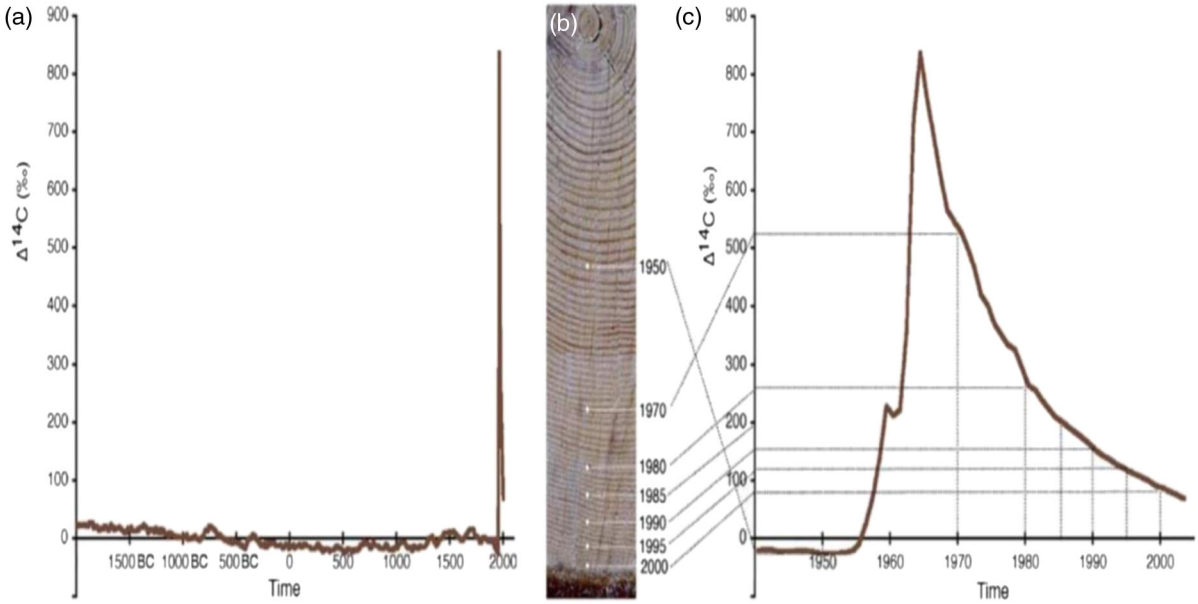

FIG. 26. (a) Deviation of the atmospheric ^{14}C content ($\Delta^{14}C$ in per mill) relative to a constant reference value ($\Delta^{14}C = 0$) and displays $\Delta^{14}C$ for the last 4000 yr. (b) Annual tree rings from a local pine tree. The ^{14}C content verified the bomb peak. Adapted from Spalding *et al.*, 2005. (c) Depiction of the sudden increase between 1955 and 1963 due to atmospheric nuclear weapons testing (cf. Fig. 3) and the gradual decrease after the Nuclear Test Ban Treaty of 1963. The latter is determined by the distribution of ^{14}C due to the CO_2 cycle. The slightly negative $\Delta^{14}C$ values before the rise of the bomb peak are due to the dilution of the natural $^{14}CO_2$ content with ^{14}C-free CO_2 from fossil fuel burning, which is known as the Suess effect (Suess, 1955).

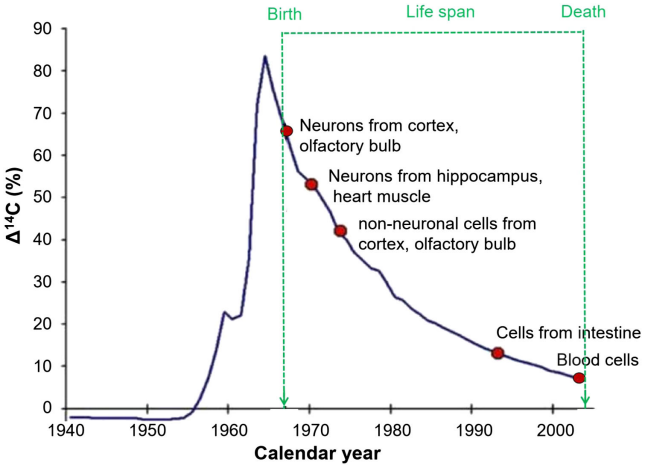

FIG. 27. Visualization of how the birth date of different cells in an individual of a known life span can be determined retrospectively by comparing the measured ^{14}C signal from DNA extracts with the ^{14}C bomb peak calibration curve. Based on work by Spalding *et al.* (2005). Adapted from Kutschera, 2022.

The ^{14}C bomb peak is a distinct signal in the second half of the 20th century, providing a rapidly running ^{14}C clock, where the contribution due to the decay of ^{14}C is negligible (~6 per mill in 50 yr). This provides a unique isotope signal to study the dynamics of systems that participate in the CO_2 cycle, in particular, the entire biosphere. The ensuing applications were fittingly called "the mushroom cloud's silver lining" (Grimm, 2008). Some of the most interesting applications are pursued at the Department of Cell and Molecular Biology of the Karolinska Institute in Stockholm. AMS measurements of ^{14}C in DNA from humans who lived through the time of the ^{14}C bomb peak allows one to retrospectively determine the birth date of cells from different parts of the brain (Spalding *et al.*, 2005, 2013; Bhardwaj *et al.*, 2006; Bergmann *et al.*, 2012). The principle of the method is depicted in Fig. 27.

Particularly interesting results were obtained by studying neuronal and non-neuronal cells from the hippocampus of 57 individuals (Spalding *et al.*, 2013). The hippocampus is part of the brain that is involved in memory formation, organization, and storage. The results are displayed in Fig. 28. Other studies of the Stockholm group investigated the renewal of heart muscle cells (Bergmann *et al.*, 2009), and also gained insight into the dynamics of fat cells (Spalding *et al.*, 2017).

3. ^{14}C bomb peak in forensic science

The ^{14}C bomb peak can play an important role in uncovering the questions in a variety of fields, such as for the authenticity of ancient and modern pieces of art, the time of

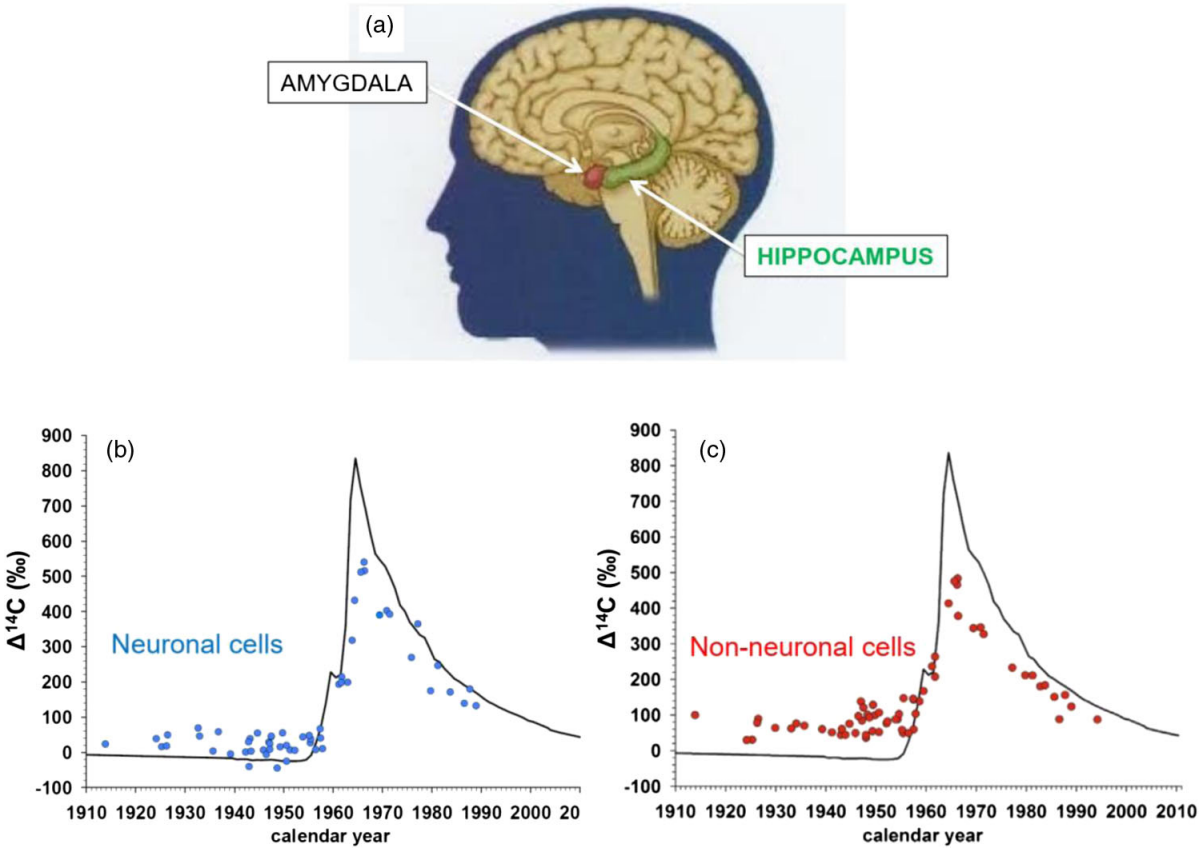

FIG. 28. Evidence for neurogenesis in the human hippocampus. (a) $\Delta^{14}C$ values of (b) neuronal and (c) non-neuronal cells from the hippocampus plotted for the birth dates of 57 individuals. Deviations from the ^{14}C bomb curve indicate the formation of new cells after birth. The offset between the atmospheric bomb curve and DNA measurements is indicative of the magnitude of cell turnover. The smaller offset of neurons indicates that their turnover is smaller than that of non-neurons. Based on work by Spalding *et al.* (2013). Adapted from Kutschera, 2022.

death or birth of humans, and the preservation of endangered animals. For example, for forgery in art the ^{14}C content of a painting supposedly produced around 1914 by the French artist Fernand Léger (1881–1955) fell in to the early rise of the bomb peak, clearly indicating that it originated from after the death of Léger (Caforio *et al.*, 2014). In a similar investigation, Beck *et al.* (2022) discovered forgeries of Impressionist and Pointillist paintings. In a court case about life insurance for two elderly women who were found dead in their apartment in around 1989, the ^{14}C content of short-lived material (hair, lipids, etc.) allowed the determination of the time of death, and within a 1σ uncertainty, one of the two women died one year earlier (Wild *et al.*, 2000). The third example concerns African elephants and efforts to protect them against poaching for the ivory trade since 1989 by the international Convention on International Trade in Endangered Species of Wild Fauna and Flora agreement. This did not stop the poaching, and ^{14}C bomb peak signals measured in ivory seized from illegal trade between 2009 and 2014 showed less than three years of lag between the killing and the seizure (Cerling *et al.*, 2016). On the other hand, the age of several elephant tusks originating from legal hunting of elephants in the 1960s and 1970s was clearly confirmed by ^{14}C bomb peak dating (Wild *et al.*, 2019).

C. Atmospheric science

Besides being the target for cosmic-ray-produced radioisotopes (Fig. 2), it is well known that the atmosphere on Earth is crucial for the development of life as we know it. One may thus argue that it is the most precious component of our planet, and we should make sure that we keep it this way. Although the atmosphere is only a thin layer of matter on the surface of Earth, its influence on temperature and climate is profound. It is also a large chemical reactor. The main gases of the atmosphere are nitrogen (78%), oxygen (21%), and argon (0.93%). Water vapor is highly variable (0% to 4%). The rest are trace gases (Meinshausen *et al.*, 2017), some of which, such as CO_2 (0.042%) and CH_4 (0.000 19%), hold considerable importance for the temperature on the ground. Other trace gases of some importance are H_2 (0.000 05%), NO_2 (0.000 04%), and O_3 (0.000 03%). In addition, aerosols contribute to the overall complexity of the atmosphere (Bzdeka and Reida, 2017), for instance, through their influence on cloud formation (Feketeová *et al.*, 2019), and have a considerable influence on the overall radiation budget (IPCC, 2021).

Here we address AMS measurements of ^{14}CO, $^{14}CO_2$, and $^{14}CH_4$, allowing one to consider some of the subtleties of atmospheric chemistry.

1. Carbon monoxide (CO) and the hydroxyl radical OH

CO has a lifetime of two to three months in the atmosphere (Jöckel, Lawrence, and Brenninkmeijer, 1999). As indicated in Fig. 3, freshly produced ^{14}C atoms first oxidize to ^{14}CO and then oxidize to $^{14}CO_2$. The second step proceeds primarily through a reaction with the hydroxyl radical OH according to $^{14}CO + OH \rightarrow {}^{14}CO_2 + H$. Although the OH concentration at any given time is extremely low in the atmosphere ($\sim 10^{-13}$), the reactive power of OH dominates this oxidation step rather than reactions with the abundant O_2 (21%). In fact, the mean lifetime of freshly produced OH [for instance, through $O_3 + h\nu \rightarrow O_2 + O(^1D)$; $O(^1D) + H_2O \rightarrow 2OH$] is only about 1 s before it is destroyed through chemical reactions. Because of this oxidizing power removing many atmospheric trace gases, the hydroxyl radical has been called the detergent of the atmosphere (Crutzen, 1997). The general importance of monitoring OH in different regions of the world was described by Lelieveld *et al.* (2006) and Brenninkmeijer, Gromov, and Jöckel (2022).

For example, for AMS measurements of ^{14}CO the seasonal behavior of the OH concentration was observed through the measurement of ^{14}CO and CO concentration in air from the high-altitude observatory on Mt. Sonnblick (3106 m a.s.l.) in the Austrian Alps (Rom *et al.*, 2000). Figure 29 displays some of the characteristics of measurements of ^{14}CO and CO concentrations in air at this site.

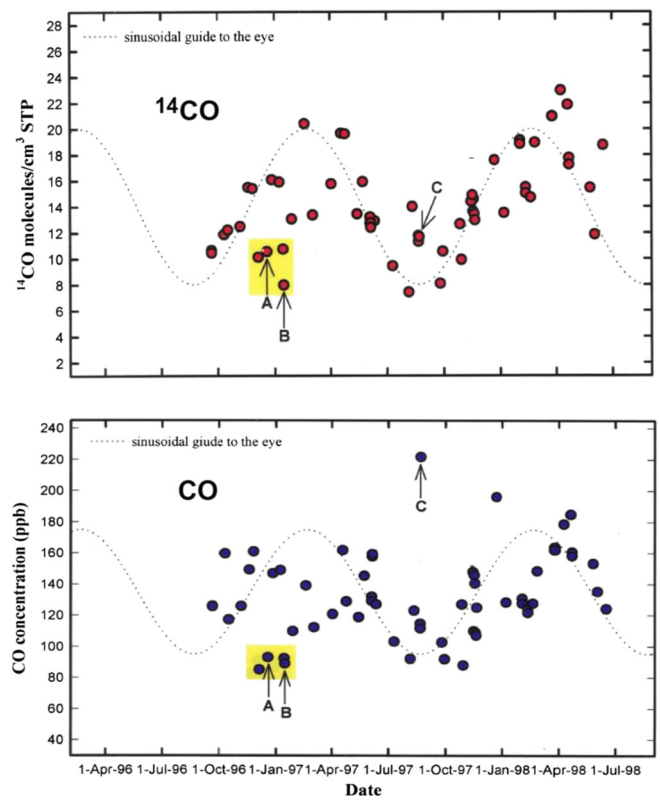

FIG. 29. Two-year record of ^{14}CO and CO concentration measurements in air from the observatory of Mt. Sonnblick (3106 m a.s.l.). The lower values during the summer are due to the depletion by reactions with increased OH concentrations. The unusually low values of both ^{14}CO and CO (marked A and B) during winter are due to the transport of air from low latitudes to Mt. Sonnblick, as verified by four-day backward trajectory calculations (Rom *et al.*, 2000). The unusually high CO value (marked C) is due to a contamination of the air by fossil fuel combustion from an emergency diesel engine running that day. Since this did not contribute any ^{14}C, the corresponding $^{14}CO_2$ value of the contaminated air remains unaffected. From Rom *et al.*, 2000.

2. The CARIBIC project: Monitoring the atmosphere on commercial airline flights

The idea to monitor trace gases and aerosols with a special instrument package on a commercial airline flight was born in the late 1990s (Brenninkmeijer *et al.*, 1999). In the ensuing years a wealth of data were collected (Brenninkmeijer *et al.*, 2007). These data allowed a direct determination of the production of radiocarbon at altitude through the measurement of ^{14}CO and $^{14}CO_2$ (Bronk Ramsey *et al.*, 2007). Long-time collection on Civil Aircraft for the Regular Investigation of the Atmosphere Based on an Instrument Container (CARIBIC) flights made it possible to model the global distribution of such important greenhouse gases as CH_4 (Zimmermann *et al.*, 2020).

3. The measurement of $^{14}CO_2$ as a sensitive tracer for anthropogenic activities

The reduction of the ^{14}C concentrations measured in modern wood was the first indication that ^{14}C-free CO_2 from fossil fuel burning affected the natural ^{14}C content in the atmosphere (Suess, 1955). This effect was offset by the dramatic increase of atmospheric ^{14}C by the nuclear weapons testing period of 1955 to 1963 (Figs. 3 and 26). After the ban of atmospheric nuclear weapons testing in 1963, the excess of ^{14}C in the atmosphere decreased gradually owing to the CO_2 cycle but was also affected by the steadily increasing contribution of ^{14}C-free CO_2 from fossil fuel burning (Levin *et al.*, 2010). Extrapolating well into the 21st century, the ^{14}C content of the atmosphere will eventually fall well below the preindustrial natural level (Graven, 2015). Figure 30 shows this trend for different representative concentration pathways of greenhouse gases (Van Vuuren *et al.*, 2011).

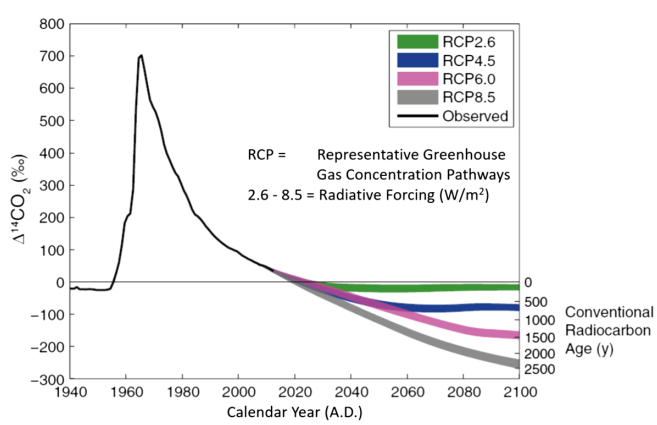

FIG. 30. Model prediction for the development of the ^{14}C content in the atmosphere from 1940 to 2100 expressed as the deviation of $^{14}CO_2$ from the natural $^{14}CO_2$ level ($\Delta^{14}CO_2 = 0$). The picture indicates the depression of ^{14}C as a function of the so-called representative concentration pathways (RCPs). The numbers following RCP in the legend depict the radiation forcing in W/m^2, depending on different scenarios to reduce the emission of greenhouse gases (Van Vuuren *et al.*, 2011). Adapted from Graven, 2015.

4. Atmospheric methane and $^{14}CH_4$ measurements

Methane is being monitored worldwide within the Advanced Global Atmospheric Gases Experiment (Saunois *et al.*, 2020). Methane is the second most important greenhouse gas in the atmosphere. Although the 2022 atmospheric concentration of CH_4 (~1.9 ppm) is still much lower than that of CO_2 (~420 ppm), the global warming potential per molecule is ~25 times larger, and the relative yearly increase is also larger. Therefore, a detailed understanding of different contributions to the rapidly increasing CH_4 concentration is of great interest. Radiocarbon measurements of atmospheric methane were performed early on with AMS (Klouda *et al.*, 1986), and considerable effort has been made in recent years to understand biogenic and fossil fuel CH_4 emissions through measurements of $\delta^{13}C$ (Nisbet *et al.*, 2016; Varga *et al.*, 2021) and ^{14}C AMS measurements in methane (Hmiel *et al.*, 2020). In $^{14}CH_4$ studies, contributions of $^{14}CH_4$ emissions from nuclear power plants must also be considered (Zazzeri *et al.*, 2017), and the distribution of ancient methane to surface waters is another aspect to be considered in the complexity of methane cycles (Sparrow *et al.*, 2018). These studies are important as input for climate modeling (Meinshausen *et al.*, 2017; Nicholls *et al.*, 2021). Efficient sampling of atmospheric methane is also essential for $^{14}CH_4$ measurements, and new sampling methods are being developed (Zazzeri, Xu, and Graven, 2021).

5. Solar energetic particle events

In 2012, unusually strong excursions of ^{14}C were found in annual tree-ring measurements of Japanese cedar trees for the time period of 774 to 775 CE (Miyake *et al.*, 2012). Similar excursions were also found for the time period of 993 to 994 CE (Miyake, Masuda, and Nakamura, 2013); see Fig. 31.

It turned out that these excursions occurred globally (Jull *et al.*, 2014; Büntgen *et al.*, 2018), and additional excursions, sometimes called Miyake events, were found to have occurred at 660 BCE (Park *et al.*, 2017), 5259 and 7176 BCE (Brehm *et al.*, 2022), and 5410 BCE (Miyake *et al.*, 2021). However, the rapid excursion happening in 3372–3371 BCE (Wang *et al.*, 2017) could not be confirmed by two additional

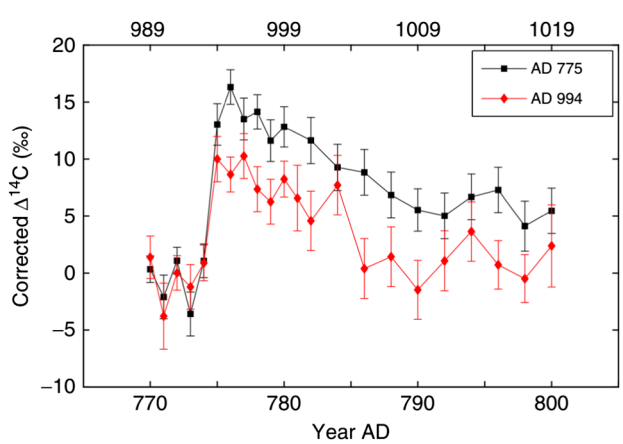

FIG. 31. Rapid ^{14}C variations observed in tree rings occurring in 774 CE and 993 CE. Adapted from Miyake, Masuda, and Nakamura, 2013.

measurements (Jull *et al.*, 2021). In addition to ^{14}C excursions in tree rings, the 774 and 993 CE events showed up in the record of ^{10}Be and ^{36}Cl in Antarctic and Greenland ice cores (Mekhaldi *et al.*, 2015). The 7176 BCE excursion of ^{14}C (Brehm *et al.*, 2022) were clearly observed in the ^{10}Be and ^{36}Cl record of different Greenland ice cores (Paleari *et al.*, 2022).

Cosmogenic radionuclides such as ^{14}C, ^{10}Be, and ^{36}Cl are produced by cosmic-ray interactions in the atmosphere, but no evidence for excessive production linked to a known supernova event has been found (Dee *et al.*, 2017), with the possible exception of the Crab Nebula supernova SN1054 (Terrasi *et al.*, 2020). Therefore, the observed excursions are considered to be produced by solar energetic particle (proton) events (Usoskin *et al.*, 2013; Mekhaldi *et al.*, 2015; Park *et al.*, 2017; Sukhodolov *et al.*, 2017; Uusitalo *et al.*, 2018; Jull *et al.*, 2020; Sakurai *et al.*, 2020). Such a "solar storm" event today would cause a massive disruption of complex electronic systems, from mobile phones to satellites to the Internet, on which we rely so much today.

The ^{14}C excursions also provide fixed points in the ^{14}C calibration curve, allow one to determine the age of historical buildings with unprecedented precision (Wacker *et al.*, 2014; Kuitems *et al.*, 2020), and enable one to fix the much-debated arrival of the first Europeans to the Americas to 1021 CE (Kuitems *et al.*, 2022).

D. Oceanographic and hydrospheric research

1. Global ocean currents

Earth is the only planet in the Solar System that carries a large amount of liquid water, and probably has during most of its existence. Since the oceans cover $2/3$ of the surface of Earth, with a mean depth of 3800 m, they have an enormous heat capacity. The oceans are also a grand dynamic system that is depicted in a simplified manner in Fig. 32 (Broecker, 1991). The figure illustrates the distribution of heat around the globe, with considerable influence on the global and regional climate. The details regarding ocean currents are much more complex; see Rahmstorf (2002).

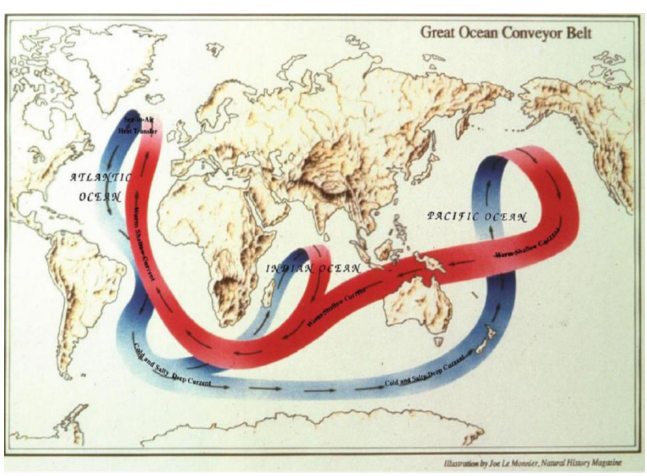

FIG. 32. Great ocean conveyor as conceived originally by Broecker (1991). It is a simplified picture of the main ocean currents transporting heat around the globe. The warm and shallow currents are indicated in red, and the cold an salty deep current are marked in blue. Illustration by Joe Le Monnier, Natural History Magazine. Adapted from Kutschera, 2013.

AMS measurements of ^{14}C in ocean water instead of beta counting reduced the sample size by a factor of about 500 (250–0.5 l), and within the World Ocean Circulation Experiment tens of thousands of ^{14}C measurements were performed (McNichol *et al.*, 2000). These measurements deliver important information to the ongoing Global Ocean Data Analysis Project (Olsen *et al.*, 2019, 2020). This then also allows one to estimate the uptake of anthropogenic CO_2 in the ocean (Gruber *et al.*, 2019), essential information for estimating the human impact on global warming. Recently the Southern Ocean has gained considerable importance for understanding the overall dynamics of global ocean currents, and a project called Southern Ocean Carbon and Climate Observations and Modeling has been launched.[3] In addition, a variety of anthropogenic radionuclides of medium-mass actinide isotopes are being developed as versatile oceanic tracers (Hain *et al.*, 2022); see also Sec. III.G.

In addition to a chemical analysis of the oceans, physical aspects of the oceans are being studied by the Argo Project (2021), an international program that uses profiling floats to measure temperature, salinity, currents, and, recently, bio-optical properties (Fig. 33). Of special interest is to quantify the heat content of the oceans.

2. Groundwater dating

Groundwater is the most important resource of fresh water on Earth. Although it constitutes only ~0.8% of all water on Earth, it is 100 times more abundant than fresh water from lakes and rivers. Understanding the groundwater systems is therefore of great importance, particularly in arid areas (Ferguson *et al.*, 2020). Depending on the study of young or old groundwater systems, multiple isotope tracers with different half-lives can be used: ^{14}C bomb peak (the last 60 yr), ^{85}Kr ($t_{1/2} = 10.8$ yr), ^{3}H (12.3 yr), ^{39}Ar (269 yr), ^{14}C (5700 yr), ^{81}Kr (2.3×10^5 yr), ^{36}Cl (3.0×10^5 yr), and ^{129}I (1.6×10^7 yr). Here the noble-gas radionuclides are of particular interest since they do not participate in chemical reactions. An early AMS study with ^{81}Kr in the Great Artesian Basin in Australia revealed groundwater ages in the range from 200 000 to 400 000 yr (Collon *et al.*, 2000). The Nubian aquifer, an even older groundwater system in Africa, was also explored with ^{81}Kr, albeit using a different technique (Sturchio *et al.*, 2004). As discussed in Sec. II.G, the laser-based ATTA (Chen *et al.*, 1999) developed into a powerful analytical tool to study noble-gas radionuclides in geoscience (Lu *et al.*, 2014), including groundwater studies with ^{39}Ar (Ritterbusch *et al.*, 2014). A particularly detailed isotope study was recently performed in the San Joaquin Valley in California, an agricultural region that is heavily reliant on groundwater (Seltzer *et al.*, 2021). AMS measurements of ^{14}C in groundwater dissolved inorganic carbon combined with other isotope tracers (^{3}H, ^{39}Ar, and ^{85}Kr) revealed a growing input of anthropogenic carbonate from soil

[3]See http://soccom.princeton.edu/content/overview.

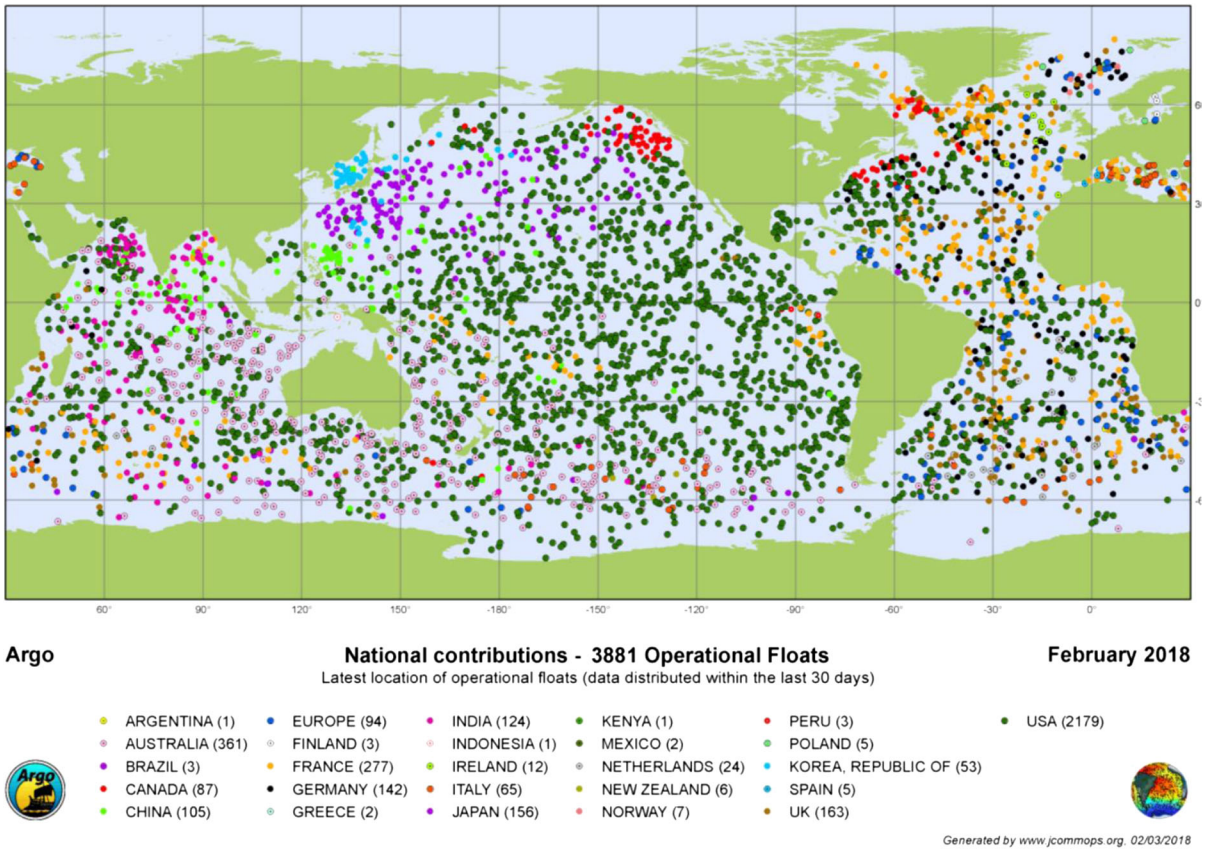

FIG. 33. Distribution of almost 4000 profiling floats across the world oceans within the Argo Project. The colors of the dots indicate the country that released the floats. Continents are marked in bright green. Adapted from the Argo Project, 2021.

amendments. This affects the estimate of groundwater residence times significantly (Seltzer *et al.*, 2021).

Groundwater is the major resource of fresh water for billions of people (Giordano, 2009), and isotope tracer studies with AMS (^{14}C) and ATTA (^{39}Ar, ^{81}Kr, and ^{85}Kr) will continue to contribute significantly to a better understanding of this vitally important resource for humans on Earth.

E. Cryospheric research

Polar ice caps and glaciers contain about 1.7% of the surface water on Earth. However, during the last ice age the amount of landlocked ice approximately doubled, reducing sea levels by ~120 m. This exposed landmasses at shallow parts of the oceans. An excellent example is the Bering Strait (~50 m depth), which then formed a landbridge between Asia and North America.

1. Polar ice sheets

The history of ice ages has been explored through extensive ice core research in both Greenland and Antarctica, with the latter going back 800 000 yr (EPICA Community Members, 2004). Stable isotope ratios of ^{2}H/^{1}H(δD) and ^{18}O/^{16}O(δ^{18}O) in ice can be used as proxies for temperature variations and revealed eight glacial cycles between cold (glacial) and warm (interglacial) periods (Fig. 34). An important contribution to the long-standing debate about the synchronization of records from different ice cores was presented on the basis of AMS measurements of cosmogenic ^{10}Be produced in the atmosphere that has been incorporated into ice cores (Raisbeck *et al.*, 2017). An interesting application of ^{81}Kr measurements with ATTA identified 120 000-year-old ice in the Taylor Glacier in Antarctica (Buizert *et al.*, 2014).

2. Glaciers

The waxing and waning of alpine glaciers are sensitive proxies for temperature and climate changes during the Holocene, the relatively stable and warm period after the end of the last ice age 11 700 yr ago (Kutschera *et al.*, 2000). The dramatic increase of atmospheric CO_2 recorded since 1956 on Mauna Loa in Hawaii (Keeling, 1998, 2008; Nisbert, 2007) is undoubtedly due to human activity and is warming the surface of the planet. While this led to a worldwide melting of ice during the 20th century (Thompson *et al.*, 2009), alpine glaciers moved considerably during the Holocene due to natural causes, with some distinct differences evident between the Northern and Southern Hemispheres (Kutschera, 2020). In these studies AMS measurements of ^{14}C in recently exposed organic matter (such as trees and peat) and ^{10}Be and ^{26}Al surface exposure dating of moraines and exposed bedrock helped to piece together the history of glacier movement during the last 10 000 yr; see Schaefer *et al.* (2009) and Kelly *et al.* (2015). The overall temperature trend during the Holocene seems to follow the Milanković theory of solar insulation variation on Earth (Milanković, 1941; Berger and

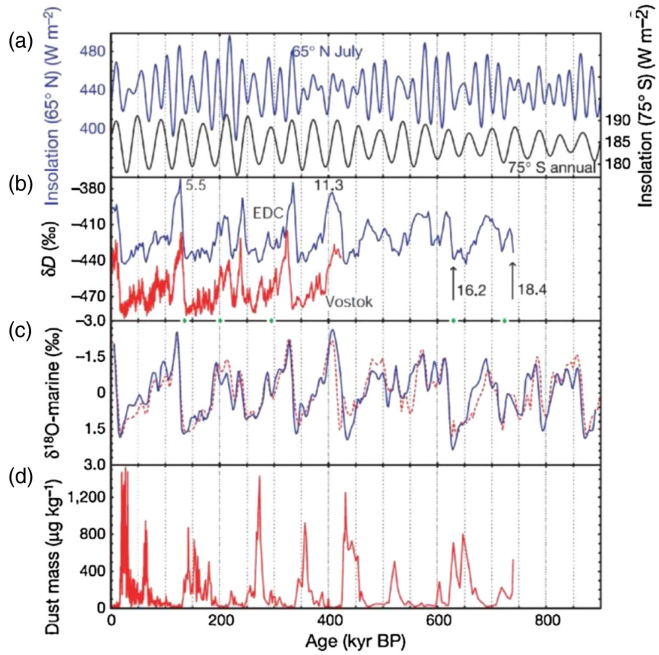

FIG. 34. Comparison of EPICA Dome C data with other paleoclimatic records (EPICA Community Members, 2004). (a) Record of the insolation at high northern and southern latitudes (Berger and Loutre, 1991). (b) Temperature record as measured with the δD signal in the EPICA Dome C (blue curve) and the Vostok ice cores (red curve). The numbers refer to the marine isotope stage (MIS), where odd numbers were originally assigned to warm periods and even ones were assigned to cold periods (Emiliani, 1955; Shackleton, 1987). However, decimal numbers later became common to distinguish details of various subperiods (Jouzel *et al.*, 2007). (c) Marine δ^{18}O signals from two different deep-sea sediment cores (solid blue line and red dashed line) that reflect both temperature and ice mass changes. (d) The dust signal, which is particularly large during cold periods. Adapted from Kutschera, 2013.

Loutre, 1991), with a cooling trend in the Northern Hemisphere in the second half of the Holocene, and the opposite in the Southern Hemisphers (Putnam *et al.*, 2012).

F. Lithospheric research

1. Surface exposure dating and geomorphology

Both solar and Galactic cosmic rays first meet the atmosphere when they encounter Earth. They produce a variety of radioisotopes by nuclear reactions with nuclei of the atmosphere (Lal and Peters, 1967; Beer, McCracken, and von Steiger, 2012; Poluianov *et al.*, 2016). However, they also produce secondary particles in these reactions such as neutrons and muons. Although they are attenuated in their passage through the atmosphere, a significant amount arrives at the surface of Earth and produces radioisotopes *in situ* in terrestrial rocks (Lal, 1988; Gosse and Phillips, 2001; Dunai, 2010; Schaefer *et al.*, 2022). The abundant mineral quartz (SiO_2) is a particularly useful target to produce ^{10}Be and ^{26}Al. In an early experiment with AMS measurements of ^{10}Be and ^{26}Al in quartz, the production rate for these radioisotopes was determined from glacially polished rocks of a known age (Nishiizumi, Kohl, Arnold *et al.*, 1991).

As a result of differing approaches to production-rate estimates, a large effort was devoted to better defining these values in a joint U.S.–European Union program known as CRONUS. This effort involved a large number of scientists from geology, geophysics, and geochemistry. A series of papers resulted (Phillips *et al.*, 2016a, 2016b) that included detailed studies at specific locations, such as the Lake Bonneville shorelines near Salt Lake City, UT (Lifton *et al.*, 2015). Several intercomparison materials were also made for distribution and cross collaboration (Blard *et al.*, 2015; Jull, Scott, and Bierman, 2015; Schaefer *et al.*, 2016). A "CRONUS calculator" originally devised by Balco *et al.* (2008) and extended by Marrero *et al.* (2016) was also revised as a result of these efforts.[4]

These improvements have been applied to a wide range of geomorphological studies, such as the incision rate of rivers (Burbank *et al.*, 1996) and the long-standing question of denudation rates in the Himalayas (Lupker *et al.*, 2012), as well as the age of moraines in glacial studies; see Sec. III.E.2 as well as Schaefer *et al.* (2009), Kelly *et al.* (2015), and Kutschera (2022). The approach has also been used in archaeological studies through the method of burial dating of sediments (Granger and Muzikar, 2001) to determine the age of the Peking man, who was mentioned in Sec. III.A.6 (Shen *et al.*, 2009). Shen *et al.* (2020) used cosmogenic nuclides to demonstrate evidence for early homonids 2.4×10^6 yr ago at the Xihoudu site in China. Similar studies helped define the first evidence of humans in Africa $(1.8 - 2.1) \times 10^6$ yr ago (Gibbon *et al.*, 2014).

2. Volcanology and sedimentology

^{10}Be is produced not only *in situ* on the surface of Earth, as described in Sec. III.F.1, but also in the atmosphere (see Fig. 2), where it is called meteoric ^{10}Be and also used for investigations in the lithosphere. One such investigation dealt with the question of subduction in island-arc volcanos (Brown *et al.*, 1982). An intensive study of meteoric ^{10}Be in a 500 000-year-old core from the large loess plateau of China has been used as a proxy for rainfall, and thus has revealed details about the history of East Asian monsoon events (Beck *et al.*, 2018). The same group also used ^{10}Be to look at geomagnetic effects beyond the Brunhes-Matuyama geomagnetic reversal, which should produce the large peak expected when Earth's magnetic field collapses and reverses. There is an offset in the ^{10}Be record relative to the magnetic record in the loess due to later "overprinting" of the geomagnetic signal in the sediment (Zhou *et al.*, 2014).

G. Anthropogenic radionuclides

Anthropogenic radionuclides, like ^{236}U and ^{239,240}Pu as well as longer-lived fission products (such as ^{129}I, ^{99}Tc, and ^{135,137}Cs), have been omnipresent in the environment since humankind started nuclear activity. These nuclides have been locally distributed but have also spread across the globe as

[4]See http://hess.ess.washington.edu.

fallout from the atmospheric weapons tests during the 1950s and 1960s (see also the discussion of the ^{14}C bomb peak in Sec. III.B.2), from releases from nuclear reprocessing facilities (Sellafield and Cap de la Hague), and via reactor accidents (Chernobyl and Fukushima) and other nuclear incidents. Depending on their source, the actinide isotope ratios as well as their absolute atom concentrations can be used as sensitive fingerprints in various applications. Owing to their isobar-free detection, AMS of Pu was suggested already in the early days of AMS (Litherland, 1980), but AMS measurements of actinides, and of ^{236}U and plutonium isotopes, in particular, were pioneered at the IsoTrace facility (Zhao, Nadeau, Garwan *et al.*, 1994; Zhao, Nadeau, Kilius, and Litherland, 1994) and later further developed by Fifield *et al.* (1996), Fifield (1999, 2008), and Fifield, Synal, and Suter (2004) at ANU. Other mass-spectrometric methods such as inductively coupled plasma mass spectrometry (ICPMS) and TIMS have also used been used for Pu measurements for many years (Ketterer and Szechenyi, 2008), but AMS provides the highest abundance sensitivity [note also that RIMS claims a high detection efficiency (Trappitsch *et al.*, 2019) but thus far has not shown this for routine measurements].

Recent major advances of AMS in detection sensitivity (Vockenhuber *et al.*, 2013; Hotchkis *et al.*, 2019) and measurement background (Chamizo *et al.*, 2022; Hain *et al.*, 2022) have opened new possibilities for the analysis of a number of long-lived radionuclides; see also Sec. IV.B for a discussion of the recent detection of interstellar ^{244}Pu. This has led to a boost in new applications in recent years. For example, actinides (^{231}Pa, ^{233,236}U, ^{237}Np, and Pu) and fission products (^{90}Sr, ^{99}Tc, ^{129}I, and ^{135,137}Cs) were measured by AMS as (1) tracers in oceanography (Casacuberta *et al.*, 2014; Chamizo *et al.*, 2022; Hain *et al.*, 2022), (2) tracers in soil erosion and sediment movement studies (Lal *et al.*, 2017; Froehlich *et al.*, 2019), (3) tracers in environmental monitoring programs (for instance, for tracing discharges from plutonium-processing and fuel reprocessing plants, and also for tracing leaking nuclear reactors and to ensure that radioactive waste is not migrating from safe storage facilities) (Christl, Casacuberta *et al.*, 2015; Tims *et al.*, 2016; Medley *et al.*, 2019), (4) nuclear forensic studies to identify the source of nuclear material (Lachner *et al.*, 2015), (5) health physics studies to estimate human exposure to radioactivity, and (6) uranium exploration to find new ore deposits.

More information on recent research programs with a focus on actinides was gathered at the following facilities: ETH Zurich (Vockenhuber *et al.*, 2013; Christl *et al.*, 2014, 2015; Christl, Casacuberta *et al.*, 2015); VERA at the University of Vienna (Steier *et al.*, 2008; Sakaguchi *et al.*, 2014; Lachner *et al.*, 2015; Hain *et al.*, 2020, 2022); Centro Nacional de Aceleradores (CAN), Seville (Chamizo *et al.*, 2022); Australian Nuclear Science and Technology Organisation (ANSTO), Sydney (Child and Hotchkis, 2013; Hotchkis *et al.*, 2019); ANU (Canberra) (Everett *et al.*, 2008; Fifield, 2008; Fifield *et al.*, 2010; Tims *et al.*, 2016; Lal *et al.*, 2017; Froehlich *et al.*, 2019); LLNL, Livermore (Brown *et al.*, 2004); and the Lalonde Laboratory, Ottawa (formerly IsoTrace, Toronto) (Cornett *et al.*, 2015).

IV. NUCLEAR PHYSICS AND ASTROPHYSICS

A. Nuclear physics

Modern accelerator mass spectrometry is a technique that was conceived by nuclear physicists and was born in nuclear physics laboratories (Bennett *et al.*, 1977; Muller, 1977; Nelson, Korteling, and Stott, 1977). As previously noted, the first experiment using an accelerator as a spectrometer was that of Alvarez and Cornog (1939a), who discovered ^{3}He as a stable isotope in natural helium (atmospheric and well helium). It is only natural that, together with the conceptual development of dating by atom counting, which captured the mind of these physicists, research soon bifurcated back to nuclear physics. The unique sensitivity and discrimination power of AMS and the counting of unambiguously identified single ions open the road to the search for rare species or processes and for the counting of specific reaction products often hard or impossible to detect otherwise. The leading principle here is the same that drove the interest to dating, namely, the far more efficient counting of atoms than counting of decays when the half-life is long relative to a measurement time. The small mass required for a sample is another major consideration. We devote this section to research in various subfields of nuclear physics, where AMS has made a contribution. We first review the determinations of half-lives of long-lived radionuclides, and the search of superheavy elements in nature. After a short background in nuclear astrophysics, we review the measurements of reaction cross sections that are of interest in nuclear astrophysics (Sec. IV.B). The large expansion of AMS toward nuclear astrophysics that started in the late 1990s now provides a technique that is well accepted in this field and in fact follows the development and vibrant activity in nuclear astrophysics in recent years.

1. Half-life of long-lived radionuclides

The basis for measuring half-lives is the radioactive decay law

$$dN_t/dt = -\lambda N_t \rightarrow N_t = N_0 e^{-\lambda t}, \tag{2}$$

where N_t is the number of radioactive atoms at time t, dN_t/dt is the decay rate at time t, N_0 is the initial number of radioactive atoms at time 0, and λ is the decay constant related to the half-life $t_{1/2}$ through $\lambda = \ln 2/t_{1/2}$. While short half-lives can be determined from the exponential decay curve, for long half-lives both dN_t/dt and N_t must be measured. For long half-lives a sufficient number of radioactive atoms N_t is required to allow a precise measurement of the decay rate. But this is often difficult to achieve.

Although the half-life of ^{14}C is now well established as 5700 ± 30 yr (Kutschera, 2013), it has always been difficult to explain why it is so long (Brookhaven National Laboratory Nuclear Data Center, 2018; Kutschera, 2019). The decay of ^{14}C to ^{14}N is a so-called Gamow-Teller β transition (Gamow and Teller, 1936), and with a normal transition strength the half-life would be only a few days. The extraordinary hindrance apparently comes from subtle details in the

structure of the nuclear states of ^{14}C and ^{14}N mediating the β transition (Maris *et al.*, 2011). The long half-life may thus be called a gift of nature to archaeology.

One of the earliest uses of AMS was the half-life measurement of the cosmogenic radionuclide ^{32}Si. In this case, N_t was determined through ^{32}Si/^{28}Si ratio measurements in artificially produced ^{32}Si material (Elmore, Anantaraman *et al.*, 1980; Kutschera *et al.*, 1980). These measurements resulted in a considerably shorter half-life than determined from geophysical measurements (DeMaster, 1980). Several more half-life measurements followed; they are summarized in Fig. 35 (Fifield and Morgenstern, 2009). Since most of the individual measurements disagree outside their respective uncertainties, a reliable half-life value of ^{32}Si has yet to be established. A new approach was initiated with the SINCHRON project, which utilized a large amount of ^{32}Si (some 10^{16} atoms) that had been produced and extracted from proton-irradiated disks at the Paul Scherrer Institute (Veicht *et al.*, 2021); an effort to redetermine the half-life is under way (Schlomberg *et al.*, 2022). The relatively short half-life of ^{32}Si makes it useful for dating recent glacier ice through AMS measurement of cosmogenic ^{32}Si deposited with snow precipitation (Morgenstern *et al.*, 2010).

The half-lives of several radionuclides that are used in AMS applications have recently been remeasured. These include ^{10}Be, $t_{1/2} = (1.387 \pm 0.012) \times 10^6$ yr, which is the weighted mean used by Chmeleff *et al.* (2010) and Korschinek *et al.* (2010); ^{41}Ca, $(9.94 \pm 0.15) \times 10^4$ yr (Jörg *et al.*, 2012); ^{44}Ti, 58.9 ± 0.3 yr (Ahmad *et al.*, 2006); ^{60}Fe, $(2.61 \pm 0.04) \times 10^6$ yr (Rugel *et al.*, 2009; Wallner, Bichler *et al.*, 2015); ^{129}I, $(16.4 \pm 0.12) \times 10^6$ yr (García-Toraño *et al.*, 2018); and ^{182}Hf, $(8.90 \pm 0.09) \times 10^6$ yr (Vockenhuber *et al.*, 2004). Among these, ^{60}Fe became of particular interest since an excess of this radionuclide found in deep-sea manganese crusts indicated an extraterrestrial origin, possibly from a supernova a few million years ago (Knie *et al.*, 1999, 2004; Wallner *et al.*, 2016a, 2021); see Sec. IV.B.3.

Half-life values are a fundamental nuclear physics quantity for dating applications where the decay in combination with its half-life value is used (note that the situation is different for ^{14}C, where an absolute time calibration independent of the half-life value has been established). The half-life is often also directly related to the isotope ratio of AMS standards, because the absolute number of the radionuclide in a sample can be deduced from its activity and the half-life value. Proper AMS standards are then diluted down to smaller AMS concentrations. New state-of-the-art AMS systems can produce highly precise data; for instance, ^{10}Be/^{9}Be ratios can be measured to better than 1%. But some ^{10}Be standards were found to differ by more than 13%. Therefore, the standards and, consequently, half-life values also need to be accurately known. In recent years it has become an important premise to have a reliable and well-known standard material or to arrive at a consensus value that suffices for the needs of the AMS community. For example, the most recent ^{10}Be half-life measurements were based on precise elastic recoil detection (Korschinek *et al.*, 2010) and ICPMS measurements (Chmeleff *et al.*, 2010) and agreed to better than 1% with each other.

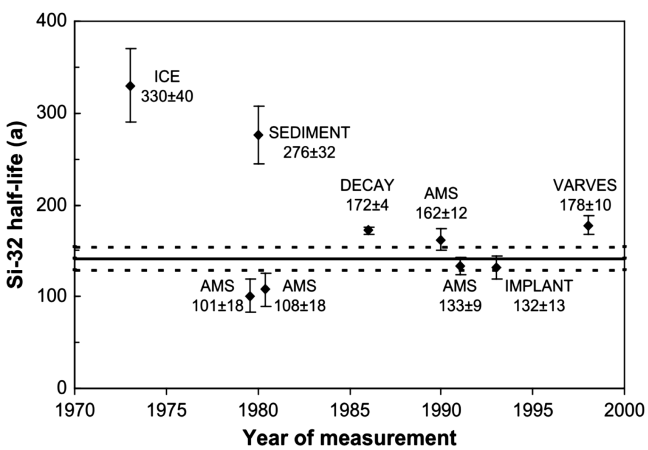

FIG. 35. Chronology of ^{32}Si half-life measurements. The solid line represents a mean value of 144 yr, with the calculations not including the ice and sediment values. The dashed line indicates a 1σ uncertainty of ± 11 yr. Adapted from Fifield and Morgenstern, 2009.

2. Search for superheavy nuclei by AMS

The search for new elements (natural or artificially produced) has been a driving force in chemistry and physics; see Fig. 36 for the current periodic table of elements. The first (and the lightest) element artificially produced whose isotopes are all radioactive was technetium ($Z = 43$), which was positively identified by Perrier and Segrè (1937, 1947). Element 43 (Tc) was produced at the Berkeley cyclotron by bombarding molybdenum with deuterons, a technique that successively led to the discovery in the following years of the heavier elements beyond naturally occurring thorium and uranium in the actinide series; see Seaborg (1968, 1995) for examinations of the production of transuranic elements using different methods.

The possible existence of an "island of stability" for still heavier nuclides possibly around $Z = 114$ (Nilsson, Thompson, and Tsang, 1969) was suggested and the term superheavy nuclei adopted in the late 1950s (Werner and Wheeler, 1958). The theoretical reasoning behind these ideas was connected to the study of the fission barrier of heavy nuclides (Swiatecki, 1956; Myers and Swiatecki, 1966; Nix, 1972) and an extension of "magic nuclei" in the frame of the shell model (Meldner, 1966, 1969). The artificial production of superheavy nuclei by a bombardment of actinides, notably with the lighter projectile ^{48}Ca (Oganessian *et al.*, 2012) at the Flerov Laboratory of Nuclear Reactions (Dubna), continues to be intensely pursued. The effort led to the identification of short-lived nuclides up to $Z = 118$ (noble-gas element oganesson) that decay by alpha emission and spontaneous fission; see Giuliani *et al.* (2019) for a review. The search for long-lived superheavy elements, possibly present in nature, started shortly after the hypothesis of an island of stability was suggested. This species could be produced using the rapid (r) neutron-capture process, as is the case in our present understanding of naturally occurring thorium and uranium; limitations to how heavy this process could be were, however, formulated (Viola, 1969). Early broad-range searches for superheavy elements were made in ores and natural materials

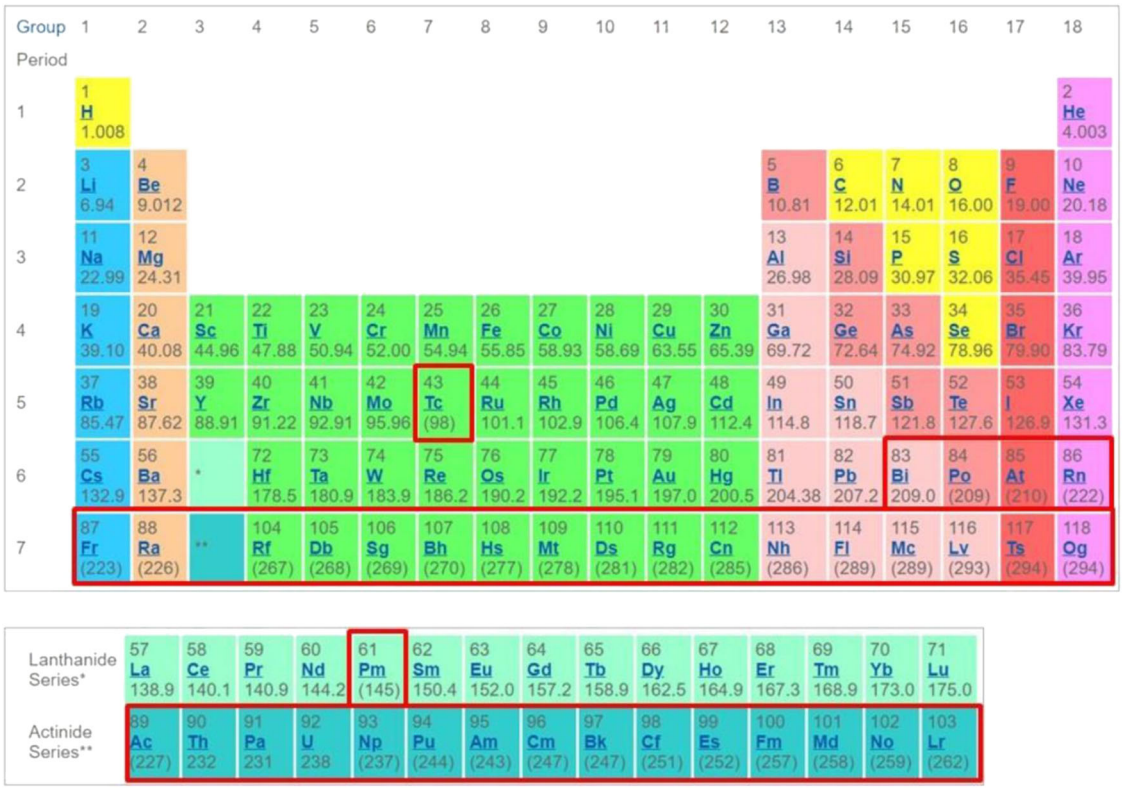

FIG. 36. The periodic table of elements as established recently following the confirmation of discovery of elements up to the noble-gas oganesson ($Z = 118$) and of their names and symbols adopted by the International Union of Pure and Applied Chemistry. The bold red frames denote elements with no stable isotopes and their longest lived isotope (in parentheses). Adapted from Los Alamos National Laboratory, 2017.

via dielectric track detectors (fission tracks) by Flerov, Druin, and Pleve (1970) or neutron counting from spontaneous fission (Grimm, Herrmann, and Schüssler, 1971; Cheifetz *et al.*, 1972). To anticipate a long and interesting science venture, we state that no superheavy species have been identified or confirmed to date in terrestrial matter, including searches using AMS that we later review.

The realization of the ultrahigh sensitivity and discrimination power of AMS in 1977 led to experiments searching for traces of new species of masses in the range $A > 300$ in terrestrial matter. Schwarzschild, Thieberger, and Cumming (1977) are to our knowledge the first to report such a search in a sample of monazite, a phosphate mineral rich in rare-earth elements and thorium. The search showed no evidence for nuclides in the range $345 \leq A \leq 355$, with an abundance sensitivity of the order of 1×10^{-10}. Another early search for a long-lived $Z = 110$ nuclide was motivated by the estimate by Schramm and Fowler (1971) that a superheavy chemical homolog of platinum could be produced in a ratio 0.02:0.06 to the abundance of ^{195}Pt by multiple neutron capture. A search at the University of Pennsylvania (Stephens, Klein, and Zurmühle, 1980) set a limit of 1×10^{-11} for the abundance of a superheavy ^{294}110 nuclide in a placer of platinum with a half-life larger than $\approx 2 \times 10^{8}$ yr.

The modern era of searches for superheavy elements by AMS benefited from technical advances at the Maier-Leibnitz Laboratory [Technical University of Munich (TUM)] (Lachner *et al.*, 2008) and the VERA Laboratory of the University of Vienna (Dellinger *et al.*, 2010; Dellinger, Forstner *et al.*, 2011; Dellinger, Kutschera *et al.*, 2011).

Some of these searches were motivated in part by a series of papers by Marinov *et al.* (2007, 2009, 2010, 2011), where evidence of long-lived neutron-deficient isotopes of elements Au and Th (and long-lived ^{261,265}Rg isotopes in Au) was presented with abundances in the range $10^{-11} - 10^{-10}$, which were based on inductively coupled plasma sector field mass spectrometry measurements and interpreted as isomeric superdeformed nuclear states. These claims were not confirmed by AMS searches performed with much higher sensitivities at both the TUM and VERA laboratories; see the previous discussion. The TUM setup based on a large high-voltage 14 MeV MP tandem accelerator is illustrated in Fig. 37(a).

Negative ions analyzed by an injection magnet and an electrostatic analyzer are accelerated to a terminal voltage between 8 and 11 MV. Stripping in the high-voltage terminal by a thin C foil results in the dissociation of all molecular ions and production of positive ions distributed over a number of charge states. These ions are analyzed in atomic-mass-to-charge (A/q) ratio in the range $292 \leq A \leq 310$ using a succession of magnets and Wien velocity filters and finally identified by a time-of-flight–multiple ΔE-Si detector telescope (Ludwig *et al.*, 2012). With no finding of positive evidence, the measurements reached limits of abundance sensitivity ranging from 10^{-12} to 10^{-16}, depending on the sample used and the mass detected. Figure 37(b) shows an example of ion identification for a setting corresponding to a

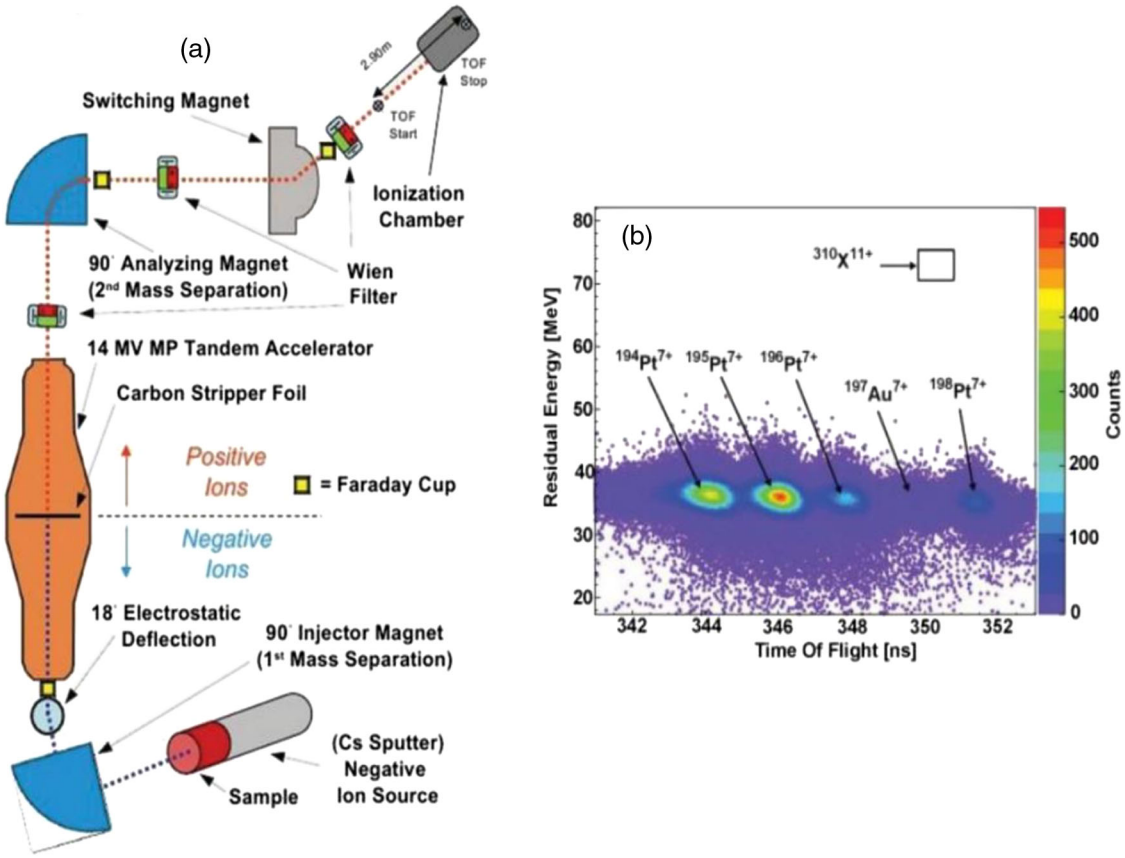

FIG. 37. (a) AMS setup used at the Maier-Leibnitz Laboratory [Technical University of Munich (TUM)] for the search for superheavy elements in natural materials. (b) Identification spectrum of ions for an accelerator setting corresponding to hypothetical $^{310}X^{11+}$ ions. The rectangular contour shows the expected location of events, based on calibration of the residual energy measured by the Si detector and the ion time of flight through the detector system shown in (a). Adapted from Ludwig *et al.*, 2012.

hypothetical $^{310}X^{11+}$ ion, illustrating the discrimination power of the setup between ions having nearby A/q values: zero counts and no background are established, corresponding to an abundance limit of 1.4×10^{-15} relative to the raw Pt material used as the sample in the ion source. Based on a lower voltage accelerator with a 3 MV terminal, and consequently different measurement systematics, experiments at the VERA Laboratory (described earlier) led to nondetection of eka-Pt, eka-Pb, and eka-Bi (Dellinger, Forstner *et al.*, 2011) isotopes, as well as to long-lived isotopes of roentgenium (Dellinger, Kutschera *et al.*, 2011) in natural gold with abundance limits in the range $10^{-13} - 10^{-16}$ relative to their respective stable chemical homologs. See the review of AMS searches for superheavy elements in terrestrial matter by Korschinek and Kutschera (2015) for further details.

B. Astrophysics

1. Background in nuclear astrophysics

Nuclear astrophysics is the microscopic constituent of astrophysics and deals with the nuclear reactions occurring at femtometric distances in the interior of objects of astronomical size. The field aims to understand the formation of the elements present in nature and their distribution across the chart of nuclides. The realization that natural elements were formed in the interior of stars dates from not earlier than 100 yr ago. Sir Arthur S. Eddington stated, in a presidential address to the Royal Society of London (Eddington, 1920) [see also Eddington (1926)], "A star is drawing on some vast reservoir of energy by means unknown to us. This reservoir can scarcely be other than the subatomic energy which, it is known, exists abundantly in all matter." He thus first identified nuclear reactions as the source of energy balancing the star's own gravity. It was then a short step forward to the concept of nucleosynthesis and to the conjecture that helium together with energy is produced out of four protons in our Sun (Eddington, 1926). The fusion of protons into helium occurred already in the primordial Universe, but nuclear astrophysics' main focus is the synthesis of heavier elements, while the former is classified as big-bang nucleosynthesis, the era predating star formation. In 1948, Alpher, Bethe, and Gamow (1948) presented a vast model of nucleosynthesis where fusion processes producing elements up to iron along a star's evolution were outlined. Neutrons were first mentioned as major players in the synthesis of heavy elements, even though the origin of neutrons was attributed to fission of shorter-lived actinides. The main origin of neutrons responsible for the nucleosynthetic processes during the nuclear burning phases of a star is now attributed to (α, n) reactions, but fission and the accompanying neutrons are now considered an important recycling path of nucleosynthesis following explosive events; see Arnould and Goriely (2020).

A culmination of decades of experimental work initiated by Clarke (1889) in the late 19th century, the review by Suess and Urey (1956) on the relative abundance of the natural elements, provided the empirical ground for nucleosynthesis models (Fig. 38).

The noteworthy works by Cameron (1957) and Burbidge, Burbidge, Fowler, and Hoyle (B2FH) (Burbidge *et al.*, 1957) followed, beginning the era of modern nuclear astrophysics. The classification of nuclides based on their nucleosynthetic production modes, the basic models, and the terminology introduced in these papers has been a part of the field since then. Without entering into the depth of the subject, which is beyond the scope of this review, one can divide the nuclear reactions that govern stellar nucleosynthesis into two broad categories of charged-particle and neutron-capture reactions. The former lead, by means of exothermic fusion of nuclei up to the region of iron, to maintaining a star in hydrodynamical equilibrium. The latter, unhindered by Coulomb repulsion, are responsible for the synthesis of the majority of heavy elements; see also the Fig. 38 caption. Explosive events (novae, supernovae, and star mergers) are the site of more exotic reactions (such as neutrino-wind driven reactions). A major impact of accelerator mass spectrometry on nuclear astrophysics was in providing measurements of cross sections of important reactions involving long-lived nuclides and in the search of fresh nucleosynthetic products deposited in minute amounts in terrestrial (and lunar) archives. We next review these recent activities. The future return to Earth and study of Solar System material collected in space missions or sampled from asteroids (Tsuda *et al.*, 2019) and Mars (Muirhead, Nicholas, and Umland, 2020) will likely further benefit from the sensitive analytical capabilities of AMS.

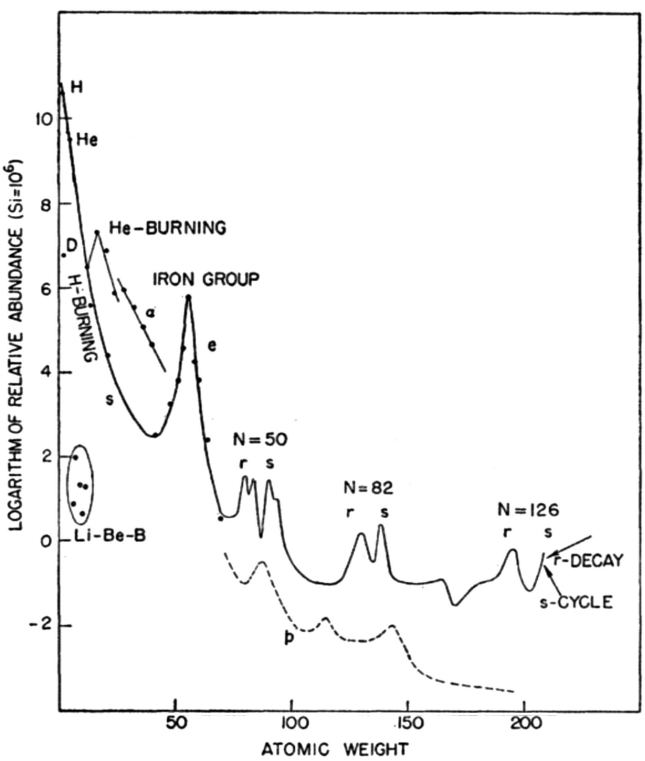

FIG. 38. Schematic curve of atomic abundances relative to that of Si as a function of atomic weight based on the data of Suess and Urey (1956), as presented by Burbidge *et al.* (1957) in the B2FH review. The curve and the B2FH review where the major nucleosynthesis processes are identified had a major impact on the development of nuclear astrophysics. Processes denoted by H–, He burning, and α refer mainly to exothermic fusion reactions up to the iron group; *s* and *r* refer, respectively, to the slow process occurring at low neutron densities in steady-state stellar conditions and rapid neutron-capture processes where extremely high neutron densities are produced in explosive stellar events. *P* refers to the rare *p*-process stable nuclides (35 in number) that are produced via nuclear reactions other than neutron capture, such as photonuclear and charged-particle reactions. Adapted from Burbidge *et al.*, 1957.

2. Reaction cross sections measured with AMS

The knowledge of nuclear reaction cross sections has always been a prime goal of experimental nuclear physics and has provided a basis for theoretical models of nuclear structure and reaction mechanisms. This information is of prime importance in nuclear astrophysics for the quantitative validation of nucleosynthesis models. These models are eventually confronted with the elemental and isotopic distribution measured in the Solar System using different analytical techniques and astronomical observations.

Nuclear cross sections are typically measured either on line using the prompt yield of the reaction products (for instance, scattered projectilelike or targetlike particles) or off line using the activation method. The latter method consists in measuring the yield of products left out in the reaction site. The classical activation method consists therefore in detecting a radioactive reaction product via its characteristic decay. Accelerator mass spectrometry had a profound impact by complementing the method by enabling atom counting of the reaction product. The ultrahigh sensitivity and discrimination power of AMS enables unambiguous identification of the product. It thus enlarged the scope of the activation method to unstable nuclides with long half-lives whose decay is practically too slow to be measurable in an experiment time or with hard-to-detect decay modes. We note here that due to the minute size of nuclear cross sections (of the order of $1\ \mathrm{b} = 10^{-24}\ \mathrm{cm}^2$, and mostly much lower) the activation method by atom counting is practical only when a reaction product does not exist as a natural stable isotope, because the reaction product would typically be overwhelmed by the presence of chemical impurities.

Wallner (2010) and, more recently, Gyürky *et al.* (2019) and Chávez *et al.* (2022) reviewed compilations of cross sections measured by AMS in different laboratories, mostly indeed related to open questions in nuclear astrophysics. To follow, we divide the reactions studied via AMS into two categories: neutron-capture reactions and reactions involving charged particles. Since AMS typically measures an isotopic ratio between a rare and an abundant isotope, the measurement of a neutron-capture reaction cross section is particularly direct, as the target and product nuclides are by definition isotopes of the same element. The cross section $\sigma_{n\gamma}$ of a target nucleus ^{A}Z is determined from the AMS-measured isotopic ratio $r = N(^{A+1}Z)/N(^{A}Z)$ by

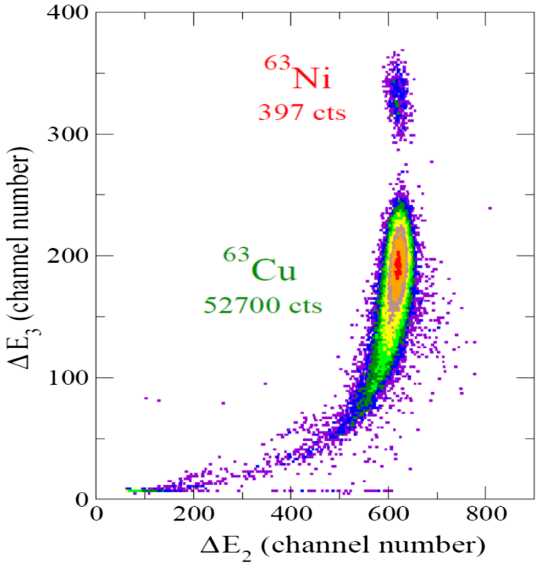

FIG. 39. AMS detection of ^{63}Ni produced by the neutron-capture reaction ^{62}Ni$(n,\gamma)^{63}$Ni. The neutron activation of an isotopically enriched ^{62}Ni target was performed at Forschungs-Zentrum Karlsruhe with a quasi-Maxwellian neutron energy distribution ($kT = 25$ keV) to study the s-process evolution in massive stars. The ^{63}Ni ions, after separation of most of the stable isobaric ^{63}Cu in a gas-filled spectrograph, are identified in the figure by the energy losses ΔE_2 and ΔE_3 measured on two successive anodes of a focal-plane ionization chamber. Adapted from Nassar *et al.*, 2005.

$$r = \sigma_{n\gamma}\Phi t, \tag{3}$$

where Φt is the time-integrated neutron flux and $\sigma_{n\gamma}$ is the capture cross section averaged over the energy distribution of the neutrons, which is rarely monoenergetic. The first reaction of this kind to be studied was the ^{62}Ni$(n,\gamma)^{63}$Ni reaction (Nassar *et al.*, 2004, 2005), leading to long-lived ^{63}Ni with a half-life of 101 yr (β^- decay and no γ rays) and thus displaying the superiority of AMS atom counting over decay counting (Fig. 39). An interesting result from the AMS-based measurement of the ^{62}Ni$(n,\gamma)^{63}$Ni reaction was the observation that this single measured cross section, notably different from that assumed thus far from theoretical calculations, impacts the evolution of elemental production throughout the entire weak s-process range as calculated using stellar evolution codes (Nassar *et al.*, 2005; Dillmann *et al.*, 2010).

The nuclear astrophysics interest in the reaction belongs to a detailed study of the slow-capture s process (Figs. 38 and 40). Roughly half of the heavy elements are made through the s process, which synthesizes them by successive neutron captures competing on timescales similar to those of β^- decay. The process brings back a newly produced radioactive nuclide toward stable nuclides and consequently evolves along or close to the valley of stability. The process occurs in two phases of stellar evolution, namely, that of relatively low-mass stars having reached the status of red giants (the main s process), providing nuclides with $90 \le A \le 209$, and in the weak s process $60 \le A \le 90$ occurring in the core of massive stars.

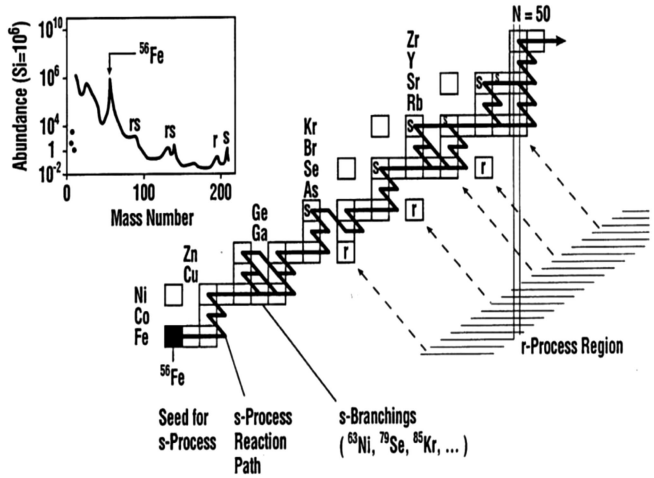

FIG. 40. Schematic representation of the s-process evolution starting from a ^{56}Fe seed preexisting in a star. The process of successive neutron captures synthesizes about half of the heavy elements in nature. Inset: reproduced distribution of natural elements shown in Fig. 38 sorted by mass number. From Käppeler *et al.*, 2011.

Charged-particle-induced reactions investigated by activation differ from neutron-induced reactions in that a different element is produced by the activation. This requires a chemical treatment involving a carrier of the new element (of natural composition or an enriched stable isotope) and usually chemical separation from the target material. The first nuclear reaction studied by activation and AMS, in the early days of AMS, was in fact a charged-particle-induced reaction, the ^{26}Mg$(p,n)^{26}$Al reaction (Paul *et al.*, 1980) (see Fig. 41),

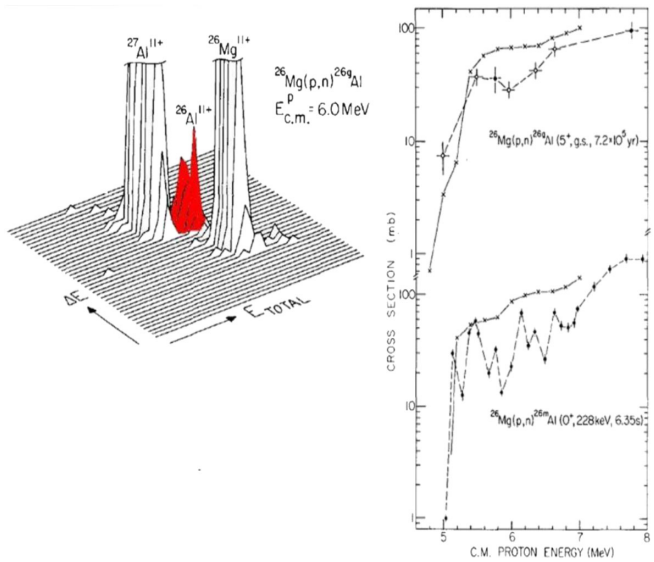

FIG. 41. Detection of ^{26}Al produced by the charged-particle reaction ^{26}Mg$(p,n)^{26g}$Al and leading to the long-lived ground state ^{26g}Al ($t_{1/2} = 7.2 \times 10^5$ yr). The reaction was studied at Argonne National Laboratory in the early years of AMS as the inverse of the destruction reaction of the important ^{26}Al radionuclide. Adapted from Paul *et al.*, 1980.

TABLE III. Measurements of nuclear reaction cross sections performed since about 2015 via activation and AMS analysis. We refer for earlier works to previous reviews and publications (Gyürky *et al.*, 2019; Chávez *et al.*, 2022). ANL, Argonne National Laboratory, USA; ANU, Australian National University, Australia; CIAE, China Institute of Atomic Energy, China; FNAL, Fermi National Accelerator Laboratory, USA; HZDR, Helmholtz-Zentrum Dresden-Rossendorf, Germany; ININ, Instituto Nacional de Investigaciones Nucleares, Mexico; IFUNAM, Instituto de Física, Universidad Nacional Autónoma de México, Mexico; KIT, Karlsruhe Institute of Technology, Germany; LEMA, Laboratorio de Espectrometría de Masas con Aceleradores; IPN, Institut de Physique Nucléaire, France; MALT, MicroAnalysis Laboratory, Tandem accelerator, Japan; ND, University of Notre Dame, USA; PRIME, Purdue Rare Isotope Measurement Laboratory, USA; RCNP, Research Center for Nuclear Physics, Osaka University, Japan; SARAF-LiLiT, Soreq Applied Research Accelerator Facility-Liquid-Lithium Target, Israel; Tohoku U, Tohoku University, Sendai, Japan; TUM, Technical University of Munich, Germany; VERA, Vienna Environmental Research Accelerator, Austria.

Reaction	Irradiation facility	Incident energy	AMS facility	Reference
^{9}Be$(n,\gamma)^{10}$Be	KIT	$kT = 25$ and 473 keV	VERA	Wallner *et al.* (2019)
^{9}Be$(n,\gamma)^{10}$Be	ININ	Thermal	LEMA	Marin-Lambarri *et al.* (2020)
^{13}C$(n,y)^{14}$C	KIT	$kT = 25$, 123 and 182 keV	VERA	Wallner *et al.* (2016b)
^{14}N$(n,p)^{14}$C	KIT	$kT = 25$, 123 and 182 keV	VERA	Wallner *et al.* (2016b)
^{28}Si$(d,\alpha)^{26}$Al	IFUNAM	3.4–4.8 MeV	LEMA	Reza *et al.* (2020)
^{33}S$(\alpha,p)^{36}$Cl	ND	3–6 MeV	ND, PRIME	Anderson *et al.* (2017)
^{34}S$(^{3}$He$,p)^{36}$Cl	ND	3.3–7.1	ND	Anderson *et al.* (2020)
^{35}Cl$(n,\gamma)^{36}$Cl	KIT, SARAF-LiLiT	$kT = 40.5$ keV	ANU, HZD, VERA	Pavetich *et al.* (2019b)
^{36,38}Ar$(n,\gamma)^{37,39}$Ar	SARAF-LiLiT	$kT = 47$ keV	ANL	Tessler *et al.* (2018)
^{54}Fe$(n,\gamma)^{55}$Fe	KIT	$kT = 25$ and 450 keV	VERA	Wallner *et al.* (2017)
^{58}Ni$(n,\gamma)^{59}$Ni	KIT	$kT = 25$ keV	TUM	Ludwig *et al.* (2017)
^{60}Ni$(n,2n)^{59}$Ni	CIAE	14 MeV	CIEA	He *et al.* (2015)
^{nat}Cu, ^{89}Y, ^{139}Tb$(p,x)^{10}$Be, ^{26}Al	FNAL, RCNP	120 GeV, 392 MeV	MALT	Sekimoto *et al.* (2015)
^{92}Zr$(n,\gamma)^{93}$Zr	SARAF-LiLiT	$kT = 40$ keV	ANU	Pavetich *et al.* (2019a, 2022)
^{93}Nb$(n,2n)^{92}$Nb	CIAE	14.6 MeV	CIAE	He *et al.* (2018)
^{147}Sm$(\gamma,n)^{146}$Sm	Tohoku U	10–50 MeV	ANL	Nusair *et al.* (2016)

which benefited from the fact that ^{26}Mg does not form stable negative ions. This reaction involved the important ^{26}Al radionuclide, which was later detected as a live radioactivity in the Galactic interstellar medium (Diehl *et al.*, 2006a, 2006b, 2021; Diehl, Martin *et al.*, 2021).

The study of the reaction was then motivated by the freshly discovered isotopic anomaly of ^{26}Mg abundance in meteoritic inclusions, which was attributed to the presence in the early Solar System of live ^{26}Al decaying *in situ* to ^{26}Mg (Lee, Papanastassiou, and Wasserburg, 1976a, 1976b). An important feature of the method is that the measurement by AMS of the isotopic ratio, for instance, in the particular case above $r_{26} = {}^{26}\mathrm{Al}/{}^{27}\mathrm{Al}$ between the reaction product (^{26}Al) and the chemical carrier (Al), allows one to determine the total number N_{26} of ^{26}Al atoms produced in the reaction. This is done via the equation $N_{26} = r_{26} \times N_{27}$, regardless of the chemical efficiency of the chemical recovery, based on the known amount of carrier ^{27}Al added.

Complementing existing reviews and compilations (Chávez *et al.*, 2022), Table III lists a number of recent measurements of cross sections by AMS, dedicated mostly to various topics of nuclear astrophysics.

3. Traces of accreted interstellar matter

a. Extraterrestrial particles

Earth is continuously bombarded by extraterrestrial matter. Approximately $30\,000 \pm 20\,000$ tons of cosmic dust reach Earth every year (Love and Brownlee, 1994), almost exclusively originating from sources within the Solar System. The majority of influx consists of small objects, such as micrometeorites with a diameter of less than a micrometer. Larger objects such as meteorites or asteroids contribute to less than 1% to the total influx; see Sec. IV.C.

Particles of extrasolar origin, i.e., originating from the interstellar medium, such as cosmic rays and interstellar dust particles, have to overcome the solar wind pressure and the magnetic field of the heliosphere in order to penetrate the Solar System (Chaikin *et al.*, 2022). The first type, Galactic cosmic-ray particles, is predominantly responsible for the production of cosmogenic nuclides both in space (meteorites, lunar surface, etc.) and on Earth. Only a small fraction, though, will survive and arrive at Earth's surface. Single atoms from interstellar space (in contrast to the highly energetic cosmic rays) are deflected away from the Solar System by the magnetic field of the heliosphere.

Interstellar dust particles are the second type of interstellar traces. The space missions of *Ulysses*, *Galileo*, and *Cassini* have observed such dust particles at orbits between 0.4 and 5 astronomical units (AU) with average diameters of 0.5 to 0.6 μm (Altobelli *et al.*, 2016). These particles were identified through their characteristic high velocities (above the escape velocity of the Solar System) and peculiar trajectories. Interstellar dust can therefore also be found in Earth's orbit.

A characteristic feature for identifying an interstellar origin for dust particles is the presence of some longer-lived radionuclides. If attached to cosmic dust particles, such nuclides may be able to enter the Solar System and can become deposited on lunar or planetary surfaces, or they may become incorporated into terrestrial archives.

b. Radionuclides as cosmic radioactive clocks

Nucleosynthesis in stars generates fresh nuclides that enrich the interstellar medium through stellar winds and stellar explosions. This includes stable nuclides and radionuclides. The presence of long-lived radionuclides contains time information as they decay and act as radioactive clocks. Prominent examples of such radionuclides with half-lives of the order of a million years are ^{26}Al and ^{60}Fe. Both nuclides are present in the interstellar medium and were observed by satellites through their characteristic γ rays associated with their decay. In addition, the early Solar System contained a number of radionuclides (here called short-lived radionuclides since their lifetimes are short compared to the age of the Solar System). Their presence at the birth of the Solar System was deduced from overabundances of their stable decay products when compared to the average terrestrial abundance ratios. Examples include the radionuclides ^{26}Al, ^{36}Cl, ^{41}Ca, ^{53}Mn, ^{60}Fe, and ^{182}Hf, as well as the actinides ^{244}Pu and ^{247}Cm; see Huss *et al.* (2009), Lugaro *et al.* (2014), and Coté *et al.* (2021).

c. Primordial radionuclides

Radionuclides with half-lives longer than 10^8 yr can still be naturally present today. A significant fraction has survived decay since the Solar System formed some 4.6 Gyr ago; these are the so-called primordial radionuclides: examples are ^{235}U and ^{238}U, ^{232}Th, and also ^{40}K with half-lives between 0.704 and 14 Gyr (10^9 yr). An interesting candidate is ^{244}Pu with a half-life of $(81.3 \pm 0.3) \times 10^6$ yr (Nesaraja, 2017). Decay would have reduced its original abundance by ~17 orders of magnitude. Hoffman *et al.* (1971) searched for the presence of primordial ^{244}Pu in a terrestrial mineral (Precambrian bastnaesite), which could potentially have enriched the Pu concentration by several orders of magnitude compared to its average terrestrial value today. Using thermal ionization mass spectrometry, they found an indication of ^{244}Pu's present existence in nature with 242 ^{244}Pu atoms identified corresponding to a concentration of 1.0×10^{-18} g ^{244}Pu/g. Note also the upper limit set by Fields *et al.* (1966) of the average terrestrial ^{244}Pu concentration of 3×10^{-22} g ^{244}Pu/g. Some 30 years later, the Munich AMS group repeated this measurement, however, applying AMS, and thus with the advantage of suppressing any molecular interference. In contrast to Hoffman *et al.* (1971), they did not observe any ^{244}Pu, which relates to an upper limit for the abundance of ^{244}Pu in their bastnaesite sample of 1.5×10^{-19} g ^{244}Pu/g (Lachner *et al.*, 2012) Recently another measurement at ETH Zurich, taking advantage of the significantly improved overall detection efficiency of actinides (Wu *et al.*, 2022), also did not find any indication for primordial ^{244}Pu, confirming the upper limit given by Lachner *et al.* (2012). Thus, the direct detection of primordial ^{244}Pu on Earth remains an open issue.

d. Search for interstellar signatures in terrestrial and lunar archives

The interstellar medium (ISM) continuously receives injections of freshly produced nuclides from dying stars and, consequently, the interplay of production and decay will alter the concentrations of radionuclides over time and space. The Solar System is ploughing through the ISM and may collect such particles.

Dedicated searches for interstellar radionuclides were conducted on lunar material (for instance, the Apollo 11 bulk sample material) by Fields *et al.* (1970) using mass spectrometry. They searched for the possible presence of ^{244}Pu or ^{247}Cm (half-life $= 1.57 \times 10^7$ yr). Both nuclides would be extinct or nearly extinct as primordial nuclides (see previous discussion), but if present they could act as indicators of "an infusion from a supernova that occurred quite close to the Solar System within the last billion years." They used a special mass spectrometer that could determine neighboring isotopes of widely disparate abundances. Finding no indication of these actinides, they concluded that the absence of ^{244}Pu and ^{247}Cm in lunar material precludes nearby supernova explosions within the last eon or two. However, this conclusion is valid only if the heavy *r*-process nuclides (including all actinides) are produced mainly by supernovae. This assumption was valid at that time, but more recent research (Cowan *et al.*, 2021) favors compact-object mergers such as neutron-star mergers) as a dominant source for the heavy *r*-process nucleosynthesis (see later discussion).

Alvarez *et al.* (1980) conducted a similar search for supernova-produced ^{244}Pu, but on terrestrial material, about 10 yr after the first measurements on lunar samples. In their paper, they demonstrated an extraterrestrial cause for the Cretaceous-Paleogen (K-Pg) (previously called Cretaceous-Tertiary) mass extinction 6.6×10^7 yr ago by measuring an enhanced concentration of Ir- and Pt-group elements in the material from the K-Pg boundary layer. Besides other convincing arguments for an asteroid impact, they also tested the hypothesis that the K-Pg extinction could have been the result of a nearby supernova, although such an event (requiring an extremely short distance of ~0.1 pc for a supernova) would have been unlikely. They measured the ^{244}Pu content by neutron activation analysis and concluded, since no ^{244}Pu was detected (with a detection limit <10% compared to the expected signal when scaled with the Ir concentration in the layers associated with the K-Pg event), that the cause for the mass extinction was not due to a nearby supernova. Their conclusion again relied on the assumption that actinides are produced in supernovae.

Soon after the advent of AMS, its potential for identifying spurious traces of extraterrestrial radionuclides was recognized. For example, right after the work by Alvarez *et al.* (1980) (see previous discussion), Litherland *et al.* (1981) pointed out that the detection of ^{244}Pu or ^{129}I at the K-Pg boundary could help to distinguish between the asteroid theory and the supernova theory for the mass extinctions. AMS would now offer a sensitivity for ^{244}Pu detection much greater than any other previous technique. However, this project was not continued during the early days of AMS, because the many other new developments changed priorities (Litherland, 2021). Therefore, it took another 15 yr until the detection of live interstellar radionuclides continued with a successful revival this time with AMS.

Ellis, Fields, and Schramm (1996) suggested searching for a number of radionuclides in terrestrial archives where isotope anomalies could signify a recent nearby supernova explosion, i.e., for the past few half-lives of a specific radionuclide. Their work was inspired by the Alvarez search (Alvarez *et al.*, 1980) and by the AMS discovery of ^{10}Be isotope anomalies about 3.5×10^4 and 6×10^4 yr ago in ice cores (Raisbeck *et al.*, 1987, 1992; Beer *et al.*, 1992) and deep-sea sediments (McHargue, Damon, and Donahue, 1995). The ^{10}Be data had triggered discussions that one or more nearby supernova explosions could be the cause for these anomalies (Raisbeck *et al.*, 1992).

A number of radionuclides were proposed by Ellis, Fields, and Schramm (1996) as potential candidates that may reflect nearby supernova explosions by isotope anomalies in the terrestrial geological record, either through their direct deposition or indirectly by leading to an enhanced cosmic-ray production in Earth's atmosphere, such as ^{10}Be. Independent of Ellis, Fields, and Schramm (1996), at the same time the Munich group also suggested utilizing ^{60}Fe as an indicator of nearby supernovae (Korschinek *et al.*, 1996).

The most promising nuclides as direct messengers from the interstellar medium turned out to be ^{26}Al, ^{53}Mn, ^{60}Fe, and ^{244}Pu. This is for two reasons: First, AMS can measure them with high sensitivity or as nearly background free. Second, the nuclides ^{60}Fe and ^{244}Pu do not exist naturally on Earth (except for the recent production of ^{244}Pu during atmospheric nuclear weapons tests), thus any signal in the terrestrial record points to extraterrestrial sources. Other isotopes of considerable interest are ^{129}I, ^{182}Hf, and ^{247}Cm, but these still suffer from interference from anthropogenic background or require measurement or chemical separation developments. Finally, enhancements in ^{10}Be or ^{14}C are not of unique origin and it is difficult to directly associate them with a supernova (SN). Recently a number of short-term variations in the ^{14}C tree-ring record were detected (Miyake *et al.*, 2012, 2021; Miyake, Masuda, and Nakamura, 2013), sometimes accompanied with measurable ^{10}Be and ^{36}Cl excursions in ice cores (Paleari *et al.*, 2022). These enhancements, however, are the results of solar energetic particle events; see Sec. III.C.5.

The expected range of deposition rates of these extraterrestrial radionuclides into geological archives is from a few atoms to 10 000 atoms/cm^2 1000 yr. Presently only AMS is sensitive enough to detect such minute signatures. In particular, recent developments in actinide detection provided a significant boost in the search for interstellar ^{244}Pu; see later discussion. Other techniques have since also demonstrated similar high selectivity, for instance, for Pu detection such as RIMS, but have not yet been applied to real samples (Trappitsch *et al.*, 2019).

e. Cases of ^{60}Fe *and* ^{244}Pu *near supernova activity and heavy element nucleosynthesis*

In the following, the two nuclides ^{60}Fe and ^{244}Pu are discussed in more detail. For both no significant natural terrestrial abundance is observed; therefore, the presence of ^{60}Fe and ^{244}Pu in terrestrial archives points to its extraterrestrial origin. These two nuclides are of particular interest for the following reasons.

- ^{60}Fe [$t_{1/2} = 2.60 \times 10^6$ yr (Rugel *et al.*, 2009; Wallner, Bichler *et al.*, 2015)] is predominately produced in massive stars and ejected in supernovae. Thus, the presence of this radionuclide is a strong indicator of nearby supernova explosions within the last few million years (within several lifetimes of ^{60}Fe).
- ^{244}Pu (8.1×10^7 yr) is an actinide and is therefore exclusively produced in the *r* process. The *r* process, i.e., the rapid neutron-capture process, is responsible for the production of half of the heavier elements above Fe and requires explosive stellar environments. The sites and frequency of this process is still under debate, with some types of supernovae and neutron-star mergers being the most promising candidates. The presence of ^{244}Pu in the interstellar medium or upper limits on its flux to Earth will provide important experimental information on nucleosynthesis of the heavier elements. With its much longer half-life compared to ^{60}Fe, ^{244}Pu could originate also from older *r*-process events, not limited to recent supernovae that can be tracked with the shorter-lived ^{60}Fe. ^{244}Pu may also be present in the interstellar medium in a quasi-steady-state equilibrium if it is produced frequently.

^{60}Fe turned out to be the most important indicator of recent nearby supernova activity. The isobar suppression capabilities using AMS was first demonstrated for ^{59}Ni measurements on meteorites and lunar material at the Argonne National Laboratory (Kutschera *et al.*, 1993) when high particles energies were combined with the gas-filled magnet technique (Paul *et al.*, 1989); see also Sec. II.D.3. Two AMS facilities pushed the limits further to achieve the required sensitivity for detection of interstellar ^{60}Fe: Munich, based on their large 14 MV MP tandem (Knie, Faestermann, and Korschinek, 1997), pioneered this research. Later, the AMS group at the 14 MV Pelletron tandem of ANU Canberra developed the AMS technique as well, and it remains the only such facility after TU Munich shut down its activities in 2020. The AMS group at ANU reported for ^{60}Fe a measurement background of ^{60}Fe/Fe as low as 3×10^{-17} (Wallner *et al.*, 2021), which is equivalent to one identified background event over ~1 d of measurement.

Interstellar ^{60}Fe was found in terrestrial archives such as deep-sea sediments (Fitoussi *et al.*, 2008), FeMn crusts, and nodules. This nuclide was also detected in Antarctic snow (Koll, Korschinek *et al.*, 2019) in addition to lunar soil

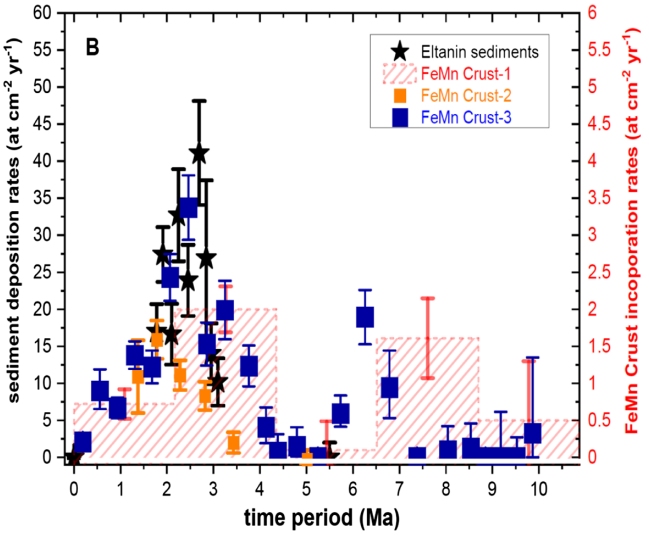

FIG. 42. Summary of ^{60}Fe measurements in different archives. Adapted from Wallner *et al.*, 2021.

samples (Fimiani *et al.*, 2016). Interstellar ^{60}Fe was found in a biogenic reservoir (fossilized magnetotactic bacteria in deep-sea sediments) (Ludwig *et al.*, 2016). All used AMS for these measurements. Independently ^{60}Fe was identified in Galactic cosmic rays (Binns *et al.*, 2016). None of these signals can be explained by terrestrial production or as being of Solar System origin, such as cosmogenic production in (micro)meteorites (Knie *et al.*, 2004; Wallner *et al.*, 2016a; Koll *et al.*, 2020).

Figure 42 shows an extensive set of AMS data from deep-sea sediments, crusts, and nodules as obtained from measurements at ANU (Wallner *et al.*, 2016a, 2020; 2021). ^{60}Fe was found in all major oceans demonstrating that the ^{60}Fe signal is a global signal; ^{60}Fe influx is extended in time and of interstellar origin from multiple events. Two broad signals point to long-term influxes of ^{60}Fe, possibly caused by several nearby SN explosions. Thus, Earth was exposed to SN ejecta or, alternatively, the Solar System could also have moved through clouds of ^{60}Fe-enriched dust.

Parallel to ^{60}Fe, the AMS technique for detection of interstellar ^{244}Pu was developed at the Hebrew University (Paul *et al.*, 2001) and at TU Munich (Wallner *et al.*, 2004). But detection of ^{244}Pu is even more challenging: the expected influx compared to ^{60}Fe would be some 3 to 5 orders of magnitudes lower (if supernovae produce actinides at all). The presence of older ^{244}Pu in the interstellar medium might add a small additional contribution to the signal.

Despite the low influx values, the extraordinary improvement in AMS detection efficiency for actinides by some 4 orders of magnitudes over the past 20 yr now makes such measurements feasible. This improvement is mainly based on the high charge-state yields using He as a gas stripper and providing essentially 100% ion transmission in compact AMS systems (Vockenhuber *et al.*, 2013). For example, the VEGA facility at ANSTO now quotes an overall detection efficiency for Pu of >1% (Hotchkis *et al.*, 2019). For comparison, this is also 2 orders of magnitude higher than the present detection efficiency for ^{60}Fe using high-voltage and more complex accelerators.

Owing to this major improvement in detection efficiency, a clear signal of ^{244}Pu well above anthropogenic production was recently found (Wallner *et al.*, 2015, 2021). This first time detection of interstellar ^{244}Pu in terrestrial samples is consistent with previous measurements that provided only upper limits. The ^{244}Pu influx seems to correlate with the ^{60}Fe data with an approximately constant ^{244}Pu/^{60}Fe ratio of $(3\text{–}5) \times 10^{-5}$ despite a low time resolution of the ^{244}Pu measurements. More ^{244}Pu measurements with a better time resolution are necessary to better understand the apparently concomitant influx of ^{60}Fe and ^{244}Pu.

The Pu data suggest that regular core-collapse supernovae are not the dominant producers of heavy *r*-process nuclides for the past few hundred million years. These data are consistent with a predominant contribution of compact-object mergers that is 100 to 1000 times less frequent than core-collapse supernovae. Nevertheless, supernovae might contribute to some extent as a minor but frequent source to the total *r*-process content of the Galaxy.

Detection for potential interstellar candidates other than ^{60}Fe and ^{244}Pu remains more difficult. ^{26}Al ($t_{1/2} = 7.18 \times 10^5$ yr) and ^{53}Mn ($t_{1/2} = 3.7 \times 10^6$ yr) were searched for in terrestrial archives. However, neither nuclide is rare on Earth. They are continuously produced naturally via cosmogenic production both directly on Earth (^{26}Al and ^{53}Mn) and, in the case of ^{53}Mn, by cosmic-ray-induced spallation reactions in planetary objects, which becomes part of the cosmic dust that is collected by Earth. Consequently, any interstellar ^{26}Al or ^{53}Mn signature must be identified on top of this "naturally existing" ^{26}Al or ^{53}Mn signal.

Interstellar ^{53}Mn is overwhelmingly produced by supernovae. By combining the ^{53}Mn data obtained from four deep-sea ferromanganese crusts, Korschinek *et al.* (2020) presented an overabundance of ^{53}Mn over that expected from cosmogenic production. Despite the difficulty in such measurements, these data are in agreement with some nucleosynthesis models. Feige *et al.* (2018) searched for the presence of interstellar ^{26}Al in deep-sea sediment samples that covered the same time period between 1.7×10^6 and 3.2×10^6 yr that showed an enhanced ^{60}Fe influx. However, no significant ^{26}Al above a dominating terrestrial signal was found. The interstellar influx limit for ^{26}Al deduced from these data is consistent with the observed ^{60}Fe-^{26}Al isotope ratios in the interstellar medium (the measured γ-ray flux ratio) and nucleosynthesis models (Diehl *et al.*, 2021, 2022).

Recent technological developments in isobar suppression might also open up new possibilities for the search of additional interstellar radionuclides. In particular, new approaches based on laser-induced selective photodetachment within an ion cooler (see Sec. II.D.3) seem promising for the near future. Detection of ^{182}Hf (Vockenhuber, Feldstein *et al.*, 2004; Forstner *et al.*, 2011; Martschini *et al.*, 2020) seems to be feasible in the near future. This nuclide ($t_{1/2} = 8.9 \times 10^6$ yr) is of particular interest for nuclear astrophysics, as it can be produced in both *s* and *r*-process nucleosynthesis. In addition, other nuclides like those identified by Ellis, Fields, and Schramm (1996) such as ^{107}Pd or

so-called *p*-process nuclides might be in reach in the near future with this new technique.

C. Extraterrestrial matter

1. Meteorites

Meteorites are messengers from the Solar System that carry information in the form of a variety of long-lived radioisotopes (including ^{14}C, ^{26}Al, ^{36}Cl, ^{41}Ca, ^{59}Ni, and ^{81}Kr) that are built up by the interaction of cosmic rays with the meteorite (Masarik and Reedy, 1994; Michel, 1999). Meteorites are derived from larger asteroids, and the collision times in space mean that the exposure times of a meteorite are typically $(5-50)\times 10^6$ yr (Eugster *et al.*, 2006). Since the exposure time in space is usually much longer than the half-lives of the respective radioisotopes, they are in secular equilibrium when a meteorite collides with Earth. Antarctic ice fields and hot desert environments are particularly fertile areas to preserve meteorites when they arrive on Earth. Among the previously mentioned radioisotopes, AMS measurements of ^{36}Cl [$t_{1/2} = (301\pm 2)\times 10^3$ yr] turned out to be best suited to determine terrestrial ages of Antarctic meteorites >25 000 yr and ^{14}C ($t_{1/2} = 5700$ yr) for $<2.5\times 10^4$ yr, with some measurements also made by ^{81}Kr (Herzog, Caffee, and Jull, 2015). Meteorites with terrestrial ages as long as 2.35×10^6 yr have been recovered (Welten *et al.*, 1997). The distribution of terrestrial ages also allows one to study glaciological aspects such as ice flow and geomorphology of Antarctic mountains (Folco *et al.*, 2006). Measurements of terrestrial ages of many meteorites have been determined by ^{14}C, ^{36}Cl, and ^{41}Ca dating (Eugster *et al.*, 2006; Jull, 2006; Welten *et al.*, 2006) The distribution of meteorites in desert environments can be affected by local geological conditions in arid environments, particularly the southwestern U.S. (Jull *et al.*, 1993; Jull, 2006), Western Australia (Jull *et al.*, 2010), the Atacama Desert (Drouard *et al.*, 2019), North Africa (Aboulahris *et al.*, 2019), and the Arabian Peninsula (Al-Kathiri *et al.*, 2005).

An interesting application of terrestrial ages of Antarctic meteorites was the determination of the ^{41}Ca half-life relative to that of ^{36}Cl measured in the same meteoritic sample material (Klein *et al.*, 1991). Figure 43 shows the result of this measurement $t_{1/2} = (103\pm 7)\times 10^3$ yr, which is consistent with that from a specific ^{41}Ca activity measurement of Paul, Ahmad, and Kutschera (1991) $t_{1/2} = (101\pm 10)\times 10^3$ yr, as well as the high-precision measurement of Jörg *et al.* (2012) $t_{1/2} = (99.4\pm 1.5)\times 10^3$ yr.

Meteorites also carry information of the early Solar System (ESS) through stable isotopic anomalies produced by the *in situ* decay of radioisotopes with half-lives much shorter than the Solar System ($\sim 4.6\times 10^9$ yr). The first evidence of live ^{26}Al being present in the ESS was the measurement of ^{26}Mg isotopic excess in the Allende meteorite (Lee, Papanastassiou, and Wasserburg, 1976a). Later the isotopic excess effects of a variety of other extinct radioisotopes were discovered, opening interesting views on nucleosynthesis in stars close to the formation of the Solar System (Wasserburg *et al.*, 2006).

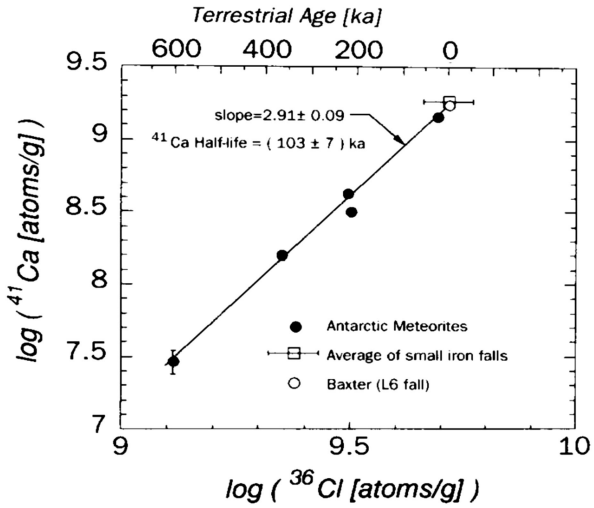

FIG. 43. Log-log plot of ^{41}Ca vs ^{36}Cl concentration measured in Antarctic meteorites of different terrestrial age. From the slope indicated and the known half-life of ^{36}Cl, a half-life of $(103\pm 7)\times 10^3$ yr was determined for ^{41}Ca. Adapted from Klein *et al.*, 1991.

2. Lunar material

The Apollo flights to the Moon between 1969 and 1972 brought back valuable material from the surface. Since the Moon has no atmosphere and no magnetic field, solar cosmic rays of low energy can reach the surface and induce nuclear reactions. The solar wind also implants nuclei in surface material. Numerous studies have been undertaken to understand the cosmic-ray exposure history of lunar soils and rocks, as recently summarized by Crawford *et al.* (2021). The high-energy cosmic rays from the Galaxy are considered to have been constant over the last few million years (Vogt, Herzog, and Reedy, 1990). However, the variability in the solar flux can be observed in the lunar record. Cosmogenic nuclides have been studied in many lunar rocks and cores [see Fink *et al.* (1998), Jull *et al.* (1998), and Nishiizumi *et al.* (2009) for summaries], and these data have been used to calculate variations in the solar and Galactic cosmic-ray record, as summarized by Jull *et al.* (2020). These records are also important for understanding the solar flare record on Earth, especially from increases in ^{14}C in terrestrial annual records such as tree rings (Miyake *et al.*, 2021). In Fig. 44, we show an example of estimates of solar proton fluxes over different times periods that gives an estimate of the maximum possible fluence limited by the lunar data (Poluianov *et al.*, 2016).

In an effort to measure the flux of solar alpha particles, AMS measurements of ^{59}Ni [$t_{1/2} = (76\pm 5)\times 10^3$ yr] produced by the reaction ^{56}Fe$(\alpha, n)^{59}$Ni in surface material from a lunar rock were performed. In this case, ATLAS was used to measure ^{59}Ni^{28+} by full stripping to separate it from the interfering stable isobar ^{59}Co^{27+} in a magnetic spectrograph (Kutschera *et al.*, 1993). In this way a specific activity of $\sim$100 dpm ^{59}Ni/kg Fe was measured, which is roughly what one expects from solar cosmic-ray alpha particle interactions.

A different use of lunar material was the measurement of stellar ^{60}Fe [$t_{1/2} = (2.61\pm 0.04)\times 10^6$ yr] accumulated in surface samples (Fimiani *et al.*, 2016), whose origin is likely

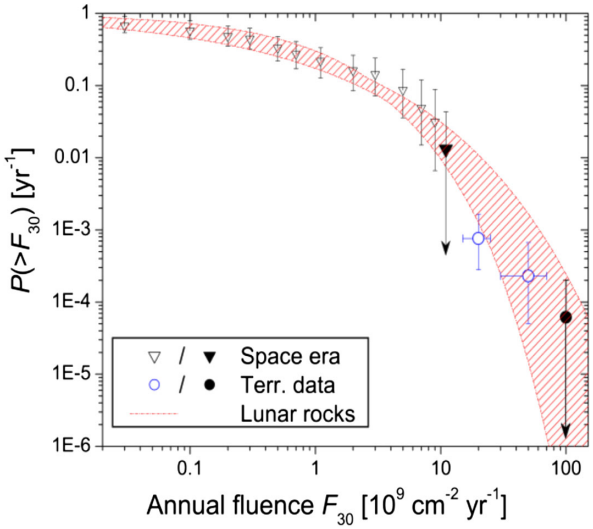

FIG. 44. Occurrence probability density function (OPDF) of solar energetic particles with the annual fluence $F > 30$ MeV exceeding the giving value. The triangles denote OPDF based on the data for the spacecraft. The circles correspond to the solar energetic particle (SEP) events derived from terrestrial cosmogenic and neutron-monitor data [modified after Usoskin *et al.* (2017)]. Open symbols indicate the measured or estimated values, whereas filled symbols indicate a conservative upper bound. Error bars bound the 68% confidence interval. The red hatched area encompasses the OPDF estimated in this work from ^{26}Al in lunar samples. Adapted from Poluianov *et al.*, 2016.

from the same nearby supernova events from several million years ago (see Fig. 42), which were detected on Earth in deep-sea manganese crusts (Wallner *et al.*, 2020, 2021).

Taricco *et al.* (2006) looked at ^{44}Ti ($t_{1/2} = 59.1 \pm 0.3$ yr) as a proxy for the variability of the cosmic-ray flux in meteorites collected over the last 235 yr and compared this to the solar-cycle record, with reasonable agreement. This study was conducted by decay counting but suggests that development of AMS measurements of other shorter-lived nuclides such as ^{32}Si ($t_{1/2} = 144 \pm 11$ yr) could be of interest in the future in a similar application.

3. Asteroid impacts

Some of the most violent events on Earth include asteroid impacts, with the most famous having been related to a mass extinction of ~70% of life on Earth 6.6×10^7 yr ago, including the demise of the dinosaurs (Alvarez *et al.*, 1980). After the Chicxulub crater in Mexico was identified as the impact crater of a giant asteroid (Schulte *et al.*, 2010), the exact date of the impact was determined with ^{40}Ar/^{39}Ar dating on tektites and bentonite associated with the impact (Renne *et al.*, 2013). The well-known Meteor Crater (Arizona) has been dated using *in situ* cosmogenic nuclides ^{10}Be and ^{26}Al to about 5×10^4 yr (Nishiizumi, Kohl, Shoemaker *et al.*, 1991).

An AMS measurement of ^{10}Be in cored material from the bottom of the lake formed at the Bosumtwi impact crater in Ghana was performed to garner details of the impact process. The inability to find ^{10}Be in the samples of suevite breccia indicated that little surface material had fallen back into the crater after the impact (Losiak *et al.*, 2013). The age of two possible impact structures in Estonia called Ilumetsa was determined from radiocarbon dating to be postglacial ~7000 yr ago (Losiak *et al.*, 2020). Recently Chen *et al.* (2021) used the radiocarbon dating of charcoal and lacustrine sediments to constrain the age of a meteorite crater in China to $\sim 4.9 \times 10^4$ yr.

Samples have been returned to Earth from Japanese space missions to the asteroids (24153) Itokawa and (162173) Ryugu. Exposure ages have been estimated from noble-gas studies (Herzog and Wieler, 2014; Meier *et al.*, 2014). Initial studies on Itokawa grains using AMS resulted in large errors (Nishiizumi, Caffee, and Welten, 2015) due to the small sample size. Samples from the Ryugu C-type asteroid are now available and will give us new information. The return of asteroidal material from a similar C-type asteroid (101995) Bennu by an American spacecraft will also add to the collection of available material.

V. CONCLUDING REMARKS

Since our material world consists of atoms, "atom sorting and counting" using AMS is one way to obtain direct information about the composition of a sample of interest. The focus of AMS is on the measurement of ultralow traces of cosmogenic and anthropogenic long-lived radionuclides. In this way, AMS is extending the widely used method of stable isotope mass spectrometry to one that includes long-lived radioisotopes as well. This allows us to use the "isotope language" to study our environment at large in unprecedented detail. In particular, depending on the half-life of the measured radionuclides, time-dependent processes can be investigated as well.

This review describes the technical aspects of the AMS method and the wide range of research possibilities. Even though an effort is made to cover as many fields of research as possible, the selection of topics is necessarily influenced by our expertise. However, a rather large bibliography is supplied to allow interested readers to pursue any of the topics in more depth.

Among the radionuclides measured with AMS, ^{14}C is by far the most used and is measured routinely at almost all AMS facilities worldwide. It offers seemingly unlimited research possibilities. Second to ^{14}C is the use of ^{10}Be, followed by ^{26}Al, ^{36}Cl, ^{41}Ca, ^{129}I, and many other long-lived radionuclides. In recent years, AMS measurements of anthropogenic isotopes of the actinides (Th, Pa, U, Np, Pu, Am, and Cm) released into the environment from the atmospheric nuclear weapons testing period and fission products from the nuclear industry have been gaining importance for a number of interesting applications, such as in oceanography (Hain *et al.*, 2022).

A rapidly increasing research field of AMS is nuclear astrophysics. The detection of rare isotope signals (such as ^{60}Fe and ^{53}Mn) in deep-sea archives (nodules and sediments) and lunar material indicate supernova explosions at $\sim 3 \times 10^6$ and $\sim 7 \times 10^6$ yr ago. The detection of ^{244}Pu in the same archives points to a production in neutron-star mergers or

other rare cosmic events. A variety of nuclear cross section measurements with AMS contribute to our understanding of nuclear synthesis in stars.

The study of extraterrestrial matter is another lively field of AMS. Besides lunar material, which is still available from the Apollo-flight era (1969–1972), the first material from asteroids has also recently been collected. Perhaps material from Mars will someday be brought to Earth, either remotely or through human travel.

The worldwide increase of the number of AMS facilities (currently approaching 160) reflects the great interest in this field. This is accompanied by technical improvements, i.e., the "small is beautiful" development of ever smaller AMS facilities, the reduction of sample size, the increase of the overall detection efficiency, the reduction of background, and the availability of new radioisotopes. The addition of laser-matter interaction techniques to AMS, unlike those from mass spectrometry and nuclear detection, bodes well for new developments. In all likelihood, this will lead to new and innovative research in the fields addressed in this review and beyond.

LIST OF SYMBOLS AND ABBREVIATIONS

AD	anno Domini
AGAGE	Advanced Global Atmospheric Gases Experiment
AMS	accelerator mass spectrometry
ANL	Argonne National Laboratory, Argonne, IL
ALICE	Accélérateur Linéaire Injecteur Cyclotron (linear accelerator and cyclotron), Orsay, France
ANIS	Aarhus negative-ion source, Aarhus, Denmark
ANSTO	Australian Nuclear Science and Technology Organisation, Sydney, Australia
ANU	Australian National University, Canberra, Australia
a.s.l.	above sea level
ATOMKI	Atommagkutató Intézet, Institute for Nuclear Research, Hungarian Academy of Sciences, Debrecen, Hungary
ATLAS	Argonne Tandem Linear Accelerator System
ATTA	atom trap trace analysis
AU	astronomical unit
B2FH	Burbidge, Burbidge, Fowler, and Hoyle (Burbidge *et al.*, 1957)
BC	before Christ
BCE	Before the Common Era; alternative form of BC
CARIBIC	Civil Aircraft for the Regular Investigation of the Atmosphere Based on an Instrument Container
CAMS	Center for Accelerator Mass Spectrometry, Lawrence Livermore National Laboratory, Livermore, CA, USA
CAMS	compact accelerator mass spectrometer, NEC, Middleton, WI
CE	Common Era; alternative expression for AD
CEDAD	Centro di Fisica Applicata, Datazione e Diagnostica (Centre for Applied Physics, Dating and Diagnostics), University of Salento, Lecce, Italy
CIAE	China Institute of Atomic Energy, Beijing, China
CIRCE	Centre for Isotopic Research on the Cultural and Environmental heritage, University of Campania, Caserta, Italy
CITES	Convention on International Trade in Endangered Species
CNA	Centro Nacional de Aceleradores (National Centre for Accelerators), Seville, Spain
C-T	Cretaceous-Tertiary
DF	degrader foil
DNA	desoxyribonucleic Acid
DREAMS	Dresden Accelerator Mass Spectrometry, Rossendorf, Dresden, Germany
D-REAMS	The Dangoor Research Accelerator Mass Spectrometry Laboratory, Weizmann Institute of Science, Rehovot, Israel
EPICA	European Project for Ice Coring in Antarctica
dTOF	delta E time of flight (energy loss plus TOF)
EA	electron affinity
ECR	electron cyclotron resonance
ERD	elastic recoil detection
ETH	Eidgenössische Technische Hochschule (Swiss Federal Institute of Technology), Zurich, Switzerland
FNAL	Fermi National Accelerator Laboratory, Batavia, IL
FS	full stripping
GAMS	gas-filled analyzing magnet system, Tandem Laboratory, Garching/Munich, Germany
GFM	gas-filled magnet
GLODAP	Global Ocean Data Analysis Project
GSI	Gesellschaft für SchwerIonen Forschung (Helmholtz Centre for Heavy Ion Research), Darmstadt, Germany

HAMSTER	Helmholtz Accelerator Mass Spectrometer for Tracing Environmental Radionuclides
HIAF	Heavy Ion Accelerator Facility, ANU Canberra, Australia
HVEE	High Voltage Engineering Europe, Amersfoort, Netherlands
HZDR	Helmholtz-Zentrum Dresden-Rossendorf, Dresden, Germany
IAEA	International Atomic Energy Agency, Vienna, Austria
IAA	Institute for Accelerator Analysis, Shirakawa, Japan
IBA	ion beam analysis
ICPMS	inductively coupled plasma mass spectrometry
ICPSFMS	inductively coupled plasma sector field mass spectrometry
IFUNAM	Instituto de Física, Universidad Nacional Atónoma de México, Mexico
IHEG-CAGS	Institute of Hydrology and Environmental Geology, Chinese Academy of Geological Science, Shijiazhuang City, China
LAMS	laser accelerator mass spectrometry
ILIAMS	ion laser interaction accelerator mass spectrometry, VERA Laboratory, University of Vienna, Vienna, Austria
ININ	Instituto Nacional de Investigaciones Nucleares, Ocoyoacac, México
ISA	isotope separator for anions, Lalonde AMS Laboratory, Ottawa, Ontario, Canada
INFN	Istituto Nationale di Fisica Nucleare (National Institute for Nuclear Physics), Italy
IPCC	Intergovernmental Panel on Climate Change
IPN	Institut de Physique Nucléaire, Nuclear Physics Institute, Orsay, France
ISM	interstellar medium
IUPAC	International Union of Pure and Applied Chemistry
KATRI	Korean Apparel Testing and Research Institute, Seoul, Korea
KIGAM	Korean Institute of Geosciences and Minerals, Deajeon, Korea
KIRAMS	Korea Institute of Radiological and Medical Sciences, Seoul, Korea
KIST	Korea Institute of Science and Technology, Seoul, Korea
KIT	Karlsruhe Institute of Technology, Karlsruhe, Germany
KOMAC	Korea Multi-purpose Accelerator Complex, Gyongi, Korea
K-Pg	Cretaceous-Paleogene boundary, formerly Cretaceous-Tertiary (K-T) boundary
KRICT	Korean Research Institute of Chemical Technology, Ulsan, Korea
LABEC	Laboratori di tecniche nucleari per l'Ambiente e i Beni Culturali (Laboratory of Nuclear Techniques for Environment and Cultural Heritage), Florence, Italy
LEA	low-energy accelerator mass spectrometry, ETH Zurich and Ionplus, Switzerland
LEMA	Laboratorio de Espectrometría de Masas con Acceleradores, Mexico
LIC	laser detachment and ion cooler or chemical reaction cell
LiLiT	Liquid-Lithium Target, SARAF, Soreq, Israel
LLNL	Lawrence Livermore National Laboratory, Livermore, CA
MALT	Micro Analysis Laboratory, Tandem accelerator, University of Tokyo, Tokyo, Japan
MICADAS	mini radiocarbon dating system, ETH Zurich and Ionplus, Switzerland
MILEA	multielement low-energy accelerator mass spectrometry, ETH Zurich and Ionplus, Switzerland
MIS	marine isotope stage
MOT	magneto-optical trap
ND	University of Notre Dame, Notre Dame, IN
NEC	National Electrostatics Corporation, Middleton, WI
NIES	National Institute of Environmental Studies, Tsukuba, Japan
NRICH	National Research Institute of Cultural Heritage, Daejon, Korea
OPDF	occurrence probability density function
ORAU	Oxford Radiocarbon Accelerator Unit, University of Oxford, Oxford, England
PA	passive absorber
PIXE	particle-induced x-ray emission
PXD	projectile x-ray detection
PIMS	positive-ion mass spectrometry
PRIME	Purdue Rare Isotope Measurement Laboratory, Purdue University, West Lafayette, IN
PSI	Paul Scherrer Institute, Villigen, Switzerland

RCNP	Research Centre for Nuclear Physics, Osaka University, Osaka, Japan
RFQ	radio-frequency quadrupole
RICH	Royal Institute for Cultural Heritage, Brussels, Belgium
RIMS	resonance ionization mass spectrometry
SARAF	Soreq Applied Research Accelerator Facility, Soreq Nuclear Research Center, Yavneh, Israel
SAVE	South Atlantic Ventilation Experiment
SN	supernova
SOCCOM	Southern Ocean Carbon and Climate Observations and Modeling
SS	Solar System
SSAMS	single stage accelerator mass spectrometry, NEC, Middleton, WI
SUERC	Scottish Universities Environmental Research Centre, East Kilbride, Scotland
TANDAR	Tandem Argentino, Buenos Aires, Argentina
TIMS	thermal ionization mass spectrometry
TNO	Toegepast Natuurwetenschappelijk Onderzoek (Netherlands Organisation for Applied Scientific Research)
TOF	time of flight
Tohoku U	Tohoku University, Sendai, Japan
TV	terminal voltage
TUM	Technical University Munich, Garching, Germany
UAMS	Upgraded Accelerator Mass Spectrometer, NEC, Middleton, WI
UNILAC	Universal Linear Accelerator, GSI Darmstadt, Germany
VERA	Vienna Environmental Research Accelerator, University of Vienna, Austria
XCAMS	extended compact AMS spectrometer, NEC, Middleton, WI

ACKNOWLEDGMENTS

This review benefited greatly from countless interactions with AMS researchers around the world. We acknowledge the dedicated work of the organizers of the 15 triennial AMS conferences, which has made it possible to follow the impressive progress of the field since 1978. We thank Joel Bourquin (Ionplus), Mark Sundquist (NEC), Hans-Arno Synal, Henri van Oosterhout (HVE), and Christof Vockenhuber (ETHZ) for supplying information on the development and distribution of worldwide AMS facilities (Sec. II.H). Helpful comments of three anonymous reviewers are gratefully acknowledged. A. J. T. J. acknowledges support from the European Union and the State of Hungary, cofinanced by the European Regional Development Fund through Project No. GINOP-2.3.4-15-2020-00007 "INTERACT." M. P. acknowledges support over the years from the Israel Science Foundation (Grants No. 43/01, No. 1387/15, and No. 876/19), the U.S.-Israel Binational Science Foundation (Grants No. 1985105, No. 1998453, and No. 2020136), and the German-Israeli Foundation (Grant No. 1500). A. W. and M. P. acknowledge support from the Australian Research Council's Discovery scheme (Projects No. DP140100136, No. DP180100495, and No. DP180100496).

Note added.—We note that Kinoshita *et al.* (2012) recently retracted their paper; see Kinoshita *et al.* (2023).

REFERENCES

Aboulahris, M., H. Chennouai Aoudjehande, P. Rochette, J. Gattacceca, A. J. T. Jull, N. Laridhi, L. Folco, and S. Buhl, 2019, "Characteristics of the Sahara as a meteorite recovery surface," Meteorit. Planet. Sci. **54**, 2908–2928.

Ahmad, I., J. P. Greene, E. F. Moore, S. Ghelberg, A. Ofan, M. Paul, and W. Kutschera, 2006, "Improved measurement of the ^{44}Ti half-life from a 14-year long study," Phys. Rev. C **74**, 065803.

Alfimov, V., and G. Possnert, 2004, "Computer simulation of ion-beam optics in a gas-filled magnetic spectrometer," Nucl. Instrum. Methods Phys. Res., Sect. B **223–224**, 180–184.

Al-Kathiri, A., B. A. Hofmann, A. J. T. Jull, and E. Gnos, 2005. "Weathering of meteorites from Oman: Correlation of chemical/mineralogical weathering proxies with ^{14}C terrestrial ages and the influence of soil chemistry," Meteorit. Planet. Sci. **40**, 1215–1239.

Alpher, R. A., H. Bethe, and G. Gamow, 1948, "The origin of chemical elements," Phys. Rev. **73**, 803–804.

Altobelli, N., *et al.*, 2016, "Flux and composition of interstellar dust at Saturn from Cassini's Cosmic Dust Analyzer," Science **352**, 312–318.

Alvarez, L. W., 1951, "Energy doubling in dc accelerators," Rev. Sci. Instrum. **22**, 705–706.

Alvarez, L. W., 1982, "The early days of accelerator mass spectrometry," Phys. Today **35**, No. 1, 25–32.

Alvarez, L. W., W. Alvarez, F. Asaro, and H. V. Michel, 1980, "Extraterrestrial cause of the Cretaceous-Tertiary extinction," Science **208**, 1095–2118.

Alvarez, L. W., and R. Cornog, 1939a, "He^3 in helium," Phys. Rev. **56**, 379.

Alvarez, L. W., and R. Cornog, 1939b, "Helium and hydrogen of mass 3," Phys. Rev. **56**, 613.

Anbar, M., 1978, "The limitation of mass spectrometric radiocarbon dating using CN-ions," in *Proceedings of the First Conference on Radiocarbon Dating with Accelerators, Rochester, 1978*, edited by H. E. Gove (University of Rochester Press, Rochester), pp. 152–164.

Anderson, T., M. Skulski, L. Callahan, A. Clark, A. Nelson, K. Ostdiek, P. Collon, G. Chmiel, T. Woodruff, and M. Caffee, 2020, "Measurement of ^{34}S(^{3}He, p)^{36}Cl cross sections for nuclide enrichment in the early Solar System," Phys. Rev. C **101**, 025801.

Anderson, T., M. Skulski, A. Clark, A. Nelson, K. Ostdiek, P. Collon, G. Chmiel, T. Woodruff, and M. Caffee, 2017, "Re-measurement of ^{33}S(α, p)^{36}Cl cross sections early Solar System nuclide enrichment," Phys. Rev. C **96**, 015803.

Andersson, P., A. O. Lindahl, D. Hanstorp, C. C. Havener, Y. Liu, and Y. Liu, 2010, "Nearly complete isobar suppression by photodetachment," J. Appl. Phys. **107**, 026102.

Arazi, A., T. Faestermann, J. O. Fernandez Niello, D. Frischke, K. Knie, G. Korschinek, H. J. Maier, E. Richter, G. Rugel, and

A. Wallner, 2004, "Magnesium suppression for ^{26}Al measurements using AlO^- ions," Nucl. Instrum. Methods Phys. Res., Sect. B **223–224**, 259–262.

Argo Project, 2021, https://en.wikipedia.org/wiki/Argo_(oceanography).

Arnold, J. R., 1987, "Decay counting in the age of AMS," Nucl. Instrum. Methods Phys. Res., Sect. B **29**, 424–426.

Arnold, J. R., and W. F. Libby, 1949, "Age determination by radiocarbon content: Checks with samples of known age," Science **110**, 678–680.

Arnould, M., and S. Goriely, 2020, "Astronuclear physics: A tale of the atomic nuclei in the skies," Prog. Part. Nucl. Phys. **112**, 103766.

Artigalas, H., *et al.*, 1993, "FT-ICR with laser ablation and AMS combined with x-ray detection, applied to the measurement of long-lived radionuclides from fission or activation: Preliminary results," Nucl. Instrum. Methods Phys. Res., Sect. B **79**, 617–619.

Aston, F. W., 1922, "Mass spectra and isotopes," Nobel Prize in Chemistry lecture; published in *Nobel Lectures, Chemistry 1922–1941*, edited by Nobel Foundation (Elsevier, Amsterdam, 1966), https://www.nobelprize.org/prizes/chemistry/1922/aston/lecture/.

Aze, T., H. Matsuzaki, H. Matsumura, H. Nagai, M. Fujimura, M. Noguchi, Y. Hongo, and Y. Yokoyama, 2007, "Improvement of the ^{36}Cl-AMS system at MALT using a Monte Carlo ion-trajectory simulation in a gas-filled magnet," Nucl. Instrum. Methods Phys. Res., Sect. B **259**, 144–148.

Balco, G., and D. L. Shuster, 2009, "^{26}Al–^{10}Be–^{21}Ne burial dating," Earth Planet. Sci. Lett. **286**, 570–575.

Balco, G., J. O. Stone, N. A. Lifton, and T. J. Dunai, 2008, "A complete and easily accessible means of calculating surface exposure ages or erosion rates from ^{10}Be and ^{26}Al measurements," Quat. Geochronol. **3**, 174–195.

Beck, J. W., W. Zhou, C. Li, Z. Wu, L. White, F. Xian, X. Kong, and Z. An, 2018, "A 550,000-year record of East Asian monsoon rainfall from ^{10}Be in loess," Science **360**, 877–881.

Beck, L., *et al.*, OCBC Collaboration, 2022, "Detecting recent forgeries of Impressionist and Pointillist paintings with high-precision radiocarbon dating," Forensic Sci. Int. **333**, 111214.

Beer, J., K. McCracken, and R. von Steiger, 2012, *Cosmogenic Radionuclides: Theory and Applications in the Terrestrial and Space Environments*, Physics of Earth and Space Environments (Springer-Verlag, Berlin).

Beer, J., *et al.*, 1992, "^{10}Be as time markers in polar ice cores," in *The Last Deglaciation: Absolute and Radiocarbon Chronologies*, edited by E. Bard and W. S. Broecker, NATO ASI, Ser. I, Vol. 12 (Springer-Verlag, New York), pp. 141–153.

Bennett, C. L., R. P. Beukens, M. R. Clover, H. E. Gove, R. B. Liebert, A. E. Litherland, K. H. Purser, and W. E. Sondheim, 1977, "Radiocarbon dating using electrostatic accelerators: Negative ions provide the key," Science **198**, 508–510.

Bennett, M. R., *et al.*, 2021, "Evidence of humans in North America during the last glacial maximum," Science **373**, 1528–1531.

Berger, A., and M. F. Loutre, 1991, "Insulation values for the climate of the last 10 million years," Quat. Sci. Rev. **10**, 297–317.

Bergmann, O., *et al.*, 2009, "Evidence for cardiomyocyte renewal in humans," Science **324**, 98–102.

Bergmann, O., *et al.*, 2012, "The age of olfactory bulb neurons in humans," Neuron **74**, 634–639.

Berkovits, D., E. Boaretto, G. Hollos, W. Kutschera, R. Naaman, M. Paul, and Z. Vager, 1989, "Selective suppression of negative ions by lasers," Nucl. Instrum. Methods Phys. Res., Sect. A **281**, 663–666.

Berkovits, D., E. Boaretto, G. Hollos, W. Kutschera, R. Naaman, M. Paul, and Z. Vager, 1990, "Study of laser interaction with negative ions," Nucl. Instrum. Methods Phys. Res., Sect. B **52**, 378–383.

Bertsche, K. J., C. A. Karadi, R. A. Muller, and C. C. Paulson, 1990, "Detection of radiocarbon in the cyclotrino," Nucl. Instrum. Methods Phys. Res., Sect. B **52**, 398–404.

Bethe, H. A., and R. F. Bacher, 1936, "Nuclear physics A. Stationary states of nuclei," Rev. Mod. Phys. **8**, 82–229.

Betz, H.-D., 1972, "Charge states and charge-changing cross sections of fast heavy ions penetrating through gaseous and solid media," Rev. Mod. Phys. **44**, 465–539.

Beukens, R. P., H. E. Gove, A. E. Litherland, W. E. Kieser, and X.-L. Zhao, 2004, "The old carbon project: How old is old?," Nucl. Instrum. Methods Phys. Res., Sect. B **223–224**, 333–338.

Bhardwaj, R. D., *et al.*, 2006, "Neocortical neurogenesis in humans is restricted to development," Proc. Natl. Acad. Sci. U.S.A. **103**, 12564–12568.

Bietak, M., 2014, "Radiocarbon and the date of the Thera eruption," Antiquity **88**, 277–282.

Binns, W. R., *et al.*, 2016, "Observation of the ^{60}Fe nucleosynthesis-clock isotope in Galactic cosmic rays," Science **352**, 677–680.

Blard, P. H., *et al.*, 2015, "An inter-laboratory comparison of cosmogenic ^{3}He and radiogenic ^{4}He in the CRONUS-P pyroxene standard," Quat. Geochronol. **26**, 11–19.

Bonani, G., S. D. Ivy, I. Hajdas, T. R. Niklaus, and M. Suter, 1994, "AMS ^{14}C age determinations of tissue, bone and grass from the Ötztal iceman," Radiocarbon **36**, 247–250.

Braucher, R., and D. Bourlès, 2015, Eds., *Proceedings of the 13th International Conference on Accelerator Mass Spectrometry, Aix-en-Provence, France, 2014*, https://www.sciencedirect.com/journal/nuclear-instruments-and-methods-in-physics-research-section-b-beam-interactions-with-materials-and-atoms/vol/361/suppl/C.

Brehm, N., *et al.*, 2022, "Tree rings reveal two strong solar proton events in 7176 and 5259 BCE," Nat. Commun. **13**, 214.

Brenninkmeijer, C. A. M., S. S. Gromov, and P. Jöckel, 2022, "Cosmogenic ^{14}CO for assessing the OH-based self-cleaning capacity of the troposphere," Radiocarbon **64**, 761–779.

Brenninkmeijer, C. A. M., *et al.*, 1999, "CARIBIC—Civil aircraft for global global measurement of trace gases and aerosols in the tropopause region," J. Atmos. Ocean. Technol. **16**, 1373–1383.

Brenninkmeijer, C. A. M., *et al.*, 2007, "Civil aircraft for the regular investigation of the atmosphere based on an instrumented container: The new CARIBIC system," Atmos. Chem. Phys. **7**, 4953–4976.

Broecker, W. S., 1991, "The great ocean conveyor," Oceanography **4**, 79–89.

Bronk, C. R., and R. E. M. Hedges, 1987, "A gas ion source for radiocarbon dating," Nucl. Instrum. Methods Phys. Res., Sect. B **29**, 45–49.

Bronk, C. R., and R. E. M. Hedges, 1990, "A gaseous ion source for routine AMS radiocarbon dating," Nucl. Instrum. Methods Phys. Res., Sect. B **52**, 322–326.

Bronk Ramsey, C., 2009, "Bayesian analysis of radiocarbon dates," Radiocarbon **51**, 337–360.

Bronk Ramsey, C., C. A. M. Brenninkmeijer, P. Jöckel, H. Kjeldsen, and J. Masarik, 2007, "Direct measurement of the radiocarbon production at altitude," Nucl. Instrum. Methods Phys. Res., Sect. B **259**, 558–564.

Bronk Ramsey, C., and R. E. M. Hedges, 1997, "Hybrid ion sources: Radiocarbon measurements from microgram to milligram," Nucl. Instrum. Methods Phys. Res., Sect. B **123**, 539–545.

Brookhaven National Laboratory Nuclear Data Center, 2018, "Nuclear structure and decay data," https://www.nndc.bnl.gov/nudat2/.

Brown, L., J. Klein, R. Middleton, I. Selwyn Sacks, and F. Tera, 1982, "^{10}Be in island-arc volcanoes and implications for subduction," Nature (London) **299**, 718–720.

Brown, T. A., A. A. Marchetti, R. E. Martinelli, C. C. Cox, J. P. Knezovich, and T. F. Hamilton, 2004, "Actinide measurements by accelerator mass spectrometry at Lawrence Livermore National Laboratory," Nucl. Instrum. Methods Phys. Res., Sect. B **223–224**, 788–795.

Browne, E., and J. X. Tuli, 2017, "Nuclear data sheets for $A = 99$," Nucl. Data Sheets **145**, 25–340.

Buizert, C., *et al.*, 2014, "Radiometric ^{81}Kr dating identifies 120,000-year-old ice at Taylor Glacier, Antarctica," Proc. Natl. Acad. Sci. U.S.A. **111**, 6876–6881.

Bunemann, O., T. E. Cranshaw, and J. A. Harvey, 1949, "Design of grid ionization chambers," Can. J. Res. **27a**, 191–206.

Büntgen, U., *et al.*, 2018. "Tree rings reveal globally coherent signature of cosmogenic radiocarbon events in 774 and 993 CE," Nat. Commun. **9**, 3605.

Burbank, D. W., J. Leland, E. Fielding, R. S. Anderson, N. Brozovic, M. R. Reid, and C. Duncan, 1996, "Bedrock incision, rock uplift and threshold hillslopes in the northwestern Himalayas," Nature (London) **379**, 505–510.

Burbidge, E. M., G. R. Burbidge, W. A. Fowler, and F. Hoyle, 1957, "Synthesis of the elements in stars," Rev. Mod. Phys. **29**, 547–650.

Bzdeka, B. R., and J. P. Reida, 2017, "Perspective: Aerosol microphysics: From molecules to the chemical physics of aerosols," J. Chem. Phys. **147**, 220901.

Caffee, M. W., D. E. Granger, and T. E. Woodruff, 2015, "The gas-filled-magnet at PRIME Lab: Increased sensitivity of cosmogenic nuclide measurements," in *Proceedings of the AGU Fall Meeting, San Francisco, 2015*, p. V31G-09, https://ui.adsabs.harvard.edu/abs/2015AGUFM.V31G..09C.

Caforio, L., M. E. Fedi, P. A. Mandò, F. Minarelli, E. Peccenini, V. Pellicori, F. C. Petrucci, P. Schwartzbaum, and F. Taccetti, 2014, "Discovering forgeries of modern art by the ^{14}C bomb peak," Eur. Phys. J. Plus **129**, 1–5.

Calcagnile, L., A. D'Onofrio, M. Fedi, P. A. Mando, G. Quarta, F. Terrasi, and C. Tuniz, 2010, Eds., *Proceedings of the Eleventh International Conference on Accelerator Mass Spectrometry, Rome, 2008*, https://www.sciencedirect.com/journal/nuclear-instruments-and-methods-in-physics-research-section-b-beam-interactions-with-materials-and-atoms/vol/268/issue/7.

Cameron, A. G. W., 1957, "Nuclear reaction in stars and nucleogenesis," Publ. Astron. Soc. Pac. **69**, 201–222.

Cao, F., Y.-L. Zhang, S. Szidat, A. Zapf, L. Wacker, and M. Schwikowski, 2013, "Microgram-level radiocarbon determination of carbonaceous particles in firn and ice samples: Petreatment and OC/EC separation," Radiocarbon **55**, 383–390.

Casacuberta, N., M. Christl, J. Lachner, M. Rutgers van der Loeff, P. Masqué, and H.-A. Synal, 2014, "A first transect of ^{236}U in the North Atlantic Ocean," Geochim. Cosmochim. Acta **133**, 34–46.

Cerling, T. E., J. E. Barnette, L. A. Chesson, I. DouglasHamilton, K. S. Gobush, K. T. Uno, S. K. Wasser, and X. Xu, 2016, Radiocarbon dating of seized ivory confirm a rapid decline in African elephant populations and provides insight into illegal trade, Proc. Natl. Acad. Sci. U.S.A. **113**, 13330.

Chadwick, J., 1932a, "Possible existence of a neutron," Nature (London) **129**, 312.

Chadwick, J., 1932b, "The existence of a neutron," Proc. R. Soc. A **136**, 692–708.

Chaikin, E., A. A. Kaurov, B. D. Fields, and C. A. Correa, 2022, "Simulations of ^{60}Fe entrained in ejecta from a near-Earth supernova: Effects of observer motion," Mon. Not. R. Astron. Soc. **512**, 712–727.

Chamizo, E., M. Christl, M. López-Lora, N. Casacuberta, A.-M. Wefing, and T. C. Kenna, 2022, "The Potential of 233U/236U as a water mass tracer in the Arctic Ocean," J. Geophys. Res. Oceans **127**, e2021JC017790.

Chávez, E., *et al.*, 2022 "Accelerator mass spectrometry, an ultrasensitive tool to measure cross sections for stellar nucleosynthesis," Nucl. Instrum. Methods Phys. Res., Sect. B **526**, 77–82.

Chebboubi, A., G. Kessedjian, H. Faust, A. Blanc, M. Jentschel, U. Koester, T. Materna, O. Meplan, C. Sage, and O. Serot, 2016, "Development of a gas-filled magnet spectrometer within the FIPPS project," Nucl. Instrum. Methods Phys. Res., Sect. B **376**, 120–124.

Cheifetz, E., R. C. Jared, E. R. Giusti, and S. G. Thompson, 1972, "Search for superheavy elements in nature," Phys. Rev. C **6**, 1348–1361.

Chen, C.-Y., Y. M. Li, K. Bailey, T. O'Connor, L. Young, and Z.-T. Lu, 1999, "Ultrasensitive isotope trace analysis with a magneto-optical trap," Science **286**, 1139–1141.

Chen, M., C. Koeberl, D. Tan, P. Ding, W. Xiao, N. Wang, Y. Chen, and X. Xie, 2021, "Yilan crater, China: Evidence for an origin by meteorite impact," Meteorit. Planet. Sci. **56**, 1274–1292.

Chen, M. B., X. S. Lu, D. Li, Y. H. Liu, W. J. Zhou, G. S. Chen, L. G. Shen, S. L. Xu, and Y. X. Zhang, 2000, "Minicyclotron (SMCAMS)-based accelerator mass spectrometry and real ^{14}C measurements," Nucl. Instrum. Methods Phys. Res., Sect. B **172**, 193–200.

Chen, M.-B., D.-M. Li, S.-L. Xu, G.-S. Chen, L.-G. Shen, Y.-J. Zhang, X.-S. Lu, W.-Y. Zhang, Y.-X. Zhang, and Z.-K. Zhong, 1994, "The successful SINR mini cyclotron AMS for ^{14}C dating," Nucl. Instrum. Methods Phys. Res., Sect. B **92**, 213–216.

Child, D. P., and M. A. C. Hotchkis, 2013, "Plutonium and uranium contamination in soils from former nuclear weapon test sites in Australia," Nucl. Instrum. Methods Phys. Res., Sect. B **294**, 642–646.

Chmeleff, J., F. von Blanckenburg, K. Kossert, and D. Jakob, 2010, "Determination of the ^{10}Be half-life by multicollector ICP-MS and liquid scintillation counting," Nucl. Instrum. Methods Phys. Res., Sect. B **268**, 192–199.

Christl, M., N. Casacuberta, C. Vockenhuber, C. Elsässer, P. Bailly du Bois, J. Herrmann, and H.-A. Synal, 2015, "Reconstruction of the ^{236}U input function for the northeast Atlantic Ocean: Implications for ^{129}I/^{236}U and ^{236}U/^{238}U-based tracer ages," J. Geophys. Res. Oceans **120**, 7282–7299.

Christl, M., X. Dai, J. Lachner, S. Kramer-Tremblay, and H.-A. Synal, 2014, "Low energy AMS of americium and curium," Nucl. Instrum. Methods Phys. Res., Sect. B **331**, 225–232.

Christl, M., *et al.*, 2015, "Status of ^{236}U analyses at ETH Zurich and the distribution of ^{236}U and ^{129}I in the North Sea in 2009," Nucl. Instrum. Methods Phys. Res., Sect. B **361**, 510–516.

Clarke, F. W., 1889, "The relative abundance of the chemical elements," Bull. Phil. Soc. Wash. **11**, 135–143.

Cohen, B. L., and C. B. Fulmer, 1958, "Fission-fragment mass separator and the nuclear charge disribution of fission fragments of s single mass," Nucl. Phys. **6**, 547–560.

Collon, P., W. Kutschera, and Z.-T. Lu, 2004, "Tracing noble gas radionuclides in the environment," Annu. Rev. Nucl. Part. Sci. **54**, 39–67.

Collon, P., *et al.*, 1997, "Measurement of ^{81}Kr in the atmosphere," Nucl. Instrum. Methods Phys. Res., Sect. B **123**, 122–127.

Collon, P., *et al.*, 2000, "^{81}Kr in the Great Artesian Basin, Australia: A new method for dating very old groundwater," Earth Planet. Sci. Lett. **182**, 103–113.

Collon, P., *et al.*, 2004, "Development of an AMS method to study ocean circulation characteristic using cosmogenic ^{39}Ar," Nucl. Instrum. Methods Phys. Res., Sect. B **223–224**, 428–434.

Combes, C., S. Cazalbou, and C. Rey, 2016, "Apatite biominerals," Minerals **6**, 34.

Corbett, L. B., P. R. Bierman, and D. H. Rood, 2016, "An approach for optimizing *in situ* cosmogenic ^{10}Be sample preparation," Quat. Geochronol. **33**, 24–34.

Cornett, R. J., Z. H. Kazi, X.-L. Zhao, M. G. Chartrand, R. J. Charles, and W. E. Kieser, 2015, "Actinide measurements by AMS using fluoride matrices," Nucl. Instrum. Methods Phys. Res., Sect. B **361**, 317–321.

Coté, B., *et al.*, 2021, "^{129}I and ^{247}Cm in meteorites constrain the last astrophysical source of solar *r*-process elements," Science **371**, 945–948.

Cowan, J. J., C. Sneden, J. E. Lawler, A. Aprahamian, M. Wiescher, K. Langanke, G. Martinez-Pinedo, and F.-K. Thielemann, 2021, "Origin of the heaviest elements: The rapid neutron-capture process," Rev. Mod. Phys. **93**, 015002.

Crawford, I. A., K. H. Joy, J. H. Pasckert, and H. H. Hiesinger, 2021, "The lunar surface as a recorder of astrophysical processes," Phil. Trans. R. Soc. A **379**, 20190562.

Crutzen, P., 1997, "My life with O_3, NO_x, and other YZO_x's," in *Nobel Lectures in Chemistry 1991–1995*, edited by G. B. Malström (World Scientific, Singapore), pp. 189–242.

Davis, R., 1994, "A review of the Homestake solar neutrino experiment," Prog. Part. Nucl. Phys. **32**, 13–32.

Dee, M., B. Pope, D. Miles, S. Manning, and F. Miyake, 2017, "Supernoae and single-year anomalies in the atmospheric radiocarbon record," Radiocarbon **59**, 293–302.

Dellinger, F., O. Forstner, R. Golser, W. Kutschera, A. Priller, P. Steier, A. Wallner, and G. Winkler, 2010, "Search for a superheavy nuclide with $A = 292$ and neutron deficient thorium isotopes in natural thorianite," Nucl. Instrum. Methods Phys. Res., Sect. B **268**, 1287–1290.

Dellinger, F., O. Forstner, R. Golser, A. Priller, P. Steier, A. Wallner, G. Winkler, and W. Kutschera, 2011, "Ultrasensitive search for long-lived superheavy nuclides in the mass range $A = 288$ to $A = 300$ in natural Pt, Pb, and Bi," Phys. Rev. C **83**, 065806.

Dellinger, F., W. Kutschera, O. Forstner, R. Golser, A. Priller, P. Steier, A. Wallner, and G. Winkler, 2011, "Upper limits for the existence of long-lived isotopes of roentgenium in natural gold," Phys. Rev. C **83**, 015801.

DeMaster, D. J., 1980, "The half-life of ^{32}Si determined from a varved Gulf of California sediment core," Earth Planet. Sci. Lett. **48**, 209–217.

Denk, E., *et al.*, 2006, "Labeling the human skeleton with ^{41}Ca to assess changes in bone calcium metabolism," Anal. Bioanal. Chem. **386**, 1587–1602.

Deviese, T., D. Comeskey, J. McCullagh, C. Bronk Ramsey, and T. Higham, 2018, "New protocol for compound-specific radiocarbon analysis of archaeological bones," Rapid Commun. Mass Spectrom. **32**, 373–379.

de Vries, H., 1958, "Variation in concentration of radiocarbon with time and location on Earth," Proc. Kon. Ned. Akad. Wet., Ser. B **61**, 94–102.

Diehl, R., A. J. Korn, B. Leibundgut, M. Lugaro, and A. Wallner, 2022, "Cosmic nucleosynthesis: A multi-messenger challenge," Prog. Part. Nucl. Phys. **127**, 103983.

Diehl, R., G. Martin, G. H. Krause, K. Kretschmer, M. Lang, M. M. M. Pleintinger, T. Siegert, W. Wang, L. Bouchet, and P. Martin, 2021, "Steady-state nucleosynthesis throughout the Galaxy," New Astron. Rev. **92**, 101608.

Diehl, R., *et al.*, 2006a, "Radioactive ^{26}Al from massive stars in the galaxy," Nature (London) **439**, 45–47.

Diehl, R., *et al.*, 2006b, "^{26}Al in the inner galaxy large-scale spectral characteristics derived with SPI/INTEGRAL," Astron. Astrophys. **449**, 1025–1031.

Diehl, R., *et al.*, 2021, "The radioactive nuclei ^{26}Al and ^{60}Fe in the Cosmos and the Solar System," Pub. Astron. Soc. Aust. **38**, e062.

Dillmann, I., M. Heil, F. Käppeler, T. Faesterman, G. Korschinek, K. Knie, A. Wallner, and T. Rauscher, 2006, "First measurements of the total and partial stellar cross section to the *s*-process branching-point ^{79}Se," Proc. Sci. NIC-IX, 089.

Dillmann, I., *et al.*, 2010, "Solving the stellar ^{62}Ni problem with AMS," Nucl. Instrum. Methods Phys. Res., Sect. B **268**, 1283–1286.

Dmitriev, I. S., and V. S. Nikolaev, 1965, "Semi-empirical method for the calculation of the equilibrium distribution of charges in a fast-ion beam," Sov. Phys. JETP **20**, 409–415.

Döbeli, M., C. Kottler, M. Stocker, S. Weinmann, H.-A. Synal, M. Grajcar, and M. Suter, 2004, Gas ionization chambers with silicon nitride windows for the detection and identification of low energy ions," Nucl. Instrum. Methods Phys. Res., Sect. B **219–220**, 415–419.

Drouard, A., *et al.* (ASTER Team), 2019, "The meteorite flux of the past 2 m.y. recorded in the Atacama Desert," Geology **47**, 673–676.

Dunai, T. J., 2010, *Cosmogenic Nuclides: Principles, Concepts and Applications in the Earth Surface Sciences* (Cambridge University Press, Cambridge, England), pp. 1–180.

Ebser, S., A. Kersting, T. Stöven, Z. Feng, L. Ringen, M. Schmidt, T. Tanhua, W. Aeschbach, and M. K. Oberthaler, 2018, "^{39}Ar dating with small samples provides new key constraints on ocean ventilation," Nat. Commun. **9**, 5046.

Eddington, A. S., 1920, "The internal constitution of stars," Nature (London) **106**, 14–20.

Eddington, A. S., 1926, *The Internal Constitution of the Stars* (Cambridge University Press, Cambridge, England).

Ehrlich, Y., L. Regev, and E. Boaretto, 2021, "Discovery of annual growth in a modern olive branch based on carbon isotopes and implications for the Bronze Age volcanic eruption of Santorini," Sci. Rep. **11**, 704.

Eliades, J., A. E. Litherland, W. E. Kieser, L. Cousins, S. J. Ye, and X. L. Zhao, 2010, "Cl/S isobar separation using an on-line reaction cell for ^{36}Cl measurement at low energies," Nucl. Instrum. Methods Phys. Res., Sect. B **268**, 839–842.

Eliades, J., X. L. Zhao, A. E. Litherland, and W. E. Kieser, 2015, "Negative ion-gas reaction studies using ion guides and accelerator mass spectrometry I: $SrF_3^-YF_3^-ZrF_3^-YF_4^-$ and ZrF_5^- in NO_2," Nucl. Instrum. Methods Phys. Res., Sect. B **361**, 294–299.

Ellis, J., B. D. Fields, and D. N. Schramm, 1996, "Geological isotope anomalies as signatures of nearby supernovae," Astrophys. J. **470**, 1227–1236.

Elmore, D., N. Anantaraman, H. W. Fulbright, H. E. Gove, H. S. Hans, K. Nishiizumi, M. T. Murrell, and M. Honda, 1980, "Half-Life of ^{32}Si from Tandem-Accelerator Mass Spectrometry," Phys. Rev. Lett. **45**, 589–592.

Elmore, D., P. W. Kubik, L. F. Tubbs, H. E. Gove, R. Teng, T. Hemmick, B. Chrunyk, and N. Conard, 1984, "The Rochester tandem accelerator mass spectrometry program," Nucl. Instrum. Methods Phys. Res., Sect. B **5**, 109–116.

Elmore, D., and F. M. Phillips, 1987, "Accelerator mass spectrometry for measurement of long-lived radioisotopes," Science **236**, 543–550.

Elmore, E., *et al.*, 1980, "Determination of ^{129}I using tandem accelerator mass spectrometry," Nature (London) **286**, 138–140.

Emiliani, C., 1955, "Pleistocene temperatures," J. Geol. **63**, 538–578.

EPICA Community Members, 2004, "Eight glacial cycles from an Antarctic ice core," Nature (London) **429**, 623–628.

Ernst, H., *et al.*, 1984, "^{205}Pb: Accelerator mass spectrometry of a very heavy radioisotope and the solar neutrino problem," Nucl. Instrum. Methods Phys. Res., Sect. B **5**, 426–429.

Eugster, O., G. F. Herzog, K. Marti, and M. W. Caffee, 2006, "Irradiation records, cosmic-ray exposure ages, and transfer times of meteorites," in *Meteorites and the Early Solar System II*, edited by D. S. Lauretta and H. Y. McSween, Jr., (University of Arizona Press, Tucson), pp. 829–851.

Everett, S. E., S. G. Tims, G. J. Hancock, R. Bartley, and L. K. Fifield, 2008, "Comparison of Pu and ^{137}Cs as tracers of soil and sediment transport in a terrestrial environment," J. Environ. Radioact. **99**, 383–393.

Feige, J., A. Wallner, R. Altmeyer, L. K. Fifield, R. Golser, S. Merchel, G. Rugel, P. Steier, S. G. Tims, and S. R. Winkler, 2018, "Limits on Supernova-Associated ^{60}Fe/^{26}Al Nucleosynthesis Ratios from Accelerator Mass Spectrometry Measurements of Deep-Sea Sediments," Phys. Rev. Lett. **121**, 221103.

Feketeová, L., P. Bertier, T. Salbaing, T. Azuma, F. Calvo, B. Farizon, M. Farizon, and T. D. Märk, 2019, "Impact of a hydrophobic ion on the early stage of atmospheric aerosol formation," Proc. Natl. Acad. Sci. U.S.A. **116**, 22540–22544.

Ferguson, G., M. O. Cuthbert, K. Befus, T. Gleeson, and J. C. McIntosh, 2020, "Rethinking groundwater age," Nat. Geosci. **13**, 592–594.

Fields, P. R., H. Diamond, D. N. Metta, C. M. Stevens, D. J. Rokop, and P. E. Moreland, 1970, "Isotopic abundances of actinide elements in lunar material," Science **167**, 499–501.

Fields, P. R., A. M. Friedman, J. Milsted, J. Lerner, C. M. Stevens, D. Metta, and W. K. Sabine, 1966, "Decay properties of plutonium-244, and comments on its existence in nature," Nature (London) **212**, 131–134.

Fifield, L. K., 1999, "Accelerator mass spectrometry and its applications," Rep. Prog. Phys. **62**, 1223–1274.

Fifield, L. K., 2008, "Accelerator mass spectrometry of the actinides," Quat. Geochronol. **3**, 276–290.

Fifield, L. K., R. G. Cresswell, M. L. di Tada, T. R. Ophel, J. P. Day, A. P. Clacher, S. J. King, and N. D. Priest, 1996, "Accelerator mass spectrometry of plutonium isotopes," Nucl. Instrum. Methods Phys. Res., Sect. B **117**, 295–303.

Fifield, L. K., D. Fink, S. H. Sie, and C. Tuniz, 1994, Eds., Proceedings of the Sixth International Conference on Accelerator Mass Spectrometry, Canberra, Australia, 1993, https://journals.scholarsportal.info/browse/0168583x/v92i1-4.

Fifield, L. K., and U. Morgenstern, 2009, "Silicon-32 as a tool for dating the recent past," Quat. Geochronol. **4**, 400–405.

Fifield, L. K., T. R. Ophel, J. R. Bird, G. E. Calf, G. B. Allison, and A. R. Chivas, 1987, "The chlorine-36 measurement program at the Australian National University," Nucl. Instrum. Methods Phys. Res., Sect. B **29**, 114–119.

Fifield, L. K., H.-A. Synal, and M. Suter, 2004, Accelerator mass spectrometry of plutonium at 300 kV," Nucl. Instrum. Methods Phys. Res., Sect. B **223–224**, 802–806.

Fifield, L. K., S. G. Tims, T. Fujioka, W. T. Hoo, and S. E. Everett, 2010, "Accelerator mass spectrometry with the 14UD accelerator at the Australian National University," Nucl. Instrum. Methods Phys. Res., Sect. B **268**, 858–862.

Fifield, L. K., S. G. Tims, L. G. Gladkis, and C. R. Morton, 2007, "^{26}Al measurements with ^{10}Be counting statistics," Nucl. Instrum. Methods Phys. Res., Sect. B **259**, 178–183.

Fimiani, L., *et al.*, 2016, "Interstellar ^{60}Fe on the Surface of the Moon," Phys. Rev. Lett. **116**, 151104.

Fink, D., 2010, "AMS-11 in Rome, 2008: Past achievements, current and future trends," Nucl. Instrum. Methods Phys. Res., Sect. B **268**, 1334–1342.

Fink, D., J. Klein, and R. Middleton, 1990, "^{41}Ca: Past, present and future," Nucl. Instrum. Methods Phys. Res., Sect. B **52**, 572–582.

Fink, D., J. Klein, R. Middleton, S. Vogt, G. F. Herzog, and R. C. Reedy, 1998, "^{41}Ca^{26}Al, and ^{10}Be in lunar basalt 74275 and ^{10}Be in the double drive tube 74002/74001," Geochim. Cosmochim. Acta **62**, 2389–2402.

Fink, D., R. Middleton, J. Klein, and P. Sharma, 1990, "^{41}Ca: Measurement by accelerator mass spectrometry and applications," Nucl. Instrum. Methods Phys. Res., Sect. B **47**, 79–96.

Finkel, R., M. Arnold, G. Aumaitre, L. Benedetti, D. Bourles, K. Keddadouche, and S. Merchel, 2013, "Improved ^{36}Cl performance at the ASTER HVE 5 MV accelerator mass spectrometer national facility," Nucl. Instrum. Methods Phys. Res., Sect. B **294**, 121–125.

Finkel, R. C., and M. Suter, 1993, *AMS in the Earth Sciences: Technique and Applications*, Advances in Analytical Geochemistry Vol. 1 (JAI Press, Greenwich, CT), pp. 1–114.

Fitoussi, C., *et al.*, 2008, "Search for Supernova-Produced ^{60}Fe in a Marine Sediment," Phys. Rev. Lett. **101**, 121101.

Flerov, G. N., V. A. Druin, and A. A. Pleve, 1970, "The stability of heavy nuclei and the limit of the periodic system of elements," Sov. Phys. Usp. **13**, 24–50.

Folco, L., K. C. Welten, A. J. T. Jull, K. Nishiizumi, and A. Zeoli, 2006, "Meteorites constrain the age of Antarctic ice at the Frontier Mountain blue ice field (northern Victoria Land)," Earth Planet. Sci. Lett. **248**, 209–216.

Forstner, O., P. Andersson, D. Hanstorp, J. Lachner, M. Martschini, J. Pitters, A. Priller, P. Steier, and R. Golser, 2015, "The ILIAS project for selective isobar suppression by laser photodetachment," Nucl. Instrum. Methods Phys. Res., Sect. B **361**, 217–221.

Forstner, O., H. Gnaser, R. Golser, D. Hanstorp, M. Martschini, A. Priller, J. Rohlén, P. Steier, C. Vockenhuber, and A. Wallner, 2011, "Reassessment of ^{182}Hf AMS measurements at VERA," Nucl. Instrum. Methods Phys. Res., Sect. B **269**, 3180–3182.

Forstner, O., L. Michlmayr, M. Auer, R. Golser, W. Kutschera, A. Priller, P. Steier, and A. Wallner, 2008, "Applications of a compact ionization chamber in AMS at energies below 1 MeV/amu," Nucl. Instrum. Methods Phys. Res., Sect. B **266**, 2213–2216.

Freeman, S. P. H. T., B. Beck, J. M. Bierman, M. W. Caffee, R. P. Heaney, L. Holloway, R. Marcus, J. R. Southon, and J. S. Vogel, 2000, "The study of skeletal calcium metabolism with ^{41}Ca and ^{45}Ca," Nucl. Instrum. Methods Phys. Res., Sect. B **172**, 930–933.

Freeman, S. P. H. T., R. P. Shanks, X. Donzel, and G. Gaubert, 2015, "Radiocarbon positive-ion mass spectrometry," Nucl. Instrum. Methods Phys. Res., Sect. B **361**, 229–232.

Freeman, S. P. H. T., *et al.*, 2021 "The PIMS project status," in *Proceedings of the 15th International Conference on Accelerator Mass Spectrometry, Sydney, 2021* (Australian Nuclear Science and Technology Organisation, Lucas Heights, Australia), Abstracts, p. 183.

Friedrich, R., B. Kromer, L. Wacker, J. Olsen, S. Remmele, S. Lindauer, A. Land, and C. Pearson, 2020, "A new annual ^{14}C dataset for calibrating the Thera eruption," Radiocarbon **62**, 953–961.

Frisch, O. R., 1942, "Isotope analysis of uranium samples by means of their α-ray groups," British Atomic Energy Project Report No. BR-49 (unpublished).

Froehlich, M. B., A. Akber, S. D. McNeil, S. G. Tims, L. K. Fifield, and A. Wallner, 2019, "Anthropogenic ^{236}U and Pu at remote sites of the South Pacific," J. Environ. Radioact. **205–206**, 17–23.

Fujioka, I., L. K. Fifield, J. O. Stone, P. M. Vasconcelos, S. G. Tims, and J. Chappel, 2010, "*In situ* cosmogenic ^{53}Mn production rate from ancient low-denudation surface in tropic Brazil," Nucl. Instrum. Methods Phys. Res., Sect. B **268**, 1209–1213.

Fulbright, H. W., 1979, "Ionization chambers," Nucl. Instrum. Methods **162**, 21–28.

Fulmer, C. B., and B. L. Cohen, 1958, "Equilibrium charges of fission fragments in gases," Phys. Rev. **109**, 94–99.

Gamow, G., and E. Teller, 1936, "Selection rules for the ß-disintegration," Phys. Rev. **49**, 895–899.

García-Toraño, E., *et al.*, 2018, "Half-life of ^{129}I," Appl. Radiat. Isot. **140**, 157–162.

Garner, R. C., 2010, "Practical experience of using human microdosing with AMS analysis to obtain early human drug metabolism and PK data," Bioanalysis **2**, 429–440.

Gelbart, W. Z., R. R. Johnson, M. Paul, D. Berkovits, A. Hershkowitz, F. Cifarelli, R. B. Schubank, and Y. Shahar, 1997, "A compact multi-sample high-intensity negative ion source," Nucl. Instrum. Methods Phys. Res., Sect. B **123**, 550–553.

Geller, R., 1990, "ECRIS: The electron cyclotron resonance ion source," Annu. Rev. Nucl. Part. Sci. **40**, 15–43.

Geller, R., 1996, *Electron Cyclotron Resonance Ion Sources and ECR Plasmas* (CRC Press, Boca Raton).

Gibbon, R. J., T. R. Pickering, M. B. Sutton, J. L. Heaton, K. Kuman, R. J. Clarke, C. K. Brain, and D. E. Granger, 2014, "Cosmogenic nuclide burial dating of hominin-bearing Pleistocene cave deposits at Swartkrans, South Africa," Quat. Geochronol. **24**, 10–15.

Giordano, M., 2009, "Global groundwater? Issues and solutions," Annu. Rev. Environ. Resour. **34**, 153–178.

Giuliani, S. A., Z. Matheson, W. Nazarewicz, E. Olsen, P.-G. Reinhard, J. Sadhukhan, B. Schuetrumpf, N. Schunk, and P. Schwerdtfeger, 2019, "Colloquium: Superheavy elements: Oganesson and beyond," Rev. Mod. Phys. **91**, 011001.

Gladkis, L. D., L. K. Fifield, C. R. Morton, T. T. Barrows, and S. G. Tims, 2007, "Manganese-53: Development of the AMS technique for exposure-age dating applications," Nucl. Instrum. Methods Phys. Res., Sect. B **259**, 236–240.

Godwin, H., 1962, "Radiocarbon dating: Fifth international conference," *Nature (London)* 195, 943–945.

Golser, R., and W. Kutschera, 2017, "Twenty years of VERA: Towards a universal facility for accelerator mass spectrometry," Nucl. Phys. News **27**, 29–34.

Gosse, J. C., and F. M. Phillips, 2001, "Terrestrial *in situ* cosmogenic nuclides: Theory and application," Quat. Sci. Rev. **20**, 1475–1560.

Gove, H. E., 1978, Ed., *Proceedings of the First Conference on Radiocarbon Dating with Accelerators, Rochester, 1978*, https://phaidra.univie.ac.at/o:1624550.

Gove, H. E., 1999, *From Hiroshima to the Iceman: The Development and Applications of Accelerator Mass Spectrometry* (Institute of Physics Publishing, Bristol, England).

Gove, H. E., A. E. Litherland, and D. Elmore, 1987, Eds., *Proceedings of the Fourth International Symposium on Accelerator Mass Spectrometry, Rochester, 1987*, https://www.osti.gov/biblio/6950633.

Gove, H. E., K. H. Purser, and A. E. Litherland, 2010, "Accelerator mass spectrometry (AMS) 1977–1987," Nucl. Instrum. Methods Phys. Res., Sect. B **268**, xvii–xxii.

Granger, D. E., and P. F. Muzikar, 2001, "Dating sediment burial with *in situ*-produced cosmogenic nuclides: Theory, techniques, and limitations," Earth Planet. Sci. Lett. **188**, 269–281.

Graven, H. D., 2015, "Impact of fossil fuel emissions on atmospheric radiocarbon and various applications of radiocarbon over this century," Proc. Natl. Acad. Sci. U.S.A. **112**, 9542–9545.

Grimm, D., 2008, "The mushroom cloud's silver lining," Science **321**, 1434–1437.

Grimm, W., G. Herrmann, and H.-D. Schüssler, 1971, "Search for Superheavy Elements in Terrestrial Matter," Phys. Rev. Lett. **26**, 1040–1043.

Gruber, N., *et al.*, 2019, "The ocean sink for anthropogenic CO_2 from 1994 to 2007," Science **363**, 1193–1199.

Guilderson, T. P., P. J. Reimer, and T. A. Brown, 2005, "The boon and bane of radiocarbon dating," Science **307**, 362–364.

Gyürky, G., Z. Fülöp, F. Käppeler, G. G. Kiss, and A. Wallner, 2019, "The activation method for cross section measurements in nuclear astrophysics," Eur. Phys. J. A **55**, 1–31.

Hain, K., B. Deneva, T. Faestermann, L. Fimiani, J. M. Gomez-Guzman, D. Koll, G. Korschinek, P. Ludwig, V. Sergeyeva, and N. Thiolla, 2018, "AMS of ^{93}Zr: Passive absorber versus gas-filled magnet," Nucl. Instrum. Methods Phys. Res., Sect. B **423**, 42–48.

Hain, K., P. Steier, M. B. Froehlich, R. Golser, X. Hou, J. Lachner, T. Nomura, J. Qiao, F. Quinto, and A. Sakaguchi, 2020, "^{233}U/^{236}U signature allows to distinguish environmental emissions of civil nuclear industry weapons fallout," Nat. Commun. **11**, 1–3.

Hain, K., *et al.*, 2022, "Developing accelerator mass spectrometry capabilities for anthropogenic radionuclide analysis to extend the set of oceanographic tracers," Front. Mar. Sci. **9**, 837515.

Hajdas, I., P. Ascough, M. H. Garnett, S. J. Fallon, C. L. Pearson, G. Quarta, K. L. Spalding, H. Yamaguchi, and M. Yoneda, 2021, "Radiocarbon dating," Nat. Rev. Methods Primers **1**, 1–26.

Hakozaki, M., F. Miyake, T. Nakamura, K. Kimura, K. Masuda, and M. Okuno, 2018, "Verification of the annual dating of the 10th century Baitoushan Volcano eruption based on an AD 774–775 radiocarbon spike," Radiocarbon **60**, 261–268.

Halsted, C. T., P. R. Bierman, and G. Balco, 2021, "Empirical evidence for latitude and altitude variation of the *in situ* cosmogenic ^{26}Al/^{10}Be production ratio," Geosciences **11**, 402.

Hatori, S., H. Nawata, M. Ohseki, H. Matsuzaki, T. Misawa, and K. Kobayashi, 2000, "Gas-filled magnet at MALT-measurement of ^{36}Cl," Nucl. Instrum. Methods Phys. Res., Sect. B **172**, 211–217.

He, G., *et al.*, 2018, "Cross section measurement for the ^{93}Nb$(n,2n)^{92g}$Nb reaction at the neutron energy of 14.6 MeV by the AMS method," Chin. Phys. C **42**, 074002.

He, M., *et al.*, 2015, "Determination of cross sections of ^{60}Ni$(n,2n)^{59}$Ni induced by 14 MeV neutrons with accelerator mass spectrometry," Nucl. Instrum. Methods Phys. Res., Sect. B **361**, 517–520.

Heaton, T. J., *et al.*, 2020, "Marine20—The marine radiocarbon age calibration curve (0–55,000 cal BP)," Radiocarbon **62**, 779–820.

Hedges, R. E. M., R. A. Housley, C. R. Bronk, and G. J. van Klinken, 1992, "Radiocarbon dates from the Oxford AMS system: Archaeometry datelist 15," Archaeometry **34**, 337–357.

Heisenberg, W., 1932, "Über den Bau der Atomkerne. I," Z. Phys. **77**, 1–11.

Henning, W., W. A. Bell, P. J. Billquist, B. G. Glagola, W. Kutschera, Z. Liu, H. F. Lucas, M. Paul, K. E. Rehm, and J. L. Yntema, 1987, "Calcium-41 concentration in terrestrial materials: Prospects for dating of Pleistocene samples," Science **236**, 725–727.

Henning, W., W. Kutschera, R. K. Smither, and J. L. Yntema, 1981, Eds., *Proceedings of the Symposium on Accelerator Mass Spectroscopy, Argonne, IL, 1981*, https://phaidra.univie.ac.at/o:1624875.

Herzog, G. F., W. M. Caffee, and A. J. T. Jull, 2015, "Cosmogenic nuclides in Antarctic meteorites," in *35 Seasons of US Antarctic Meteorites (1976–2010): A Pictorial Guide to the Collection*, American Geophysical Union Special Publication Vol. 68, edited

by K. Righter, C. Corrigan, T. McCoy, and R. Harvey (Wiley, New York), pp. 153–172.

Herzog, G. F., and R. Wieler, 2014, "Cosmogenic nuclides in the inner Solar System: Surface exposure ages for Mars and asteroid 25143 Itokawa," Elements **10**, 335–336.

Hmiel, B., *et al.*, 2020, "Preindustrial $^{14}CH_4$ indicates greater anthropogenic fossil CH_4 emissions," Nature (London) **578**, 409–412.

Hoffman, D. C., F. O. Lawrence, J. L. Mewherter, and F. M. Rouke, 1971, "Detection of plutonium-244 in nature," Nature (London) **234**, 132–134.

Hogg, A. G., *et al.*, 2020, "SHCal20 Southern Hemisphere calibration, 0–50,000 years cal BP," Radiocarbon **62**, 759–778.

Horiuchi, K., I. Oniyanagi, H. Wasada, and H. Matsuzaki, 2013, "^{10}Be measurements at MALT using reduced-size samples of bulk sediments," Nucl. Instrum. Methods Phys. Res., Sect. B **294**, 72–76.

Hotchkis, M. A. C., D. P. Child, M. B. Froehlich, A. Wallner, K. Wilcken, and M. Williams, 2019, "Actinides AMS on the VEGA accelerator," Nucl. Instrum. Methods Phys. Res., Sect. B **438**, 70–76.

Huss, G. R., B. S. Meyer, G. Srinivasan, J. N. Goswami, and S. Sahijpal, 2009, "Stellar sources of the short-lived radionuclides in the early Solar System," Geochim. Cosmochim. Acta **73**, 4922–4945.

IPCC, 2021, "Sixth assessment report of the Intergovernmental Panel on Climate Change (2021/2022)," https://www.ipcc.ch/assessment-report/ar6/.

Ireland, T. R., 2013, "Recent developments in isotope-ratio mass spectrometry for geochemistry and cosmochemistry," Rev. Sci. Instrum. **84**, 011101.

Jiang, W., *et al.*, 2012, "An atom counter for measuring ^{81}Kr and ^{85}Kr in environmental samples," Geochim. Cosmochim. Acta **91**, 1–6.

Jöckel, P., M. G. Lawrence, and C. A. M. Brenninkmeijer, 1999, "Simulations of cosmogenic ^{14}CO using the three-dimensional atmospheric model MATCH: Effects of production distribution and the solar cycle," J. Geophys. Res. **104**, 11733–11743.

Johnson, R. R., D. Berkovits, E. Boaretto, Z. Gelbart, S. Ghelberg, O. Meirav, M. Paul, J. Prior, V. Sossi, and E. Venczel, 1994, "Calcium resorption from bone in a human studied by ^{41}Ca tracing," Nucl. Instrum. Methods Phys. Res., Sect. B **92**, 483–488.

Jörg, G., A. Amelin, K. Kossert, and C. Lierse von Gostomski, 2012, "Precise and direct determination of the half-life of ^{41}Ca," Geochim. Cosmochim. Acta **88**, 51–65.

Jouzel, J., *et al.*, 2007, "Orbital and millennial Antarctic climate variability over the past 800,000 years," Science **317**, 793–796.

Jull, A. J. T., 2006. "Terrestrial ages of meteorites," in *Meteorites and the Early Solar System II*, edited by D. S. Lauretta and H. Y. McSween, Jr. (University of Arizona Press, Tucson), pp. 889–905.

Jull, A. J. T., J. W. Beck, and G. S. Burr, 1997, Eds., *Proceedings of the Seventh International Conference on Accelerator Mass Spectrometry, Tucson, 1996* [Nucl. Instrum. Methods Phys. Res., Sect. B **123**, 1–612].

Jull, A. J. T., and G. S. Burr, 2006, "Accelerator mass spectrometry: Is the future big or small?," Earth Planet. Sci. Lett. **243**, 305–325.

Jull, A. J. T., S. Cloudt, D. J. Donahue, J. M. Sisterson, R. C. Reedy, and J. Masarik, 1998, "^{14}C depth profiles in Apollo 15 and 17 cores and lunar rock 68815," Geochim. Cosmochim. Acta **62**, 3025–3036.

Jull, A. J. T., D. J. Donahue, E. Cielaszyk, and F. Wlotzka, 1993, "^{14}C terrestrial ages and weathering of 27 meteorites from the Southern High Plains and adjacent areas (USA)," Meteoritics **28**, 188–195.

Jull, A. J. T., D. J. Donahue, and T. H. Zabel, 1983, "Target preparation for radiocarbon dating by tandem accelerator mass spectrometry," Nucl. Instrum. Methods Phys. Res. **218**, 509–514.

Jull, A. J. T., A. Feinberg, G. Kovaltsov, F. Mekhaldi, R. Muscheler, S. Poluianov, E. Rozanov, T. Sukhodolov, and I. G. Usoskin, 2020, "Cosmogenic isotopes as proxies for solar energetic particles," in *Extreme Solar Particle Storms: The Hostile Sun*, edited by F. Miyake, I. Usoskin, and S. Poluianov (Institute of Physics, London), Chap. 4, https://iopscience.iop.org/book/edit/978-0-7503-2232-4/chapter/bk978-0-7503-2232-4ch4.

Jull, A. J. T., L. R. McHargue, P. A. Bland, R. C. Greenwood, A. W. R. Bevan, K. J. Kim, M. D. Giscard, S. E. LaMotta, and J. A. Johnson, 2010, "Terrestrial ^{14}C and ^{14}C/^{10}Be ages of meteorites from the Nullarbor Plain, Australia," Meteorit. Planet. Sci. **45**, 1271–1283.

Jull, A. J. T., I. P. Panyushkina, T. E. Lange, V. V. Kukarskih, V. S. Myglan, K. J. Clark, M. W. Salzer, G. S. Burr, and S. W. Leavitt, 2014, "Excursions in the ^{14}C record at A.D. 774–775 in tree rings from Russia and America," Geophys. Res. Lett. **41**, 3004–3010.

Jull, A. J. T., I. P. Panyushkina, M. Molnár, T. Varga, L. Wacker, N. Brehm, E. Laszló, C. Baisan, M. W. Salzer, and W. Tegel, 2021, "Rapid ^{14}C excursion at 3372–3371 BCE not observed at two different locations," Nat. Commun. **12**, 712.

Jull, A. J. T., E. M. Scott, and P. Bierman, 2015, "The CRONUS-Earth intercomparison for cosmogenic analysis," Quat. Geochronol. **26**, 3–10.

Käppeler, F., R. Gallino, S. Bisterzo, and W. Aoki, 2011, "The *s* process: Nuclear physics, stellar models, and observations," Rev. Mod. Phys. **83**, 157–193.

Keeling, C. D., 1998, "Rewards and penalties of monitoring the Earth," Annu. Rev. Energy Environ. **23**, 25–82.

Keeling, R., 2008, "Recording Earth's vital signs," Science **319**, 1771.

Keller, A., *et al.*, 2012, "New insights into the Tyrolean iceman's origin and phenotype as inferred by whole-genome sequencing," Nat. Commun. **3**, 698.

Kelly, M. A., T. V. Lowell, P. J. Applegate, F. M. Phillips, J. M. Schaefer, C. A. Smith, H. Kim, K. C. Leonard, and A. Hudson, 2015 "A locally calibrated, late glacial ^{10}Be produced rate from a low-latitude, high-altitude site in the Peruvian Andes," Quat. Geochronol. **26**, 70–85.

Ketterer, M. E., and S. C. Szechenyi, 2008, "Determination of plutonium and other transuranic elements by inductively coupled plasma mass spectrometry: A historical perspective and new frontiers in the environmental sciences," Spectrochim. Acta B **63**, 719–737.

Kieser, W. E., I. D. Clark, C. A. Crann, X.-L. Zhao, and J. Gosse, 2020, Eds., *Proceedings of the Fourteenth International Conference on Accelerator Mass Spectrometry, Ottawa, 2017*, https://www.sciencedirect.com/journal/nuclear-instruments-and-methods-in-physics-research-section-b-beam-interactions-with-materials-and-atoms/special-issue/10C30FPLFD8.

Kim, Y. H., *et al.*, 2020, "Development of a gas-filled magnet for FIPPS phase II," Nucl. Instrum. Methods Phys. Res., Sect. B **463**, 269–271.

King, S. J., *et al.*, 1997, "The influence of dissolved silicate on the physiological chemistry of aluminium, studied in humans using tracer ^{26}Al and accelerator mass spectrometry," Nucl. Instrum. Methods Phys. Res., Sect. B **123**, 254–258.

Kinoshita, N., *et al.*, 2012, "A shorter ^{146}Sm half-life measured and implications for ^{146}Sm-^{142}Nd chronology in the Solar System," Science **335**, 1614–1617.

Kinoshita, N., *et al.*, 2023, "Retraction," Science **379**, 1307.

Kislinger, G., C. Steinhausen, M. Alvarez-Brückmann, C. Winklhofer, T.-H. Ittel, and E. Nolte, 1997, "Investigations of human aluminium biokinetics with ^{26}Al and AMS," Nucl. Instrum. Methods Phys. Res., Sect. B **123**, 259–265.

Klein, J., D. Fink, R. Middleton, K. Nishiizumi, and J. Arnold, 1991, "Determination of the half-life of ^{41}Ca from measurements of Antarctic meteorites," Earth Planet. Sci. Lett. **103**, 79–83.

Klouda, G. A., L. A. Currie, D. J. Donahue, A. J. T. Jull, and M. H. Naylor, 1986, "Urban atmospheric ^{14}CO and $^{14}CH_4$ measurements by accelerator mass spectrometry," Radiocarbon **28**, 625–633.

Knezovich, J., T. Brown, B. Buchholz, R. Finkel, T. Guilderson, M. Kashgarian, G. Nimz, T. Ognibene, S. Tumey, and J. Vogel, 2007, Eds., Proceedings of the Tenth International Conference on Accelerator Mass Spectrometry, Berkeley, 2005, https://www.sciencedirect.com/journal/nuclear-instruments-and-methods-in-physics-research-section-b-beam-interactions-with-materials-and-atoms/vol/259/issue/1.

Knie, K., T. Faestermann, and G. Korschinek, 1997, "AMS at the Munich gas-filled analyzing magnet system GAMS," Nucl. Instrum. Methods Phys. Res., Sect. B **123**, 128–131.

Knie, K., T. Faestermann, G. Korschinek, G. Rugel, W. Rühm, and C. Wallner, 2000, "High-sensitivity AMS for heavy nuclides at the Munich tandem accelerator," Nucl. Instrum. Methods Phys. Res., Sect. B **172**, 717–720.

Knie, K., G. Korschinek, T. Faestermann, E. A. Dorfi, G. Rugel, and A. Wallner, 2004, "^{60}Fe Anomaly in a Deep-Sea Manganese Crust and Implications for a Nearby Supernova Source," Phys. Rev. Lett. **93**, 171103.

Knie, K., G. Korschinek, T. Faestermann, C. Wallner, J. Scholten, and W. Hillebrandt, 1999, "Indication for Supernova Produced ^{60}Fe Activity on Earth," Phys. Rev. Lett. **83**, 18–21.

Koll, D., T. Faestermann, G. Korschinek, and A. Wallner, 2020, "Origin of recent interstellar ^{60}Fe on Earth," EPJ Web Conf. **232**, 02001.

Koll, D., G. Korschinek, T. Faestermann, J. M. Gómez-Guzmán, S. Kipfstuhl, S. Merchel, and J. M. Welch, 2019, "Interstellar ^{60}Fe in Antarctica," Phys. Rev. Lett. **123**, 072701.

Koll, D., *et al.*, 2019, "Recent developments for AMS at the Munich tandem accelerator," Nucl. Instrum. Methods Phys. Res., Sect. B **438**, 180–183.

Korschinek, G., T. Faestermann, K. Knie, and C. Schmidt, 1996, "^{60}Fe, a promising AMS isotope for many applications," Radiocarbon **38**, 68–69.

Korschinek, G., T. Faestermann, M. Poutivtsev, A. Arazi, K. Knie, G. Rugel, and A. Wallner, 2020, "Supernova-Produced ^{53}Mn on Earth," Phys. Rev. Lett. **125**, 031101.

Korschinek, G., and W. Kutschera, 2015, "Mass spectrometric searches for superheavy elements in terrestrial matter," Nucl. Phys. **A944**, 190–203.

Korschinek, G., *et al.*, 2010, "A new value for the half-life of ^{10}Be by heavy-ion elastic recoil detection and liquid scintillation counting," Nucl. Instrum. Methods Phys. Res., Sect. B **268**, 187–191.

Krohn, V. E., 1962, "Emission of negative ions from metal surfaces bombarded by positive cesium ions," J. Appl. Phys. **33**, 3523–3525.

Kubik, P. W., D. Elmore, T. K. Hemmick, and W. Kutschera, 1989, "The gas-filled magnet: An isobar separator for accelerator mass spectrometry," Nucl. Instrum. Methods Phys. Res., Sect. B **40–41**, 741–744.

Kuitems, M., A. Panin, A. Scifoa, I. Arzhantsevad, Y. Kononov, P. Doeve, A. Neocleous, and M. Dee, 2020, "Radiocarbon-based approach capable of subannual precision resolves the origins of the site of Por-Bajin," Proc. Natl. Acad. Sci. U.S.A. **117**, 14038–14041.

Kuitems, M., *et al.*, 2022, "Evidence for European presence in the Americas in AD 1021," Nature (London) **601**, 388–341.

Kutschera, W., 1983, "Accelerator mass spectrometry: From nuclear physics to dating," Radiocarbon **25**, 677–691.

Kutschera, W., 2005, "Progress in isotope analysis at ultra-trace level with AMS," Int. J. Mass Spectrom. **242**, 145–160.

Kutschera, W., 2013, "Applications of accelerator mass spectrometry," Int. J. Mass Spectrom. **349–350**, 203–218.

Kutschera, W., 2016, "Accelerator mass spectrometry: State of the art and perspectives," Adv. Phys. X **1**, 570–595.

Kutschera, W., 2018, "Applications of ^{14}C, the most versatile radionuclide to explore our world," in *The Euroschool on Exotic Beams*, Vol. 5, Lecture Notes in Physics Vol. 948, edited by C. Scheidenberger and M. Pfützner (Springer-Verlag, Heidelberg), pp. 1–30.

Kutschera, W., 2019, "The half-life of ^{14}C—Why is it so long?," Radiocarbon **61**, 1135–1142.

Kutschera, W., 2020, "On the enigma of dating the Minoan eruption of Santorini," Proc. Natl. Acad. Sci. U.S.A. **117**, 8677–8679.

Kutschera, W., 2022, "The versatile uses of the ^{14}C bomb peak," Radiocarbon **64**, 1295–1308.

Kutschera, W., 2023, "An overview of world-wide AMS facilities," Nucl. Instrum. Methods Phys. Res., Sect. B **538**, 87–94.

Kutschera, W., I. Ahmad, B. G. Glagola, R. C. Pardo, K. E. Rehm, D. Berkovits, M. Paul, J. R. Arnold, and K. Nishiizumi, 1993, "Accelerator mass spectrometry of ^{59}Ni in extraterrestrial matter," Nucl. Instrum. Methods Phys. Res., Sect. B **73**, 403–412.

Kutschera, W., R. Golser, A. Priller, and B. Strohmaier, 2000, Eds., *Proceedings of the Eighth International Conference on Accelerator Mass Spectrometry, Vienna, 1999* [Nucl. Instrum. Methods Phys. Res., Sect. B **172**, 1–977].

Kutschera, W., W. Henning, M. Paul, R. K. Smither, E. J. Stephenson, J. L. Yntema, D. E. Alburger, J. B. Cumming, and G. Harbottle, 1980, "Measurement of the ^{32}Si Half-Life via Accelerator Mass Spectrometry," Phys. Rev. Lett. **45**, 592–596.

Kutschera, W., and W. Müller, 2003, "Isotope language of the alpine iceman investigated with AMS and MS," Nucl. Instrum. Methods Phys. Res., Sect. B **204**, 705–719.

Kutschera, W., and M. Paul, 1990, "Accelerator mass spectrometry in nuclear physics and astrophysics," Annu. Rev. Nucl. Part. Sci. **40**, 411–438.

Kutschera, W., M. Paul, I. Ahmad, T. A. B. G. Glagola, R. Harkewicz, M. Hellstrom, K. E. Rehm, B. M. Sherrill, and M. Steiner, 1994, "Long-lived noble gas radionuclides," Nucl. Instrum. Methods Phys. Res., Sect. B **92**, 241–248.

Kutschera, W., *et al.*, 1989, "Studies towards a method for radiocalcium dating of bones," Radiocarbon **31**, 311–323.

Kutschera, W., *et al.*, 2014, "Evidence for early human presence at high altitudes in the Ötztal Alps (Austria/Italy)," Radiocarbon **56**, 923–947.

Lachner, J., I. Dillmann, T. Faestermann, G. Korschinek, M. Poutivtsev, and G. Rugel, 2008, "Search for long-lived isomeric states in neutron-deficient thorium isotopes," Phys. Rev. C **78**, 064313.

Lachner, J., I. Dillmann, T. Faestermann, G. Korschinek, M. Poutivtsev, G. Rugel, C. Liers von Gostomski, A. Türler, and U. Gerstmann, 2012 "Attempt to detect primordial ^{244}Pu on Earth," Phys. Rev. C **85**, 015801.

Lachner, J., M. Kasberger, M. Martschini, A. Priller, P. Steier, and R. Golser, 2015, "Developments towards detection of ^{135}Cs at VERA," Nucl. Instrum. Methods Phys. Res., Sect. B **361**, 440-444.

Lachner, J., C. Marek, M. Martschini, A. Priller, P. Steier, and R. Golser, 2019, "^{36}Cl in a new light: AMS measurements assisted by

ion-laser interaction," Nucl. Instrum. Methods Phys. Res., Sect. B **456**, 163–168.

Lachner, J., M. Martschini, A. Kalb, M. Kern, O. Marchhart, F. Plasser, A. Priller, P. Steier, A. Wieser, and R. Golser, 2021, "Highly sensitive ^{26}Al measurements by ion-laser-interaction mass spectrometry," Int. J. Mass Spectrom. **465**, 116576.

Lal, D., 1988, "*In situ*-produced cosmogenic isotopes in terrestrial rocks," Annu. Rev. Earth Planet. Sci. **16**, 355–388.

Lal, D., 1991, "Cosmic ray labeling of erosion surfaces: *In situ* nuclide production rates and erosion rates," Earth Planet. Sci. Lett. **104**, 424–439.

Lal, D., and B. Peters, 1967, "Cosmic ray produced radioactivity on the Earth," in *Encyclopedia of Physics*, Vol. 46, edited by K. Sitte (Springer-Verlag, Berlin), pp. 551–612.

Lal, R., L. K. Fifield, S. G. Tims, and R. J. Wasson, 2017, "^{239}Pu fallout across continental Australia: Implications on ^{239}Pu use as a soil tracer," J. Environ. Radioact. **178–179**, 394–403.

Lee, T., D. A. Papanastassiou, and G. J. Wasserburg, 1976a, "Demonstration of ^{26}Mg excess in Allende and evidence for ^{26}Al," Geophys. Res. Lett. **3**, 41–44.

Lee, T., D. A. Papanastassiou, and G. J. Wasserburg, 1976b, "Correction to 'Demonstration of ^{26}Mg excess in Allende and evidence for ^{26}Al,' " Geophys. Res. Lett. **3**, 109–112.

Lelieveld, J., *et al.*, 2006, "New directions: Watching over tropospheric hydroxyl (OH)," Atmos. Environ. **40**, 5741–5743.

Levin, I., S. Hammer, B. Kromer, S. Preunkert, R. Weller, and D. E. Worthy, 2022, "Radiocarbon in global tropospheric carbon dioxide," Radiocarbon **64**, 781–791.

Levin, I., and V. Hesshaimer, 2000, "Radiocarbon—A unique tracer of global carbon cycle dynamics," Radiocarbon **42**, 69–80.

Levin, I., T. Naegler, B. Kromer, M. Diehl, R. J. Francey, A. J. Gomez-Pelaet, L. P. L. Steele, D. Wagenbach, R. Weller, and D. E. Worthy, 2010, "Observations and modelling of the global distribution and long-term trend of atmospheric $^{14}CO_2$," Tellus B **62**, 26–46.

Leya, I., *et al.*, 2020, "^{53}Mn and ^{60}Fe in iron meteorites—New data and model calculations," Meteorit. Planet. Sci. **55**, 818–831.

Libby, W. F., E. C. Anderson, and J. R. Arnold, 1949, "Age determination by radiocarbon content: World-wide assay of natural radiocarbon," Science **109**, 227–228.

Lifton, N., *et al.*, 2015, "*In situ* cosmogenic nuclide production rate calibration for the CRONUS-Earth Project from Lake Bonneville, Utah, shoreline features," Quat. Geochronol. **26**, 56–69.

Litherland, A. E., 1980, "Ultrasensitive mass spectrometry with accelerators," Annu. Rev. Nucl. Part. Sci. **30**, 437–473.

Litherland, A. E., 2021 (private communication).

Litherland, A. E., R. P. Beukens, L. R. Kilius, J. C. Rucklidge, H. E. Gove, D. Elmore, and K. H. Purser, 1981, "Ultra-sensitive mass spectrometry with tandem accelerators," Nucl. Instrum. Methods Phys. Res. **186**, 463–477.

Litherland, A. E., I. Tomski, X. L. Zhao, L. M. Cousins, J. P. Doupé, G. Javahery, and W. E. Kieser, 2007, "Isobar separation at very low energy for AMS," Nucl. Instrum. Methods Phys. Res., Sect. B **259**, 230–235.

Litherland, A E., X.-L. Zhao, and W. E. Kieser, 2011, "Mass spectrometry with accelerators," Mass Spectrom. Rev. **30**, 1037–1072.

Liu, Y., J. R. Beene, C. C. Havener, and J. F. Liang, 2005, "Isobar suppression by photodetachment in a gas-filled rf quadrupole ion guide," Appl. Phys. Lett. **87**, 113504.

Loosli, H. H., and H. Oeschger, 1968, "Detection of ^{39}Ar in atmospheric argon," Earth Planet. Sci. Lett. **5**, 191–198.

Loosli, H. H., H. Oeschger, and W. Wiest, 1970, "Argon 37, argon 39, and krypton 81 in the atmosphere and tracer studies based on these isotopes," J. Geophys. Res. **75**, 2895–2900.

Los Alamos National Laboratory, 2017, "Los Alamos National Laboratory periodic table of elements," https://periodic.lanl.gov/index.shtml.

Losiak, A., A. Joeleht, J. Plado, M. Szyszka, K. Kirsomäe, E. M. Wild, P. Steier, C. M. Belcher, A. M. Jazwa, and R. Helde, 2020, "Determining the age and possibility for an extraterrestrial impact formation mechanism of the Ilumetsa structures (Estonia)," Meteorit. Planet. Sci. **55**, 274–293.

Losiak, A., E. M. Wild, L. Michlmayr, and C. Koeberl, 2013, "^{10}Be content in suevite breccia from the Bosumtwi impact crater," Geophys. Res. Abstr. **15**, EGU2013-6381, https://meetingorganizer.copernicus.org/EGU2013/EGU2013-6381.pdf.

Love, S. G., and D. Brownlee, 1994, "Peak atmospheric entry temperatures of micrometeorites," Meteoritics **29**, 69–71.

Lu, Z.-T., 2016, "Radiokrypton dating coming of age," Natl. Sci. Rev. **3**, 172–173.

Lu, Z.-T., 2022, "A primer on atom trap trace analysis (ATTA)," https://atta.ustc.edu.cn/en-us/events/attaprimer_publication.html.

Lu, Z.-T., *et al.*, 2014, "Tracer applications of noble gas radionuclides in the geosciences," Earth-Sci. Rev. **138**, 196–214.

Ludwig, P., T. Faestermann, G. Korschinek, G. Rugel, I. Dillmann, L. Fimiani, S. Bishop, and P. Kumar, 2012, "Search for superheavy elements with $292 \leq A \geq 310$ in nature with accelerator mass spectrometry," Phys. Rev. C **85**, 024315.

Ludwig, P., *et al.*, 2016, "Time-resolved 2-million-year-old supernova activity discovered in Earth's micro-fossil record," Proc. Natl. Acad. Sci. U.S.A. **113**, 9232–9237.

Ludwig, P., *et al.*, 2017, "Measurement of the stellar $^{58}\mathrm{Ni}(n,\gamma)^{59}\mathrm{Ni}$ cross section with accelerator mass spectrometry," Phys. Rev. C **95**, 035803.

Lugaro, M., A. Heger, D. Osrin, S. Goriely, K. Zuber, A. I. Karakas, B. K. Gibson, C. L. Doherty, J. C. Lattanzio, and U. Ott, 2014, "Stellar origin of the ^{182}Hf cosmochronometer and the presolar history of Solar System matter," Science **345**, 650–653.

Lupker, M., P.-H. Blard, J. Lavé, C. France-Lanord, L. Leanni, N. Puchol, J. Charreau, and D. Bourlès, 2012, "^{10}Be-derived Himalayan denudation rates and sediment budgets in the Ganga basin," Earth Planet. Sci. Lett. **333–334**, 146–156.

Maher, S., F. P. M. Jjunju, and S. Taylor, 2015, "Colloquium: 100 years of mass spectrometry: Perspectives and future trends," Rev. Mod. Phys. **87**, 113–135.

Manning, S. W., B. Kromer, M. Cremaschi, M. W. Dee, R. Friedrich, C. Griggs, and C. S. Hadden, 2020, "Mediterranean radiocarbon offsets and calendar dates for prehistory," Sci. Adv. **6**, eaoz1096.

Marin-Lambarri, D. J., *et al.*, 2020, "Measurement of the thermal neutron capture cross section by ^{9}Be using the neutron flux from a nuclear research reactor and the AMS technique," Phys. Rev. C **102**, 044601.

Marinov, A., A. Pape, D. Kolb, L. Halicz, I. Segal, N. Tepliakov, and R. Brandt, 2011, "Enrichment of superheavy element roentgenium (Rg) in natural Au," Int. J. Mod. Phys. E **20**, 2391–2401.

Marinov, A., I. Rodushkin, Y. Kashiv, L. Halicz, I. Segal, A. Pape, R. V. Gentry, H. W. Miller, D. Kolb, and R. Brandt, 2007, "Existence of long-lived isomeric states in naturally-occurring neutron-deficient Th isotopes," Phys. Rev. C **76**, 021303.

Marinov, A., I. Rodushkin, D. Kolb, A. Pape, Y. Kashiv, R. Brandt, R. V. Gentry, and H. W. Miller, 2010, "Evidence fort he possible existence of a long-lived superheavy nucleus with atomic mass number $A = 292$ and atomic number $Z = 122$ in natural Th," Int. J. Mod. Phys. E **19**, 131–140.

Marinov, A., I. Rodushkin, A. Pape, Y. Kashiv, D. Kolb, R. Brandt, R. V. Gentry, H. W. Miller, L. Halicz, and I. Segal, 2009, "Existence of long-lived isotopes of a superheavy element in natural Au," Int. J. Mod. Phys. E **18**, 621–629.

Maris, P., J. P. Vary, P. Navrátil, W. E. Ormand, H. Nam, and D. J. Dean, 2011, "Origin of the Anomalous Long Lifetime of ^{14}C," Phys. Rev. Lett. **106**, 202502.

Marom, A., J. S. O. McCullagh, T. F. G. Higham, and R. E. M. Hedges, 2013, "Hydroxyproline dating: Experiments on the ^{14}C analysis of contaminated and low-collagen bones," Radiocarbon **55**, 698–708.

Marrero, S. M., F. M. Phillips, B. Borchers, N. Lifton, R. Aumer, and G. Balco, 2016, "Cosmogenic nuclide systematics and the `CRONUScalc` program," Quat. Geochronol. **31**, 160–187.

Martschini, M., L. K. Fifield, M. B. Froehlich, G. Leckenby, S. Pavetich, S. G. Tims, B. Tranter, and A. Wallner, 2019, "New and upgraded ionization chambers for AMS at the Australian National University," Nucl. Instrum. Methods Phys. Res., Sect. B **438**, 141–147.

Martschini, M., D. Hanstorp, J. Lachner, C. Marek, A. Priller, P. Steier, P. Wasserburger, and R. Golser, 2019, "The ILIAMS project—An RFQ ion beam cooler for selective laser photodetachment at VERA," Nucl. Instrum. Methods Phys. Res., Sect. B **456**, 213–217.

Martschini, M., J. Lachner, S. Merchel, A. Priller, P. Steier, A. Wallner, A. Wieser, and R. Golser, 2020, "The quest for AMS of ^{182}Hf—Why poor gas gives pure beams," EPJ Web Conf. **232**, 02003.

Martschini, M., *et al.*, 2017, "Selective laser photodetachment of intense atomic and molecular negative ion beams with the ILIAS RFQ ion beam cooler," Int. J. Mass Spectrom. **415**, 9–17.

Martschini, M., *et al.*, 2022, "5 years of ion-laser interaction mass spectrometry—Status and prospects of isobar suppression in AMS by lasers," Radiocarbon **64**, 555–568.

Masarik, J., and R. C. Reedy, 1994, "Effects of bulk composition on nuclide production processes in meteorites," Geochim. Cosmochim. Acta **58**, 5307–5317.

Massey, H. S. W., 1950, in *Negative Ions*, edited by N. Feather and D. Shoenberg(Cambridge University Press, Cambridge, England).

McAninch, J. E., L. J. Hainsworth, A. A. Marchetti, M. R. Leivers, P. R. Jones, A. E. Dunlop, R. Mauthe, J. S. Vogel, I. D. Proctor, and T. Straume, 1997, "Measurement of ^{63}Ni and ^{59}Ni by accelerator mass spectrometry using characteristic projectile x-rays," Nucl. Instrum. Methods Phys. Res., Sect. B **123**, 137–143.

McHargue, L. R., P. E. Damon, and D. J. Donahue, 1995, "Enhanced cosmic-ray production of ^{10}Be coincident with the Mono Lake and Laschamp geomagnetic excursions," Geophys. Res. Lett. **22**, 659–662.

McNichol, A. P., R. J. Schneider, K. F. von Reden, A. R. Gagnon, K. L. Elder, R. M. Key, and P. D. Quay, 2000, "Ten years after—The WOCE AMS radiocarbon program," Nucl. Instrum. Methods Phys. Res., Sect. B **172**, 479–484.

Medley, P., S. G. Tims, M. B. Froehlich, L. K. Fifield, A. Bollhöfer, A. Wallner, and S. Pavetich, 2019, "Development of ^{231}Pa AMS measurements to improve radiological dose assessment from uranium mining and milling," Nucl. Instrum. Methods Phys. Res., Sect. B **438**, 66–69.

Meier, M. M. M., *et al.*, 2014, "A precise cosmic-ray exposure age for an olivine grain from the surface of near-Earth asteroid (25143) Itokawa," Lunar Planet. Sci. **45**, 1247, https://ui.adsabs.harvard.edu/abs/2014LPI....45.1247M/abstract.

Meinshausen, M., *et al.*, 2017, "Historical greenhouse gas concentrations for climate modelling (CMIP6)," Geosci. Model Dev. **10**, 2057–2116.

Mekhaldi, F., *et al.*, 2015, "Multiradionuclide evidence for the solar origin of the cosmic-ray events of AD 774/5 and 993/4," Nat. Commun. **6**, 8611.

Meldner, H., 1966, "Prediction of new magic regions and masses for super-heavy nuclei from calculations with realistic shell model single particle Hamiltonians," in *Proceedings of Why and How Should We Investigate Nucleides Far Off the Stability Line?, Lysekil, Sweden, 1966*, https://escholarship.org/uc/item/28q2j00w.

Meldner, H., 1969, "Realistic nuclear single particle Hamiltonians and the proton shell 114," Phys. Rev. **178**, 1815–1826.

Michel, R., 1999, "Long-lived radionuclides as tracers in terrestrial and extraterrestrial matter," Radiochim. Acta **87**, 47–73.

Middleton, R., 1983, "A versatile high intensity negative ion source," Nucl. Instrum. Methods Phys. Res. **214**, 139–150.

Middleton, R., 1984a, "A review of ion sources for accelerator mass spectrometry," Nucl. Instrum. Methods Phys. Res., Sect. B **5**, 193–199.

Middleton, R., 1984b, "A versatile high intensity negative ion source," Nucl. Instrum. Methods Phys. Res. **220**, 105–106.

Middleton, R., D. Fink, J. Klein, and P. Sharma, 1989, "^{41}Ca concentration in modern bone and their implications for dating," Radiocarbon **31**, 305–310.

Milanković, M., 1941, *Kanon der Erdbestrahlung und seine Anwendung auf das Eiszeitenproblem* (Königliche Serbische Akademie, Belgrade); English translation, Milanković, M., *Canon of Insolation and the Ice-Age Problem* (Zavod za udžbenike i nastavna sredstva, Belgrade, 1998), p. 634.

Miyake, F., K. Masuda, and T. Nakamura, 2013, "Another rapid event in the carbon-14 content of tree rings," Nat. Commun. **4**, 1748.

Miyake, F., K. Nagaya, K. Masuda, and T. Nakamura, 2012, "A signature of cosmic-ray increase in AD 774–775 from tree rings in Japan," Nature (London) **486**, 240–242.

Miyake, F., *et al.*, 2021, "A single-year cosmic ray event at 5410 BCE registered in ^{14}C of tree rings," Geophys. Res. Lett. **48**, e2021GL093419.

Molnár, M., *et al.*, 2021, "Gas ion source performance of the EnviroMICADAS at HEKAL Laboratory, Debrecen, Hungary," Radiocarbon **63**, 499–511.

Morgenstern, U., L. K. Fifield, S. G. Tims, and R. G. Ditchburn, 2010, "Progress in AMS measurement of natural ^{32}Si for glacier dating," Nucl. Instrum. Methods Phys. Res., Sect. B **268**, 739–743.

Mueller, D., B. Bante, T. Faestermann, A. Gillitzer, H. J. Körner, G. Korschinek, and U. Bittner, 1992, "Accelerator mass spectrometry with a gas-filled magnetic spectrograph," Nucl. Instrum. Methods Phys. Res., Sect. B **68**, 313–318.

Muirhead, B. K., A. Nicholas, and J. Umland, 2020, "Mars sample return mission concept status," in *Proceedings of the 2020 IEEE Aerospace Conference, Big Sky, MT, 2020* (IEEE, New York), pp. 1–8, https://ieeexplore.ieee.org/stamp/stamp.jsp?tp=&arnumber=9172609.

Muller, R. A., 1977, "Radioisotope dating with a cyclotron: The sensitivity of radioisotope dating is improved by counting atoms rather than decays," Science **196**, 489–494.

Muller, R. A., 1979, "Radioisotope dating with accelerators," Phys. Today, No. 2, **32**, 23–30.

Muller, R. A., 2010, "Submarines, quarks, and radioisotope dating," Radiocarbon **52**, 209–218.

Muller, R. A., L. W. Alvarez, W. R. Holley, and E. J. Stephenson, 1977, "Quarks with unit charge: A search for anomalous hydrogen," Science **196**, 521–523.

Müller, A. M., M. Christl, J. Lachner, M. Suter, and H.-A. Synal, 2010, "Competitive ^{10}Be measurements below 1 MeV with the

upgraded ETH-TANDY AMS facility," Nucl. Instrum. Methods Phys. Res., Sect. B **268**, 2801–2807.

Müller, W., H. Fricke, A. N. Halliday, M. T. McCulloch, and J.-A. Wartho, 2003, "Origin and migration of the alpine iceman," Science **302**, 862–866.

Myers, W. D., and W. J. Swiatecki, 1966, "Nuclear masses and deformations," Nucl. Phys. **81**, 1–60.

Nakamura, T., K. Kobayashi, H. Matsuzaki, M. Murayama, Y. Nagashima, H. Oda, Y. Shibita, T. Tanaka, and M. Furukawa, 2004, Eds., Proceedings of the Ninth International Conference on Accelerator Mass Spectrometry, Nagoya, Japan, 2002, https://www.sciencedirect.com/journal/nuclear-instruments-and-methods-in-physics-research-section-b-beam-interactions-with-materials-and-atoms/vol/223/suppl/C.

Nassar, H., *et al.*, 2004, "Production and isobaric separation of ^{63}Ni ions for determination of the ^{62}Ni$(n,\gamma)^{63}$Ni reaction cross section at stellar temperatures," Nucl. Phys. **A746**, 613–616.

Nassar, H., *et al.*, 2005, "Stellar (n,γ) Cross Section of ^{62}Ni," Phys. Rev. Lett. **94**, 092504.

Nelson, D. E., 2010, "Personal recollections of a good experiment," Radiocarbon **52**, 219–227.

Nelson, D. E., R. G. Korteling, and W. R. Stott, 1977, "Carbon-14: Direct detection at natural concentrations," Science **198**, 507–508.

Nesaraja, C. D., 2017, "Nuclear data sheets for $A = 244$," Nucl. Data Sheets **146**, 387–510.

Newton, D., and R. J. Talbot, 2012, "Long-term retention of injected aluminium-26," Hum. Exp. Toxicol. **31**, 1195–1198.

Nicholls, Z. *et al.*, 2021, "Reduced complexity model intercomparison project phase 2: Synthesizing Earth system knowledge for probabilistic climate projections," Earth's Future **9**, e2020EF001900, https://agupubs.onlinelibrary.wiley.com/doi/10.1029/2020EF001900.

Nilsson, S. G., S. G. Thompson, and C. F. Tsang, 1969, "Stability of superheavy nuclei and their possible occurrence in nature," Phys. Lett. **28B**, 458–461.

Nisbert, E., 2007, "Cinderella science," Nature (London) **450**, 789–790.

Nisbet, E. G., *et al.*, 2016, "Rising atmospheric methane: 2007–2014 growth and isotopic shift," Global Biogeochem. Cycles **30**, 1356–1370.

Nishiizumi, K., J. R. Arnold, C. P. Kohl, M. W. Caffee, J. Masarik, and R. C. Reedy, 2009, "Solar cosmic ray records in lunar rock 64455," Geochim. Cosmochim. Acta **73**, 2163–2176.

Nishiizumi, K., M. W. Caffee, and K. C. Welten, 2015, "Measurements of cosmogenic radionuclides in a Hayabusa sample," Lunar Planet. Sci. **46**, 2499, https://www.hou.usra.edu/meetings/lpsc2015/pdf/2499.pdf.

Nishiizumi, K., C. P. Kohl, J. R. Arnold, J. Klein, D. Fink, and R. Middleton, 1991, "Cosmic ray produced ^{10}Be and ^{26}Al in Antarctic rocks: Exposure and erosion history," Earth Planet. Sci. Lett. **104**, 440–454.

Nishiizumi, K., C. P. Kohl, E. M. Shoemaker, J. R. Arnold, J. Klein, and R. Middleton, 1991, "*In situ* ^{10}Be–^{26}Al exposure ages at Meteor Crater, Arizona," Geochim. Cosmochim. Acta **55**, 2699–2703.

Nishiizumi, K., E. L. Winterer, C. P. Kohl, J. Klein, R. Middleton, D. Lal, and J. R. Arnold, 1989 "Cosmic ray production rates of ^{10}Be and ^{26}Al in quartz from glacially polished rocks," J. Geophys. Res. **94**, 17907–17915.

Nix, J. R., 1972, "Calculation of fission barriers for heavy and superheavy nuclei," Annu. Rev. Nucl. Sci. **22**, 65–120.

Nusair, O., *et al.*, 2016, "Accelerator mass spectrometry in laboratory nuclear astrophysics," J. Phys. Conf. Ser. **665**, 012076.

Oeschger, H., J. Houtermans, H. Loosli, and M. Wahlen, 1970, "The constancy of cosmic radiation from isotope studies in meteorites and the Earth," in *Proceedings of the 12th Nobel Symposium on Radiocarbon Variations and Absolute Chronology, Uppsala, Sweden, 1969*, edited by I. U. Olsson (John Wiley & Sons, New York), pp. 471–498.

Oganessian, Y. T., *et al.*, 2012, "Production and Decay of the Heaviest Nuclei ^{293,294}117 and ^{294}118," Phys. Rev. Lett. **109**, 162501.

Olsen, A. *et al.*, 2019, "GLODAPv2.2019—An update of GLODAPv2," Earth Syst. Sci. Data **11**, 1437–1461.

Olsen, A., *et al.*, 2020, "An updated version of the global interior ocean biochemical data product, GLODAPv2.2020," Earth Syst. Sci. Data **12**, 3653–3678.

Oppenheimer, C., *et al.*, 2017 "Multi-proxy dating the 'millennium eruption' of Changbaishan to late 946 CE," Quat. Sci. Rev. **158**, 164–171.

Paleari, C. I., *et al.*, 2022, "Cosmogenic radionuclides reveal an extreme solar particle storm near a solar minimum 9125 years BP," Nat. Commun. **13**, 214.

Park, J., J. Southon, S. Fahrni, P. P. Creasman, and R. Mewaldt, 2017, "Relationship between solar activity and Δ^{14}C peaks in AD 775, AD 994, and 660 BC," Radiocarbon **59**, 1147–1156.

Paul, M., I. Ahmad, and W. Kutschera, 1991, "Half-life of ^{41}Ca," Z. Phys. A **340**, 249–254.

Paul, M., D. Berkovits, L. D. Cecil, H. Feldstein, A. Hershkovitz, Y. Kashiv, and S. Vogt, 1997, "Environmental ^{90}Sr measurements," Nucl. Instrum. Methods Phys. Res., Sect. B **123**, 394–399.

Paul, M., B. C. Glagola, W. Henning, J. G. Keller, W. Kutschera, Z. Liu, K. E. Rehm, B. Schneck, and R. Siemssen, 1989, "Heavy ion separation with a gas-filled magnetic spectrograph," Nucl. Instrum. Methods Phys. Res., Sect. A **277**, 418–430.

Paul, M., W. Henning, W. Kutschera, E. J. Stephenson, and J. L. Yntema, 1980, "Measurement of the ^{26}Mg$(p,n)^{26}$Al$g(7.2\times10^5\ \mathrm{yr})$ cross section via accelerator mass spectrometry," Phys. Lett. **94B**, 303–306.

Paul, M., R. C. Pardo, P. Collon, W. Kutschera, K. E. Rehm, R. Scott, and R. C. Vondrasek, 2019, "Positive-ion accelerator mass spectrometry at atlas: Peaks and pits," Nucl. Instrum. Methods Phys. Res., Sect. B **456**, 222–229.

Paul, M., *et al.*, 2001, "Experimental limit to interstellar ^{244}Pu abundance," Astrophys. J. **558**, L133–L135.

Pavetich, S., *et al.*, 2014, "Interlaboratory study of the ion source memory effect in ^{36}Cl accelerator mass spectrometry," Nucl. Instrum. Methods Phys. Res., Sect. B **329**, 22–29.

Pavetich, S., *et al.*, 2019a, "^{93}Zr developments at the heavy ion accelerator facility at ANU," Nucl. Instrum. Methods Phys. Res., Sect. B **438**, 77–83.

Pavetich, S., *et al.*, 2019b, "Accelerator mass spectrometry measurement of the reaction ^{35}Cl$(n,\gamma)^{36}$Cl at keV energies," Phys. Rev. C **99**, 015801.

Pavetich, S., *et al.*, 2022, "Accelerator mass spectrometry measurements of ^{93}Zr for astrophysical and nuclear technology applications," Nucl. Instrum. Methods Phys. Res., Sect. B **527**, 45–51.

Pavicevic, M. K., G. Amthauer, V. Cvetkovic, B. Boev, V. Pejovic, W. F. Henning, F. Bosch, Y. A. Litvinov, and R. Wagner, 2018, "Lorandite from Allchar as geochemical detector for pp-solar neutrinos," Nucl. Instrum. Methods Phys. Res., Sect. A **895**, 62–73.

Pearson, C., M. Salzer, L. Wacker, P. Brewer, A. Sookdeod, and P. Kuniholm, 2020, "Securing timelines in the ancient Mediterranean using multiproxy annual tree-ring data," Proc. Natl. Acad. Sci. U.S.A. **117**, 8410–8415.

Pearson, C. L., P. W. Brewer, D. Brown, T. J. Heaton, G. W. L. Hodgins, A. J. T. Jull, T. Lange, and M. W. Salzer, 2018, "Annual

radiocarbon record indicates 16th century BCE date for the Thera eruption," Sci. Adv. **4**, eaar8241.

Perrier, C., and E. Segrè, 1937, "Some chemical properties of element 43," J. Chem. Phys. **5**, 712–716.

Perrier, C., and E. Segrè, 1947, "Technetium: The element of atomic number 43," Nature (London) **159**, 24.

Petrenko, V. V., *et al.*, 2016, "Measurements of ^{14}C in ancient ice from Taylor Glacier, Antarctica constrain *in situ* cosmogenic $^{14}CH_4$ and ^{14}CO production rates," Geochim. Cosmochim. Acta **177**, 62–77.

Petrunin, V. V., H. H. Andersen, P. Balling, and T. Andersen, 1996, "Structural Properties of the Negative Calcium Ion: Binding Energies and Fine-Structure Splitting," Phys. Rev. Lett. **76**, 744–747.

Phillips, F. M., *et al.* 2016a, The CRONUS-Earth Project: A synthesis," Quat. Geochronol. **31**, 119–154.

Phillips, F. M., *et al.*, 2016b, "Where now? Reflections on future directions for cosmogenic nuclide research from the CRONUS projects," Quat. Geochronol. **31**, 155–159.

Poluianov, S., G. A. Kovaltsov, A. L. Mishev, and I. G. Usoskin, 2016, "Production of cosmogenic isotopes ^{7}Be, ^{10}Be, ^{14}C, ^{22}Na and ^{36}Cl in the atmosphere: Altitudinal profiles of yield functions," J. Geophys. Res. Atmos. **121**, 8125–8136.

Purser, K. H., R. B. Liebert, A. E. Litherland, R. P. Beukens, H. E. Gove, C. L. Bennet, H. R. Clover, and W. E. Sondheim, 1977, "An attempt to detect stable N− ions from a sputter ion source and some implications of the results on the design of tandems for ultra-sensitive carbon analysis," Rev. Phys. Appl. **12**, 1487–1492.

Purser, K. H., and A. E. Litherland, 2020, "Accelerator mass spectrometry: A remarkable week in May 1977," Nucl. Instrum. Methods Phys. Res., Sect. B **479**, 254–263.

Purtschert, R., *et al.*, 2021, "Underground production of ^{81}Kr detected in subsurface fluids," Geochim. Cosmochim. Acta **295**, 65–79.

Putnam, A. E., J. M. Schaefer, G. H. Denton, D. J. A. Barrell, R. C. Finkel, B. G. Andersen, R. Schwartz, T. J. H. Chinn, and A. M. Doughty, 2012, "Regional climate control of glaciers in New Zealand and Europe during the pre-industrial Holocene," Nat. Geosci. **5**, 627–630.

Quiles, A., *et al.*, 2016, "A high-precision chronological model for the decorated Upper Paleolithic cave of Chauvet-Pont d'Arc, Ardèche, France," Proc. Natl. Acad. Sci. U.S.A. **113**, 4670–4675.

Quinto, F., *et al.*, 2019, "Ultratrace determination of ^{99}Tc in small natural water samples by accelerator mass spectrometry with the gas-filled analyzing magnet system," Anal. Chem. **91**, 4585–4591.

Rahmstorf, S., 2002, Ocean circulation and climate during the past 120,000 years, Nature (London) **419**, 207–214.

Raisbeck, G. M., and F. Yiou, 1979, "Possible use of ^{41}Ca for radioactive dating," Nature (London) **277**, 42–44.

Raisbeck, G. M., and F. Yiou, 1980, "Progress report on the possible use of ^{41}Ca for radioactive dating," Rev. Archaeom. **4**, 121–125, https://www.persee.fr/doc/arsci_0399-1237_1980_num_4_1_1118.

Raisbeck, G. M., F. Yiou, D. Bourles, C. Loriuss, J. Jouzel, and N. I. Barkov, 1987, "Evidence for two intervals of enhanced ^{10}Be deposition in Antarctic ice during the last glacial period," Nature (London) **326**, 273–277.

Raisbeck, G. M., F. Yiou, D. Bourlès, J. Lestringuez, and D. Deboffle, 1984, "Measurement of ^{10}Be with a tandetron accelerator operating at 2 MV," Nucl. Instrum. Methods Phys. Res., Sect. B **5**, 175–178.

Raisbeck, G. M., F. Yiou, M. Fruneau, and J. M. Loiseaux, 1978, "Beryllium-10 mass spectrometry with a cyclotron," Science **202**, 215–217.

Raisbeck, G. M., F. Yiou, J. Jouzel, J. R. Petit, N. I. Barkov, and E. Bard, 1992, "^{10}Be deposition at Vostok, Antarctica during the last 50,000 years and its relationship to possible cosmogenic production variations during this period," in *The Last Deglaciation: Absolute and Radiocarbon Chronologies*, NATO ASI, Series I, Vol. 12, edited by E. Bard and W. S. Broecker (Springer-Verlag, New York), pp. 127–139.

Raisbeck, G. M., F. Yiou, A. Peghaire, J. Quillot, and J. Uzureau, 1981, "Instability of KH_3^- and potential implications for detection of ^{41}Ca with a tandem electrostatic accelerator," in *Proceedings of the Second International Conference on Accelerator Mass Spectroscopy, Argonne, IL, 1981*, edited by W. Henning, W. Kutschera, R. K. Smither, and J. L. Yntema (Argonne National Laboratory Report No. ANL/PHY 81-1), pp. 426–430, https://phaidra.univie.ac.at/o:1624875.

Raisbeck, G. M., F. Yiou, and C. Stephan, 1979, "^{26}Al measurement with a cyclotron," J. Phys. (Paris), Lett. **40**, 241–244.

Raisbeck, G. M., *et al.*, 2017, "An improved north-south synchronization of ice core records around the 41 kyr ^{10}Be peak," Clim. Past **13**, 217–229.

Ram, R., *et al.*, 2021, "Controls on the ^{36}Cl/Cl input ratio of paleo-groundwater in arid environments: New evidence from ^{81}Kr/Kr data," Sci. Total Environ. **762**, 144106.

Reimer, P. J., *et al.*, 2020, "The Intcal20 Northern Hemisphere radiocarbon age calibration curve (0–55 cal kBP)," Radiocarbon **62**, 725–757.

Renfrew, C., and P. Bahn, 2020, *Archaeology: Theories, Methods and Practice*, (Thames & Hudson, London), p. 672.

Renne, P. R., A. L. Deino, F. J. Hilgen, K. F. Kuiper, D. F. Mark, W. S. Mitchell III., L. E. Morgan, R. Mundil, and J. Smit, 2013, "Time scales of critical events around the Cretaceous-Paleogene boundary," Science **339**, 684–687.

Renne, P. R., W. D. Sharp, A. L. Deino, G. Orsi, and L. Civetta, 1997, "^{40}Ar/^{39}Ar dating into the historical realm: Calibration against Pliny the Younger," Science **277**, 1279–1280.

Reza, G., *et al.*, 2020, "AMS cross-section measurement for the ^{28}Si$(d,\alpha)^{26}$Al reaction near the Coulomb barrier," Eur. Phys. J. Plus **135**, 899.

Ritterbusch, F., S. Ebser, J. Welte, T. Reichel, A. Kersting, R. Purtschert, W. Aeschbach-Hertig, and M. K. Oberthaler, 2014, "Groundwater dating with atom trap trace analysis of ^{39}Ar," Geophys. Res. Lett. **41**, 6758–6764.

Ritterbusch, F., *et al.*, 2022, "A Tibetan ice core covering the past 1,300 years radiometrically dated with ^{39}Ar," Proc. Natl. Acad. Sci. U.S.A. **119**, e2200835119.

Rom, W., *et al.*, 2000, "A detailed 2-year record of atmospheric ^{14}CO in the temperate Northern Hemisphere," Nucl. Instrum. Methods Phys. Res., Sect. B **161–163**, 780–785.

Ruff, M., S. Szidat, H. W. Gäggeler, M. Suter, H.-A. Synal, and L. Wacker, 2010, "Gaseous radiocarbon measurements of small samples," Nucl. Instrum. Methods Phys. Res., Sect. B **268**, 790–794.

Rugel, G., I. Dillmann, T. Faestermann, M. Heil, F. Käppeler, K. Knie, G. Korschinek, W. Kutschera, M. Poutivtsev, and A. Wallner, 2007, "Measurement of (n,γ) reaction cross sections at stellar energies for ^{58}Ni and ^{78}Se," Nucl. Instrum. Methods Phys. Res., Sect. B **259**, 683–687.

Rugel, G., T. Faestermann, K. Knie, G. Korschinek, A. A. Marchetti, J. E. McAninch, Rühm, W., T. Straume, and C. Wallner, 2000, "Accelerator mass spectrometry of ^{63}Ni using a gas-filled magnet at

the Munich Tandem Laboratory," Nucl. Instrum. Methods Phys. Res., Sect. B **172**, 934–938.

Rugel, G., T. Faestermann, K. Knie, G. Korschinek, M. Poutivtsev, D. Schumann, N. Kivel, I. Günther-Leopold, R. Weinreich, and M. Wohlmuther, 2009, "New Measurement of the ^{60}Fe Half-Life," Phys. Rev. Lett. **103**, 072502.

Rühm, W., *et al.*, 2007, "Neutron-induced ^{63}Ni in copper samples from Hiroshima and Nagasaki: a comprehensive presentation of results obtained at the Munich Maier-Leibnitz Laboratory," Radiat. Environ. Biophys. **46**, 327–338.

Rühm, W., *et al.*, 2010, "^{41}Ca in tooth enamel. Part II: A means for retrospective biological neutron dosimetry in atomic bomb survivors," Radiat. Res. **174**, 146–154.

Sadier, B., J.-J. Delannoya, L. Benedetti, D. L. Bourlès, S. Jaillet, J.-M. Geneste, A.-E. Lebatard, and M. Arnold, 2012, "Further constraints on the Chauvet Cave artwork elaboration," Proc. Natl. Acad. Sci. U.S.A. **109**, 8002–8006.

Sakaguchi, A., P. Steier, Y. Takahashi, and M. Yamamoto, 2014, "Isotopic compositions of ^{236}U and Pu isotopes in 'black substances' collected from roadsides in Fukushima Prefecture: Fallout from the Fukushima Dai-ichi Nuclear Power Plant accident," Environ. Sci. Technol. **48**, 3691–3697.

Sakurai, H., F. Tokanai, F. Miyake, K. Horiuchi, K. Masuda, H. Miyahara, M. Ohyama, M. Sakamoto, T. Mitsutani, and T. Moriya, 2020, "Prolonged production of ^{14}C during the ∼660 BCE solar proton event from Japanese tree rings," Sci. Rep. **10**, 660.

Sann, H., H. Damjantschitsch, D. Hebbard, J. Junge, D. Pelte, B. Povh, D. Schwalm, and D. B. Tran Thoai, 1975, "A position-sensitive ionization chamber," Nucl. Instrum. Methods **124**, 509–519.

Santos, G. M., J. R. Southon, S. Griffin, S. R. Beaupre, and E. R. M. Druffel, 2007, "Ultra small-mass AMS ^{14}C sample preparation and analyses at KCCAMS/UCI Facility," Nucl. Instrum. Methods Phys. Res., Sect. B **259**, 293–302.

Saunois, M., *et al.*, 2020, "The global methane budget 2000–2017," Earth Syst. Sci. Data **12**, 1561–1623.

Schaefer, J. M., A. T. Codilean, J. K. Willenbring, Z.-T. Lu, B. Keisling, R.-H. Fülöp, and P. Val, 2022, "Cosmogenic nuclide techniques," Nat. Rev. Methods Primers **2**, 1–22.

Schaefer, J. M., G. Winckler, P. H. Blard, G. Balco, D. L. Shuster, R. Friedrich, A. J. T. Jull, R. Wieler, and C. Schluechter, 2016, "Performance of CRONUS-P—A pyroxene reference material for helium analysis," Quat. Geochronol. **31**, 237–239.

Schaefer, J. M., *et al.*, 2009 "High-frequency Holocene glacier fluctuations in New Zealand differ from the northern signature," Science **324**, 622–625.

Schlomberg, M., C. Vockenhuber, H.-A. Synal, D. Schumann, M. Veicht, I. Mihalcea, and D. Schumann, 2022, "Isobar separation of ^{32}Si from ^{32}S in AMS using a passive absorber," Nucl. Instrum. Methods Phys. Res., Sect. B **533**, 56–60.

Schramm, D., and W. A. Fowler, 1971, "Synthesis of superheavy elements in the *r*-process," Nature (London) **231**, 103–106.

Schulte, P., *et al.*, 2010, "The Chicxulub asteroid impact and mass extinction at the Cretaceous-Paleogene boundary," Science **327**, 1214–1218.

Schulze-König, T., S. R. Dueker, J. Giacomo, M. Suter, J. S. Vogel, and H.-A. Synal, 2010, "BioMICADAS: Compact next generation AMS system for pharmaceutical science," Nucl. Instrum. Methods Phys. Res., Sect. B **268**, 891–894.

Schwarzschild, A. Z., P. Thieberger, and J. B. Cumming, 1977, "A search for superheavy elements in nature—The tandem van de Graaff as a high sensitivity mass spectrometer," Bull. Am. Phys. Soc. **22**, 94.

Schwarzschild, B., 1988, "Negative calcium ions are stable—in spite of the conventional wisdom," Phys. Today **41**, No. 6, 21–24.

Scognamiglio, G., E. Chamizo, J. M. López-Gutiérrez, A. M. Müller, S. Padilla, F. J. Santos, M. López-Lora, C. Vivo-Vilches, and M. García-León, 2016, "Recent developments of the 1 MV AMS facility at the Centro Nacional de Aceleradores," Nucl. Instrum. Methods Phys. Res., Sect. B **375**, 17–25.

Scognamilio, G., M. Klein, F. L. van de Hoef, N. C. Podaru, and D. J. W. Mous, 2021, "Low-energy ^{14}C and multi-element HVE AMS systems," Nucl. Instrum. Methods Phys. Res., Sect. B **492**, 29–33.

Seaborg, G. T., 1968, "Elements beyond 100, present status and future prospects," Annu. Rev. Nucl. Sci. **18**, 53–152.

Seaborg, G. T., 1995, "Transuranium elements: The synthetic actinides," Radiochim. Acta **70–71**, 69–90.

Sekimoto, S., *et al.*, 2015, "Measurement of production cross sections of ^{10}Be and ^{26}Al by 120 GeV and 392 MeV proton bombardment of ^{89}Y^{159}Tb, and ^{nat}Cu targets," Nucl. Instrum. Methods Phys. Res., Sect. B **361**, 685–688.

Seltzer, A. M., D. V. Bekaert, P. H. Barry, K. E. Durkin, E. K. Mace, C. E. Aalseth, J. C. Zappala, P. Mueller, B. Jurgens, and J. T. Kulongoski, 2021, "Groundwater residence time estimates obscured by anthropogenic carbonate," Sci. Adv. **7**, eabf3503.

Shackleton, N. J., 1987, "Oxygen isotopes, ice volumes and sea levels," Quat. Sci. Rev. **6**, 183–190.

Shapira, D., R. M. deVries, H. W. Fulbright, J. Toke, and M. R. Clover, 1975, "The Rochester heavy ion detector," Nucl. Instrum. Methods **129**, 123–130.

Shen, G., X. Gao, B. Gao, and D. E. Granger, 2009, "Age of Zhoukoudian *Homo erectus* determined with ^{26}Al/^{10}Be burial dating," Nature (London) **458**, 198–200.

Shen, G., Y. Wang, H. Tu, H. Tong, Z. Wu, K. Kuman, D. Fink, and D. E. Granger, 2020. "Isochron ^{26}Al/^{10}Be burial dating of Xihoudu: Evidence for the earliest human settlement in northern China," Anthropologie **124**, 102790.

Simpson, J. A., 1983, "Elemental and isotopic composition of the Galactic cosmic rays," Annu. Rev. Nucl. Part. Sci. **33**, 323–381.

Sistemich, K., *et al.*, 1975, "The isotope identification and the β-decay chain analysis at the fission product separator 'JOSEF,'" Nucl. Instrum. Methods **130**, 491–497.

Skoglund, P., and D. Reich, 2016, "A genomic view of the peopling of the Americas," Curr. Opin. Genet. Dev. **41**, 27–35.

Soddy, F., 1913, "Intra-atomic charge," Nature (London) **92**, 399–400.

Spalding, K. L., R. D. Bhardwaj, B. A. Buchholz, H. Druid, and J. Frisén, 2005, "Retrospective birth dating of cells in humans," Cell **122**, 133–143.

Spalding, K. L., *et al.*, 2013, "Dynamics of hippocampal neurogenesis in adult humans," Cell **153**, 1219–1227.

Spalding, K. L., *et al.*, 2017, "Impact of fat mass and distribution on lipid turnover in human adipose tissue," Nat. Commun. **8**, 15253.

Sparrow, K. J., J. D. Kessler, J. R. Southon, F. Garcia-Tigreros, K. M. Schreiner, C. D. Ruppel, J. B. Miller, S. J. Lehman, and X. Xu, 2018, "Limited contribution of ancient methane to surface waters of the U.S. Beaufort Sea shelf," Sci. Adv. **4**, eaao4842.

Steier, P., K. Hain, U. Klötzli, J. Lachner, A. Priller, S. Winkler, and R. Golser, 2019, "The actinide beamline at VERA," Nucl. Instrum. Methods Phys. Res., Sect. B **458**, 82–89.

Steier, P., J. Liebl, W. Kutschera, E. M. Wild, and R. Golser, 2017, "Preparation method of μg carbon samples for ^{14}C measurements," Radiocarbon **59**, 803–814.

Steier, P., *et al.*, 2008, "Natural and anthropogenic ^{236}U in environmental samples," Nucl. Instrum. Methods Phys. Res., Sect. B **266**, 2246–2250.

Steier, P., *et al.*, 2019, "Comparison of methods for the detection of ^{10}Be with AMS and a new approach based on a silicon nitride foil stack," Int. J. Mass Spectrom. **444**, 116175.

Stephens, W., J. Klein, and R. Zurmühle, 1980, "Search for naturally occurring superheavy element $Z = 110$, $A = 294$," Phys. Rev. C **21**, 1664–1666.

Stone, J. O., G. L. Allan, L. K. Fifield, and R. G. Cresswell, 1996, "Cosmogenic chlorine-36 from calcium spallation," Geochim. Cosmochim. Acta **60**, 679–692.

Straume, T., *et al.*, 2003, "Measuring fast neutrons in Hiroshima at distances relevant to atomic-bomb survivors," Nature (London) **424**, 539–542.

Straume, T., *et al.*, 2004, "Addendum: Measuring fast neutrons in Hiroshima at distances relevant to atomic-bomb survivors," Nature (London) **430**, 483.

Sturchio, N. C., *et al.*, 2004, "One million year old groundwater in the Sahara revealed by krypton-81 and chlorine-36," Geophys. Res. Lett. **31**, L05503.

Suess, H. E., 1955, "Radiocarbon concentration in modern wood," Science **122**, 415–417.

Suess, H. E., and H. C. Urey, 1956, "Abundances of the elements," Rev. Mod. Phys. **28**, 53–74.

Sukhodolov, T., *et al.*, 2017, "Atmospheric impacts of the strongest known solar particle storm of 775 AD," Sci. Rep. **7**, 45257.

Suter, M., 2004, "25 years of AMS—A review of recent developments," Nucl. Instrum. Methods Phys. Res., Sect. B **223–224**, 139–148.

Suter, M., M. Döbeli, M. Grajcar, A. Müller, M. Stocker, G. Sun, H.-A. Synal, and L. Wacker, 2007, "Advances in particle identification in AMS at low energies," Nucl. Instrum. Methods Phys. Res., Sect. B **259**, 165–172.

Suter, M., S. Jacob, and H.-A. Synal, 1997, "AMS of ^{14}C at low energies," Nucl. Instrum. Methods Phys. Res., Sect. B **123**, 148–152.

Swiatecki, W. J., 1956, "Systematics of fission thresholds," Phys. Rev. **101**, 97–99.

Synal, H.-A., 2013, "Developments in accelerator mass spectrometry," Int. J. Mass Spectrom. **349–350**, 192–202.

Synal, H.-A., 2022, "Accelerator mass spectrometry: Ultra-sensitive detection technique of long-lived radionuclides," Chimia **76**, 45–51.

Synal, H.-A., J. Beer, G. Bonani, H. J. Hofmann, M. Suter, and W. Wölfli, 1987, "Detection of ^{32}Si and ^{36}Cl with the ETH/SIN EN-Tandem," Nucl. Instrum. Methods Phys. Res., Sect. B **29**, 146–150.

Synal, H.-A., M. Döbeli, S. Jacob, M. Stocker, and M. Suter, 2004, Radiocarbon AMS towards its low-energy limits," Nucl. Instrum. Methods Phys. Res., Sect. B **223–224**, 339–345.

Synal, H.-A., M. Stocker, and M. Suter, 2007, "MICADAS: A New compact radiocarbon AMS system," Nucl. Instrum. Methods Phys. Res., Sect. B **259**, 7–13.

Szabo, J., I. Carmi, D. Segal, and E. Mintz, 1997, "An attempt at absolute ^{14}C dating," Radiocarbon **40**, 77–83.

Taricco, C., N. Bhandari, D. Cane, P. Colombetti, and N. Verma, 2006, "Galactic cosmic ray flux decline and periodicities in the interplanetary space during the last 3 centuries revealed by ^{44}Ti in meteorites," J. Geophys. Res. **111**, A08102.

Taylor, R. E., and Ofer Bar-Josef, 2014, *Radiocarbon Dating: An Archaeological Perspective* (Routledge, New York), p. 404.

Terrasi, F., *et al.*, 2020, "Can the ^{14}C production in 1055 CE be affected by SN1054?," Radiocarbon **62**, 1403–1418.

Tessler, M., *et al.*, 2018, "Stellar $^{36,38}\mathrm{Ar}(n,\gamma)^{37,39}\mathrm{Ar}$ Reactions and Their Effect on Light Neutron-Rich Nuclide Synthesis," Phys. Rev. Lett. **121**, 112701.

Thielemann, F.-K., 2019, "Explosive nucleosynthesis: What we learned and what we still do not understand," in *Nuclei in the Cosmos XV*, Springer Proceedings in Physics Vol. 219, edited by A. Formicola, M. Junker, L. Gialanella, and G. Imbriani (Springer, Cham, Switzerland), pp. 125–134, 10.1007/978-3-030-13876-9_21.

Thoennessen, M., 2016, *The Discovery of Isotopes* (Springer International Publishing, Cham, Switzerland), p. 413.

Thompson, L. G., H. H. Brecher, E. Mosley-Thompson, D. R. Hardy, and B. G. Mark, 2009, "Glacier loss on Kilimanjaro continues unabated," Proc. Natl. Acad. Sci. U.S.A. **106**, 19770–19775.

Thomson, J. J., 1913, "Bakerian lecture: Rays of positive electricity," Proc. R. Soc. A **89**, 1–20.

Tims, S. G., M. B. Froehlich, L. K. Fifield, A. Wallner, and M. De Cesare, 2016, "^{236}U and ^{239,240}Pu ratios from soils around an Australian nuclear weapons test site," J. Environ. Radioact. **151**, 563–567.

Tong, A. L., J.-Q. Gu, G. M. Yang, S.-M. Hu, W. Jianga, Z.-T. Lu, and F. Ritterbusch, 2021, "An atom trap system for ^{39}Ar dating with improved precision," Rev. Sci. Instrum. **92**, 063204.

Trappitsch, R., M. R. Savina, J. M. Rolison, L. N. Harrison, and N. Dauphas, 2019, "Towards the 1000 atom detection limit for ^{244}Pu," in *Proceedings of the 50th Lunar and Planetary Science Conference, The Woodlands, TX, 2019*, LPI Contribution No. 2132, https://www.hou.usra.edu/meetings/lpsc2019/pdf/2978.pdf.

Tsuda, Y., M. Yoshikawa, T. Saiki, S. Nakazawa, and S. Watanabe, 2019, "Hayabusa2-sample return and kinetic impact mission to near-Earth asteroid Ryugu," Acta Astronaut. **156**, 387–393.

Tuniz, C., J. R. Bird, D. Fink, and G. F. Herzog, 1998, *Accelerator Mass Spectrometry—Ultrasensitive Analysis for Global Science* (CRC Press, Boca Raton).

Turteltaub, K. W., J. S. Felton, B. L. Gledhill, J. S. Vogel, J. R. Southon, M. W. Caffee, R. C. Finkel, D. E. Nelson, D. Proctor, and J. C. Davis, 1990, "Accelerator mass spectrometry in biomedical dosimetry: Relationship between low-level exposure and covalent binding of heterocyclic amine carcinogens to DNA," Proc. Natl. Acad. Sci. U.S.A. **87**, 5288–5292.

Tykesson, P., H. H. Andersen, and J. Heinemeier, 1976, "Further investigation of ANIS (the Aarhus Negative Ion Source)," IEEE Trans. Nucl. Sci. **23**, 1104–1108.

Usoskin, I. G., A. Gil, G. A. Kovaltsov, A. L. Mishev, and V. V. Mikhailov, 2017, "Heliospheric modulation of cosmic rays during the neutron monitor era: Calibration using PAMELA data for 2006–2010," J. Geophys. Res. Space Phys. **122**, 3875–3887.

Usoskin, I. G., B. Kromer, F. Ludlow, J. Beer, M. Friedrich, G. A. Kovaltsov, S. K. Solanki, and L. Wacker, 2013, "The AD775 cosmic event revisited: The Sun is to blame," Astron. Astrophys. **552**, L3.

Uusitalo, J., *et al.*, 2018, "Solar superstorm of AD 774 recorded subannually by Arctic tree rings," Nat. Commun. **9**, 3495.

Van Vuuren, D. P., J. A. Edmonds, M. Kainuma, K. Riahi, and J. Weyant, 2011, "The representative concentration pathways in climatic change," Clim. Change **109**, 5–31.

Varga, T., R. E. Fisher, J. L. France, L. Haszpra, A. J. T. Jull, D. Lowry, I. Major, M. Molnár, E. G. Nisbet, and E. Lászlo, 2021, "Identification of potential methane source regions in Europe using $\delta^{13}\mathrm{C}_{\mathrm{CH4}}$ measurements and trajectory modeling," J. Geophys. Res. Atmos. **126**, e2020JD033963.

Veicht, M., I. Mihalcea, Đ. Cvjetinovic, and D. Schumann, 2021, "Radiochemical separation and purification of non-carrier-added silicon-32," Radiochim. Acta **109**, 735–741.

Villa, I. M., N. E. Holden, A. Possolo, R. B. Ickert, D. B. Hibbert, and P. R. Renne, 2020, "IUPAC-IUGS recommendation on the half-lives of ^{147}Sm and ^{146}Sm," Geochim. Cosmochim. Acta **285**, 70–77.

Viola, V. E., 1969, "On the production of nucleides with $A > 250$ in stellar nucleosynthesis," Nucl. Phys. **A139**, 188–202.

Vockenhuber, C., I. Ahmad, R. Golser, W. Kutschera, V. Liechtenstein, A. Priller, P. Steier, and S. Winkler, 2003, "Accelerator mass spectrometry of heavy long-lived radionuclides," Int. J. Mass Spectrom. **223–224**, 713–732.

Vockenhuber, C., V. Alfimov, M. Christl, J. Lachner, T. Schulze-König, M. Suter, and H.-A. Synal, 2013, "The potential of He stripping in heavy ion AMS," Nucl. Instrum. Methods Phys. Res., Sect. B **294**, 382–386.

Vockenhuber, C., C. Feldstein, M. Paul, N. Trubnikov, M. Bichler, R. Golser, W. Kutschera, A. Priller, P. Steier, and S. Winkler, 2004, "Search for live ^{182}Hf in deep-sea sediments," New Astron. Rev. **48**, 161–164.

Vockenhuber, C., K.-U. Miltenberger, and H.-A. Synal, 2019, "^{36}Cl measurements with a gas-filled magnet at 6 MV," Nucl. Instrum. Methods Phys. Res., Sect. B **455**, 190–194.

Vockenhuber, C., *et al.*, 2004, "New Half-Life Measurement of ^{182}Hf: Improved Chronometer for the Early Solar System," Phys. Rev. Lett. **93**, 172501.

Vogt, S., G. F. Herzog, and R. C. Reedy, 1990, "Cosmogenic nuclides in extraterrestrial materials," Rev. Geophys. **28**, 253–275.

Wacker, L., D. Güttler, J. Goll, J. P. Hurni, H.-A. Synal, and N. Walti, 2014, "Radiocarbon dating to a single year by means of rapid atmospheric ^{14}C changes," Radiocarbon **56**, 573–579.

Wacker, L., M. Nemec, and J. Bourquin, 2010, "A revolutionary graphitization system: Fully automated, compact and simple," Nucl. Instrum. Methods Phys. Res., Sect. B **268**, 931–934.

Wacker, L., *et al.*, 2020, "Findings from an in-depth annual tree-ring radiocarbon calibration," Radiocarbon **62**, 873–882.

Wallner, A., 2010, "Nuclear astrophysics and AMS—Probing nucleosynthesis in the lab," Nucl. Instrum. Methods Phys. Res., Sect. B **268**, 1277–1282.

Wallner, A., M. Bichler, K. Buczak, R. Dressler, L. K. Fifield, D. Schumann, J. H. Sterba, S. G. Tims, G. Wallner, and W. Kutschera, 2015, "Settling the Half-Life of ^{60}Fe: Fundamental for a Versatile Astrophysical Chronometer," Phys. Rev. Lett. **114**, 041101.

Wallner, A., S. V. Chuvaev, A. A. Filatenkov, Y. Ikeda, W. Kutschera, G. Mertens, A. Priller, W. Rochow, P. Steier, and H. Vonach, 2003, "Precise measurement of the ^{27}Al$(n, 2n)^{26g}$Al excitation function near threshold and its relevance for fusion-plasma technology," Eur. Phys. J. A **17**, 285–296.

Wallner, A., L. K. Fifield, M. B. Froehlich, D. Koll, G. Leckenby, M. Martschini, S. Pavetich, S. G. Tims, D. Schumann, and Z. Slavkovská, 2023, "Accelerator mass spectrometry with ANU's 14 million volt accelerator," Nucl. Instrum. Methods Phys. Res., Sect. B **534**, 48–53.

Wallner, A., W. Rühm, G. Rugel, N. Nakamura, A. Arazi, T. Faestermann, K. Knie, H. J. Maier, and G. Korschinek, 2010, "^{41}Ca in tooth enamel. Part I: A biological signature of neutron exposure in atomic bomb survivors," Radiat. Res. **174**, 137–145.

Wallner, A., *et al.*, 2014, "Novel Method to Study Neutron Capture of ^{235}U and ^{238}U Simultaneously at keV Energies," Phys. Rev. Lett. **112**, 192501.

Wallner, A., *et al.*, 2015, "Abundance of live ^{244}Pu in deep-sea reservoirs on Earth points to rarity of actinide nucleosynthesis," Nat. Commun. **6**, 5956.

Wallner, A., *et al.*, 2016a, "Recent near-Earth supernovae probed by global deposition of interstellar radioactive ^{60}Fe," Nature (London) **532**, 69.

Wallner, A., *et al.*, 2016b, "Accelerator mass spectrometry measurements of the ^{13}C$(n,\gamma)^{14}$C and ^{14}N$(n,p)^{14}$C cross sections," Phys. Rev. C **93**, 045803.

Wallner, A., *et al.*, 2017, "Precise measuement of the thermal and stellar ^{54}Fe$(n,\gamma)^{55}$Fe cross secions via accelerator mass spectrometry," Phys. Rev. C **96**, 025808.

Wallner, A., *et al.*, 2019, "Stellar and thermal neutron capture cross section of ^{9}Be," Phys. Rev. C **99**, 015804.

Wallner, A., *et al.*, 2020, "^{60}Fe deposition during the late Pleistocene and the Holocene echoes past supernova activity," Proc. Natl. Acad. Sci. U.S.A. **117**, 21873–21879.

Wallner, A., *et al.*, 2021, "^{60}Fe and ^{244}Pu deposited on Earth constrain the *r*-process yields of recent nearby supernovae," Science **372**, 742–745.

Wallner, C., T. Faestermann, U. Gerstmann, K. Knie, G. Korschinek, C. Lierse, and G. Rugel, 2004, "Supernova produced and anthropogenic ^{244}Pu in deep sea manganese encrustations," New Astron. Rev. **48**, 145–150.

Wang, F. Y., H. Yu, Y. C. Zou, Z. G. Dai, and K. S. Cheng, 2017, "A rapid cosmic-ray increase in BC 3372–3371 from ancient buried tree rings in China," Nat. Commun. **8**, 1487.

Wasserburg, G. J., M. Busso, R. Gallino, and K. M. Nollett, 2006, "Short-lived nuclei in the early Solar System: Possible AGB sources," Nucl. Phys. **A777**, 5–69.

Waters, M. R., 2019, "Late Pleistocene exploration and settlement of the Americas by modern humans," Science **365**, eeat5447.

Waters, M. R., T. W. Stafford, Jr., and D. L. Carlson, 2020, "The age of Clovis—13,050 to 12,750 cal yr B.P.," Sci. Adv. **6**, eaaz0455.

Weiner, S., and P. Price, 1986, "Disaggregation of bone into crystals," Calcif. Tissue Int. **39**, 365–375.

Welch, J. J., K. J. Bertsche, P. G. Friedman, D. E. Morris, R. A. Muller, and P. P. Tans, 1986, "A low energy cyclotron for radiocarbon dating," Nucl. Instrum. Methods Phys. Res., Sect. B **18**, 202–214.

Welte, C., L. Wacker, B. Hattendorf, M. Christl, J. Koch, H. Synal, and D. Günther, 2016, "Novel laser ablation sampling device for the rapid radiocarbon analysis of carbonate samples by accelerator mass spectrometry," Radiocarbon **58**, 419–435.

Welte, C., *et al.*, 2016, "Laser ablation–accelerator mass spectrometry: An approach for rapid radiocarbon analyses of carbonate archives at high spatial resolution," Anal. Chem. **88**, 8570–8576.

Welten, K. C., C. Alderliesten, K. van der Borg, L. Lindner, T. Loeken, and L. Schultz, 1997, "Lewis Cliff 86360: An Antarctic L-chondrite with a terrestrial age of 2.35 million years," Meteorit. Planet. Sci. **32**, 775–780.

Welten, K. C., K. Nishiizumi, M. W. Caffee, D. J. Hillegonds, J. A. Johnson, A. J. T. Jull, R. Wieler, and L. Folco, 2006, "Terrestrial ages, pairing and concentration mechanisms of Antarctic chondrites from Frontier Mountain, northern Victoria Land," Meteorit. Planet. Sci. **41**, 1081–1094.

Wendt, K. D. A., 2002, "The new generation of resonant ionization mass spectrometers: Becoming competitive in selective atomic ultra-trace determination?," Eur. J. Mass Spectrom. **8**, 273–285.

Wendt, K. D. A., N. Trautmann, and B. A. Bushaw, 2000, "Resonant laser ionization mass spectrometry: An alternative to AMS?," Nucl. Instrum. Methods Phys. Res., Sect. B **172**, 162–169.

Werner, F. G., and J. A. Wheeler, 1958, "Superheavy nuclei," Phys. Rev. **109**, 126–144.

White, N. R., R. E. M. Hedges, J. O. Wand, and E. T. Hall, 1981, The radiocarbon facility at the research laboratory for archaeology in Oxford—A review," in *Proceedings of the Second International Conference on Accelerator Mass Spectroscopy, Argonne, IL, 1981*, edited by W. Henning, W. Kutschera, R. K. Smither, and

J. L. Yntema (Argonne National Laboratory Report No. ANL/PHY 81-1), pp. 472–483, https://phaidra.univie.ac.at/o:1624875.

Wielandt, D., and M. Bizzarro, 2011, "A TIMS-based method for the high-precision measurements, of the three-isotope potassium composition of small samples," J. Anal. At. Spectrom. **26**, 366–377.

Wild, E. M., K. A. Arlamovsky, R. Golser, W. Kutschera, A. Priller, S. Puchegger, W. Rom, P. Steier, and W. Vycudilik, 2000, "^{14}C dating with the bomb peak: An application to forensic medicine," Nucl. Instrum. Methods Phys. Res., Sect. B **172**, 944–950.

Wild, E. M., W. Kutschera, A. Meran, and P. Steier, 2019, "^{14}C bomb peak analysis of African elephant tusks and its relation to CITES," Radiocarbon **61**, 1619–1624.

Wölfli, W., H. A. Polach, and H. H. Andersen, 1984, Eds., *Proceedings of the Third Symposium on Accelerator Mass Spectrometry, Zürich, 1984* (North-Holland, Amsterdam) [Nucl. Instrum. Methods Phys. Res., Sect. B **5**, 91–448].

Wu, Y., X. Dai, S. Xing, M. Luo, M. Christl, H.-A. Synal, and S. Hou, 2022, "Direct search for primordial ^{244}Pu in Bayan Obo bastnaesite," Chin. Chem. Lett. **33**, 3522–3526.

Yamaguchi, Y., 1963, "Possible use of ^{41}Ca in nuclear dating," Prog. Theor. Phys. **30**, 567, https://academic.oup.com/ptp/article/30/4/567/1882467.

Yiou, F., and G. M. Raisbeck, 1990, Eds., Proceedings of the Fifth International Conference on Accelerator Mass Spectrometry, Paris, 1990 [Nucl. Instrum. Methods Phys. Res., Sect. B **52**, 211–630].

Yokochi, R., J. C. Zappala, R. Purtschert, and P. Mueller, 2021, "Origin of water masses in Floridan aquifer system revealed by ^{81}Kr," Earth Planet. Sci. Lett. **569**, 117060.

Zappala, J. C., D. Baggenstos, C. Gerber, W. Jiang, B. M. Kennedy, Z.-T. Lu, J. Masarik, P. Mueller, R. Purtschert, and A. Visser, 2020, "Atmospheric ^{81}Kr as an integrator of cosmic-ray flux on the hundred-thousand-year time scale," Geophys. Res. Lett. **47**, e2019GL086381.

Zazzeri, G., D. Lowry, R. E. Fisher, J. L. France, M. Lanoisellé, C. S. B. Grimmond, and E. G. Nisbet, 2017, "Evaluating methane inventories by isotopic analysis in the London region," Sci. Rep. **7**, 4854.

Zazzeri, G., X. Xu, and H. Graven, 2021, "Efficient sampling of atmospheric methane for radiocarbon analysis and quantification of fossil methane," Environ. Sci. Technol. **55**, 8535–8541.

Zhao, X.-L., and A. E. Litherland, 2007, "The anions of the Li, Be and B fluorides: The super-halogens and AMS," Nucl. Instrum. Methods Phys. Res., Sect. B **259**, 224–229.

Zhao, X.-L., M.-J. Nadeau, M. A. Garwan, L. R. Kilius, and A. E. Litherland, 1994, "Radium, actinides, and their molecular negative ions from a cesium sputter ion source," Nucl. Instrum. Methods Phys. Res., Sect. B **92**, 258–264.

Zhao, X.-L., M.-J. Nadeau, L. R. Kilius, and A. E. Litherland, 1994, "The first detection of naturally-occurring ^{236}U with accelerator mass spectrometry," Nucl. Instrum. Methods Phys. Res., Sect. B **92**, 249–253.

Zhou, W. J., W. Beck, X. Kong, Z. S. An, X. Qiang, K. Wu, F. Xian, and H. Ao, 2014, "Timing of the Brunhes-Matayama magnetic polarity reversal in Chinese loess using ^{10}Be," Geology **42**, 467–470.

Zhou, W. J., M. B. Chen, Y. H. Liu, D. Donahue, J. Head, X. F. Lu, A. J. T. Jull, and L. Deng, 2000, "Radiocarbon determinations using a minicyclotron: applications in archaeology," Nucl. Instrum. Methods Phys. Res., Sect. B **172**, 201–205.

Zimmermann, P. H., C. A. M. Brenninkmeijer, A. Pozzer, P. Jöckel, F. Winterstein, A. Zahn, S. Houweling, and J. Lelieveld, 2020, "Model simulations of atmospheric methane (1997–2016) and their evaluation using NOAA and AGAGE surface and IAGOS-CARIBIC aircraft," Atmos. Chem. Phys. **20**, 5787–5809.

Zondervan, A., C. Prior, F. Bruhn, and R. Sparks, 2013, Eds., Proceedings of the Twelfth International Conference on Accelerator Mass Spectrometry, Wellington, New Zealand, 2011, https://www.sciencedirect.com/journal/nuclear-instruments-and-methods-in-physics-research-section-b-beam-interactions-with-materials-and-atoms/vol/294/suppl/C.

Zoppi, U., P. W. Kubik, M. Suter, H.-A. Synal, H. R. von Gunten, and D. Zimmermann, 1994, "High intensity isobar separation at the Zürich AMS facility," Nucl. Instrum. Methods Phys. Res., Sect. B **92**, 142–145.